

# Spinal Stabilisation for Disc-Associated Cervical Spondylomyelopathy in Large-Breed Dogs

Thesis submitted in accordance with the requirements of the University  
of Liverpool for the degree of Doctor of Philosophy

by

Victor Daniel Lopez Tapia

November 2023



UNIVERSITY OF  
LIVERPOOL

---

## Abstract

This thesis describes work performed for the development of distraction-stabilisation implants for disc-associated Cervical Spondylomyelopathy (CSM) in large-breed dogs. Few products or systems are designed specifically for this application, and none are universally accepted as being consistently successful. This thesis also presents work performed to generate meaningful scientific data to understand how surgical distraction-stabilisation devices and stabilisation impact these.

A virtual multi-body dynamic model of a large breed dog was developed to generate the basic scientific data required to optimise the development of breed-specific spinal implants for breed dogs at high risk of CSM. Vertebral kinematics and kinetics data of large breed dogs were obtained via gait lab analysis. A neck dissection was performed to obtain the muscle architecture of a large breed dog. The tensile properties of three nuchal ligaments were analysed to complement the muscle data. A multi-body dynamics model was developed based on Computed Tomography (CT) data and all the generated data. This final model can serve as a basis for in-silico testing of CSM implants (e.g. FEA models) and optimise their development.

Novel virtual orientation and distraction techniques for canine cervical vertebrae were developed. This technique served as a guideline for developing canine patient-specific custom-designed titanium interbody devices. In-silico manipulation of pre-operative CT scans facilitated the additive manufacture of woven titanium interbody devices that conformed to patient vertebral end-plate morphology. A pilot study was undertaken to assess the medium-term outcome of the implants.

**Clinical significance:** By using the interbody spacers developed in this thesis, instrumented distraction-stabilisation in dogs with disc-associated cervical spondylomyelopathy (DA-CSM) was achieved with satisfactory medium-term outcomes with no significant complications. The device design facilitated CT-determined fusion with no or mild vertebral subsidence.

---

## Acknowledgements

The author would like to thank everyone who provided support for this project, in particular my supervisors Dr Dan Jones, Dr Karl Bates, Dr Thomas Maddox, Ben Walton, and Rob Pettitt for their continuous support and guidance throughout these years; my research group fellows, Itayetzi Rodarte, Alice Brettle, and James Sage for their help with the inter-observer validation study; the UoL Additive Manufacturing group, especially Dr Phanphong Kongphan, Dr Sam Evans, Dr Michael Head, Dr Rodrigo Magana, and Paul Whittle for their guidance with additive manufacturing equipment; Dr Brendan Geraghty for his invaluable guidance with instron testing; Dr James Charles for his extensive guidance with musculoskeletal modelling; Dr Sophie Macaulay who helped with the neck dissection; Dr James Gardiner for his help with the gait lab setup; all staff from the Veterinary Teaching Suite, Institute of Veterinary Science, University of Liverpool, for their help with cadaver-related matters, specially Dr Zeeshan Durrani who helped with the nuchal ligament dissection; Dr Colin Driver and Jeremy Rose for kindly providing clinical guidance for implant development and performing surgeries for the clinical pilot study; Rory Fentem and Andrew Tomlinson for also contributing to the clinical pilot study; Kiran Mann for kindly providing PBS solutions for the ligament testing; the technical staff at the School of Engineering for their assistance with manufacturing matters; and the dog volunteers and their owners for contributing to this research. Additional thanks go to Consejo Nacional de Ciencia y Tecnologia (CONACYT) from Mexico for funding this project and providing financial support.

I would like to extend further gratitude to my primary supervisor Dr Dan Jones, who not only made me feel welcome in the research group since the beginning of the project but also provided invaluable support at a personal level at all times.

A very warm thank you to my colleague and best friend; my dear wife Itayetzi Rodarte, for her support and immense love that impelled me over the last years to complete my research. Additionally, thank you to my baby Isabella; she has brightened my life and given me the motivation I needed over the last months to get through the thesis

---

writing over difficult times. Finally, thank you to my parents Ana Tapia and Alberto Lopez, my brothers Alberto and Luis, and all my family and friends in Mexico who always supported me across the pond; and my friends in Liverpool that became family and were there to lighten my life over the last years.

---

# Contents

Abstract.....	i
Acknowledgements.....	ii
Contents.....	iv
1. Introduction .....	1
2. Background .....	4
2.1. Clinical Anatomy of the Canine Cervical Vertebral Column.....	4
2.1.1. Cervical Vertebrae .....	4
2.1.2. Intervertebral Discs .....	5
2.2. Disc-associated Cervical Spodylomyelopathy .....	6
2.2.1. Aetiology.....	6
2.2.2. Pathophysiology .....	7
2.2.3. Morphology of the Cervical Vertebrae and IVDs .....	10
2.3. Management Options for CSM .....	11
2.3.1. Medical Treatment .....	11
2.3.2. Surgical Treatment .....	11
Ventral Slot .....	13
Dorsal Laminectomy .....	14
Distraction-Stabilisation.....	15
2.3.3. Advancements in CSM Distraction-Stabilisation Devices.....	18
2.4. Identification and Selection of Study Breed Dog .....	21
2.4.1. Breed Predispositions to CSM .....	21
2.5. Additive Manufacturing for Novel Veterinary Devices .....	22
Selective Laser Sintering/Melting (SLS/SLM).....	23
Manufacturing of Anatomical Plates.....	23
Manufacturing of Surgical Guides .....	24
2.6. Software for 3D-Modelling and Implant Designing .....	25
2.7. Proposition of Stabilisation System .....	26
3. Design and Development of Patient-Specific Implant Prototypes .....	28
3.1. Introduction.....	28

---

3.2. Collation and Assembly of a Library of Anatomic Images.....	29
3.3. Development of Endplate-conforming Interbody Spacers .....	30
3.3.1. Identifying CT Scan Sample .....	30
3.3.2. Generation of 3D-Bone Models.....	30
3.3.3. Development of Cervical Vertebrae Orientation Technique .....	34
3.3.3.1. Intra- and Inter- Observer Variability .....	39
3.3.4. Virtual Orientation of Cervical Vertebrae .....	42
3.3.5. Development of Virtual Distraction Technique.....	43
3.3.6. Mapping of Endplate Morphology .....	44
3.3.7. CAD Profile Modelling .....	45
3.3.8. Analysis of Spacer Dimensions and Shapes.....	46
3.3.9. Distraction Level and Implant Construct .....	47
3.3.10. Manufacturing by Selective Laser Melting.....	48
3.4. Development of Ventral Anatomical Plate .....	49
3.4.1. Mapping of Ventral Vertebra Bodies.....	49
3.4.2. CAD Profile Modelling .....	50
3.4.3. Identification of Screw Trajectories .....	51
3.5. Results .....	52
4. In-silico Modelling of the Kinematics and Kinetics of a Native Canine Cervical Vertebral Column.....	54
4.1. Introduction.....	54
4.2. Non-invasive Gait Analysis of Neck Movements in a Normal Dog .....	56
4.2.1. Subject Recruitment .....	56
4.2.2. Quantification of Gait Kinematics and Kinetics .....	57
Gait Study Protocol .....	57
Data Acquisition .....	59
4.2.3. Quantification of Gross Body Proportions .....	62
4.2.4. Identification of Reference Gait Cycle .....	63
4.3. Analysis of Muscle Architecture: Neck Dissection .....	64
4.3.1 Sample Acquisition .....	64
4.3.2. Dissection Protocol and Muscle Architecture .....	64

---

4.4. Ex-vivo Nuchal Ligament Test– Tensile Strength .....	66
4.4.1. Experimental Design .....	66
4.4.2. Sample Acquisition and Dissection of the Nuchal Ligament .....	66
4.4.3. Measurement of Cross-Sectional Areas .....	68
4.4.4. Sample Preparation .....	69
4.4.5. Tensile Strength – Testing Protocol.....	70
4.4.6. Nuchal Ligament Properties .....	71
4.5. Generation of 3D-Reconstructed Skin-Bone Model .....	73
4.5.1. In-Silico Mesh Models .....	73
4.5.2. Generation of 3D-Reconstructed Skin-Bone Model.....	75
4.6. Results: Multi-Body Dynamics Model .....	78
4.6.1. Musculoskeletal Model .....	78
4.6.2. OpenSim model .....	83
4.6.3. Inverse Kinematics.....	85
4.6.4. Inverse Dynamics.....	86
4.6.5. Summary.....	88
5. Pilot Clinical Study.....	89
5.1. Introduction.....	89
5.2. Materials and Methods .....	90
5.2.1. Animals .....	90
5.2.2. Pre-Operative Imaging.....	90
5.2.3. Device Design and Manufacture .....	91
5.2.4. Surgical Procedure.....	92
5.2.5. Post-Operative Imaging .....	94
5.2.6. Statistical Analysis .....	95
5.3. Results .....	95
5.3.1. Demographics and Diagnosis .....	95
5.3.2. Surgery.....	96
5.3.3. Clinical Outcomes .....	97
5.3.4. Radiologic Outcomes .....	98
5.4. Discussion.....	101

---

6. Conclusion.....	106
6.1. Perspectives on Future Applications.....	107
References .....	108
Appendices.....	119



# 1. Introduction

Cervical spondylomyelopathy (CSM) is a clinical syndrome that is suffered in many species of mammals, including humans, horses and dogs. CSM is also commonly referred to as Wobbler Syndrome. Degeneration and herniation of intervertebral discs, with or without concomitant developmental abnormalities of the osseous structures of the vertebral column, results in static and dynamic compression of the spinal cord in the neck. These symptoms, in turn, result in pain and neurologic deficits in all four limbs. In dogs, this manifests as an ataxic gait and neck pain and is more common in large and giant breed dogs than small and miniature breed dogs. (da Costa, 2010).

Management options include medical treatment, surgical decompression, disc replacement, and surgical stabilisation of the adjacent vertebrae. Nowadays, there are more than 20 different approaches for CSM in veterinary practice, reflecting that the biomechanical principles of CSM must be carefully analysed and understood to achieve more effective techniques (da Costa, 2010). Surgical stabilisation eliminates motion and stress at the diseased segment and can be therapeutically successful. However, it is technically highly challenging. Safely placing implants that offer sufficient stability without compromising vital structures is very difficult. Limited products or systems are designed specifically for this application, and none are universally accepted as being consistently successful.

Therefore, this project aims to design and develop a functional distraction-stabilisation system for the surgical treatment of Cervical Spondylomyelopathy in large-breed dogs that can improve surgical outcomes. The following objectives have been set in order to achieve this:

1. To carry out a detailed literature review on CSM aetiology, pathophysiology, and the current surgical approaches for CSM.

2. To design and manufacture the implants and 3D bone models required to perform cervical distraction-stabilisation using Additive Manufacturing technology.
3. To carry out in-silico modelling of the kinematics and kinetics of a native canine cervical vertebral column to understand how distraction-stabilisation impacts these for implant optimisation.
4. To undertake a pilot study of clinical case series.

The initial intention for this project was to follow specific dog breeds and set the guidelines and workflow for future stratified approaches. During the literature review, two forms of CSM were identified: osseous-associated CSM accounting for approximately 15% of clinical CSM cases in canines, and disc-associated CSM affecting the other 85%. Due to the significant difference in affected population, this project only focuses on the disc-associated form. Furthermore, during the identification of breed predispositions to CSM, Dobermans were initially selected as the study dog breed because their predisposition and prevalence to CSM are significantly higher than any other breed dog. Thus, the library of medical images was intended to be primarily comprised of Doberman scans assembled during this project's first months. Subsequently, the gait lab analysis was carried out with 3 Doberman participants, and the in-silico model was started using Doberman CT scans. Likewise, a neck dissection

There were various constraints linked to this project. The first challenges are in regards to getting cadaveric material for the neck dissection and nuchal ligament testing. It was complicated to receive Doberman cadavers at the Veterinary Teaching Suite (VTS). After a year of waiting –while working on the initial stages- no Doberman cadavers were donated for this research. It was decided to use Hound cadaveric material instead due to their availability and similarity in neck size and shape to a Doberman. The second set of challenges arose from the Covid-19 pandemic, which affected the course of the project over the second half of its allocated time. The effects of Covid-19 change normal University activities unexpectedly, resulting in drawbacks to following the initial objectives for this project. The closure of University facilities

curtailed and limited access, thereby preventing any practical work over the different national lockdown stages. Likewise, access to research and additive manufacturing facilities was limited and experimenting on animal parts was not permitted. Additionally, cadaveric material was limited and the people assisting with this specialised work were also not readily available.

These delays impacted the project's comprehensive course for 24 months until the end of the allocated period for experimental work. A considerable effort was made to continue with the project, following as much as possible the initial objectives. However, the development shifted from a specific dog breed (Doberman) approach to a large-breed dog (mainly hound dogs). This shift will be noticed throughout the chapters. After all, by changing this approach, the final aim of this project was achieved for a large-breed dog cohort by designing and developing a functional distraction-stabilisation system for the surgical treatment of Cervical Spondylomyelopathy in large-breed dogs. Additionally, a multi-body dynamics model of a large-breed dog was developed to generate meaningful data for further implant testing (e.g. Finite Element Analysis) and optimisation.

---

## 2. Background

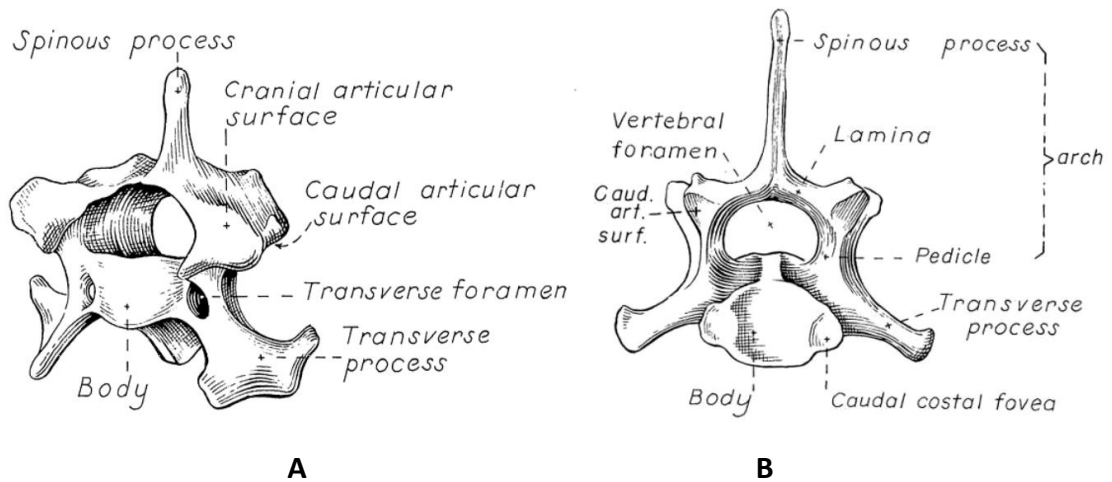
As with every engineering approach, it is paramount to understand not only the state-of-the-art techniques for performing stabilisation of the cervical vertebral column, but all parameters involved in this matter, commencing with the anatomy and physiology of the canine cervical vertebral column. A careful analysis of the interaction between biological matters (e.g. bones, ligaments and tendons) and the implants is needed to design a functional stabilisation system.

### 2.1. Clinical Anatomy of the Canine Cervical Vertebral Column

#### 2.1.1. Cervical Vertebrae

Understanding the morphology of the cervical vertebrae, intervertebral discs (IVDs), and their joint functionality is crucial when designing anatomical implants as potential replacement elements. The canine vertebral column is divided into five sections: cervical, thoracic, lumbar, sacral, and caudal. Typical vertebrae consist of a body, a vertebral arch (with left/right pedicles and laminae), and processes (transverse, articular, and spinous). The vertebra bodies are convex and concave in their cranial and caudal ends (also known as endplates). Figure 2-1 illustrates the anatomy of cervical vertebrae 5 (C5) and 7 (C7), applicable to all canine breeds.

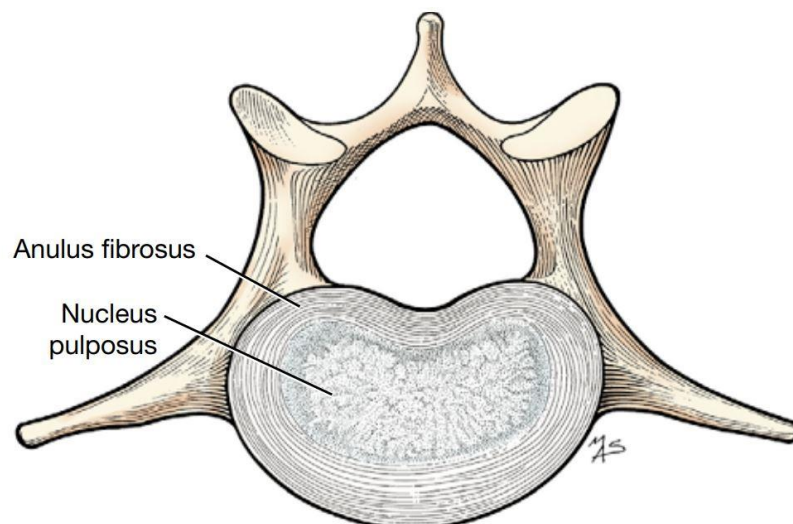
Key anatomic landmarks associated with CSM syndrome in the ventral aspect include the vertebral body, annulus fibrosus of IVDs (dorsal fibres) and the dorsal longitudinal ligament. Regarding the dorsal aspect, the joint capsules, articular facets, and dorsal vertebral lamina are components involved in the disease (Birchard and Sherding, 2006). These landmarks are relevant, and such terminologies are necessary throughout this project.



**Figure 2-1. (A) Craniolateral aspect of the canine C5, (B) Caudal view of the canine C7 (Miller and Evans, 1993).**

### 2.1.2. Intervertebral Discs

Intervertebral Discs (IVDs) are fibro-cartilage structures that interconnect adjacent vertebrae. An IVD consists of a soft central nucleus pulposus surrounded by the annulus fibrosus. They allow the motion of the vertebrae and absorb pressure and forces acting on the vertebral column (Evans and DeLahunta, 2017). Figure 2-2 illustrates a lumbar IVD of a young dog.



**Figure 2-2. Lumbar Intervertebral Disc of a young dog (cranial view) (Evans and DeLahunta, 2017).**

## **2.2. Disc-associated Cervical Spodylomyelopathy**

Cervical Spondylomyelopathy (CSM) is a clinical syndrome of the canine cervical vertebral column and manifests as spinal cord compression caused by abnormal development of the cervical vertebrae. This compression in turn, results in instability of the vertebral column leading to pain and neurologic deficits in all four limbs. In dogs, this manifests as an ataxic gait and neck pain and is more common in large and giant breed dogs than small and miniature breed dogs. (da Costa, 2010).

The disease is more apparent in large and giant dog breeds rather than medium, small and miniature dog breeds. Although cervical spondylomyelopathy is the most common term used in recent literature to describe the disease, a wide number of alternative terminologies have been utilised by veterinary surgeons and researchers over the years, namely cervical spondylopathy, caudal cervical spondylopathy, cervical spondylolisthesis, cervical vertebral malformation-malarticulation, cervical spinal instability, and cervical vertebral stenotic-myelopathy comprise the most common terms (da Costa, 2010, Lorenz et al., 2011, Jeffery, 1995). This degenerative disorder is colloquially known as 'Wobbler Syndrome' because the CSM-affected dogs suffer unstable gait, which in turn creates 'wobbly' movements. Although the term 'Wobbler Syndrome' is controversial because it does not necessarily describe the aetiology of its correspondent vertebral column lesion, it is a practical term for veterinary surgeons, facilitating communication with dog owners (Jeffery, 1995).

### **2.2.1. Aetiology**

The main characteristics of CSM-affected dogs include static or dynamic compression(s) of the cervical spinal cord and nerve roots which lead to various neurologic deficiencies (e.g. tetraparesis and ataxia) and pain across the cervical region. Such degenerations are associated with abnormal development and degenerative disease of the caudal section of the cervical vertebral column (Jeffery, 1995, da Costa, 2010).

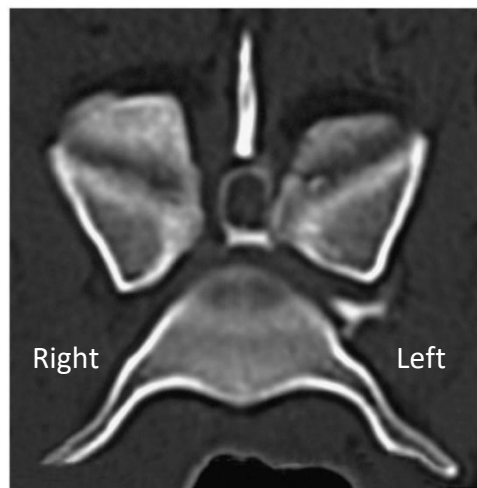
---

CSM is considered a syndrome since its aetiology is thought to be related to multiple factors, namely heredity, body conformation, and nutritional and congenital disorders. However, a well-established aetiology is still not clear. Regarding heredity factors, several studies -including a large study from the University of Liverpool in 1989- have attempted to describe any possible genetic origin for the syndrome but have failed to elicit any underlying genetic cause, for example (Burbidge et al., 1994, Lewis, 1989b). Secondly, body conformation as a possible aetiological factor has been studied since the early 1970s (Wright et al., 1973). In 1994, Burbidge and colleagues demonstrated no significant association between head/neck dimensions and CSM radiographic abnormalities of over 100 CSM-affected Dobermans (Burbidge et al., 1994). Furthermore, whether nutritional factors play a role in CSM is still questionable. However, congenital factors do appear to play a more significant role when compared to the previously mentioned ones since it has been demonstrated that most Dobermans are born with some degree of canal stenosis (da Costa, 2010).

### **2.2.2. Pathophysiology**

According to da Costa (da Costa et al., 2006) and De Decker (De Decker et al., 2010), a proportion of the clinically healthy Doberman population presents some degree of CSM characteristics without any clinical signs of having the disease. Approximately one-quarter of all healthy Dobermans possess some degree of spinal cord compression; approximately three-quarters of the population present clinically 'silent' IVD degenerations. It has been demonstrated that vertebral canal stenosis is present in all CSM-affected dogs to some extent (da Costa et al., 2006, De Decker et al., 2010). Stenosis can be severe, causing a direct compression on the spinal cord and CSM-related neurological signs, or less severe and pre-dispose to the development of clinical signs of CSM if further compression develops, from disc protrusion, for example (da Costa et al., 2006). The term *osseous-associated cervical spondylomyelopathy* (OACSM) is generally used if the CSM is associated with osseous malformation. The term *disc-associated cervical spondylomyelopathy* (DACSM) is applicable if the CSM is associated with IVD herniation.

CSM generally affects two main groups of dogs; young giant-breed dogs and adult-elderly large-breed dogs (Lorenz et al., 2011, Jeffery, 1995, Birchard and Sherding, 2006). OACSM accounts for approximately 15 % of clinical cases of canine CSM, with the vast majority of them Great Danes and other giant breeds. Common osseous malformations include vertebral body flattening and tilting, vertebral canal stenosis (at one or multiple levels), osteoarthritis at the articular process(es) and hypertrophy of the vertebral facet joints and interarcuate ligaments (Figure 2-3), leading to dorsal and dorsolateral compressions. The most commonly affected sites are C5, C6 and C7 in Great Danes; and C3 and C4 in Rottweilers and Basset hounds for this particular group (Jeffery, 1995, Birchard and Sherding, 2006, Lorenz et al., 2011).



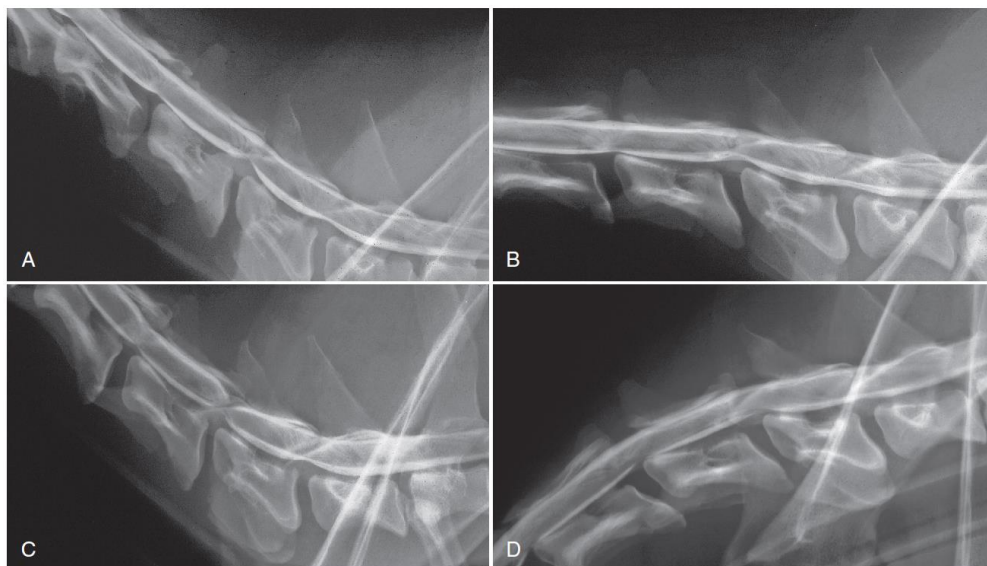
**Figure 2-3. Transverse CT/myelogram image of C6 vertebra after myelography from a 1.5-year-old male Great Dane with severe pelvic limb general proprioceptive (GP) ataxia and tetraparesis. Note proliferative articular processes causing lateral spinal cord compression more severe on the left (Lorenz et al., 2011).**

The second and most significant group comprises the other 85% of the CSM-affected population, of which approximately 80% are Dobermans (Birchard and Sherding, 2006, Jeffery, 1995). Such a group is more prone to suffer from degenerative diseases of the IVDs (e.g. flattening or tilting of the bone), which further causes spinal cord compression (Lorenz et al., 2011, Birchard and Sherding, 2006, Jeffery, 1995). Additional pathological characteristics involve hypertrophy of the dorsal longitudinal



and interarcuate ligaments (Figure 2-4). The most commonly affected joint in DACSM-affected Dobermans is C6-C7 (Jeffery, 1995, Lorenz et al., 2011).

Observations from Figure 2-4 include: (A) Neutral position showing spinal cord is severely compressed ventrally at C5-C6 vertebrae and mildly compressed at C6-C7. Compression is most likely caused by ligamentous proliferation in this area. (B) Traction of the cervical vertebral column demonstrates improvement of compression, indicating a dynamic lesion. (C) Extended cervical vertebral column positioning demonstrates that compression is more pronounced both dorsally and ventrally (recommended not to operate on this position, owing to the risk of worsening neurologic status). (D) Flexed positioning of the cervical vertebral column, demonstrating improvement of vertebral compression (Lorenz et al., 2011).



**Figure 2-4. Lateral myelogram with dynamic positioning of caudal cervical vertebral column from a Doberman with severe CSM at C5-C6 and mild at C6-C7 (Lorenz et al., 2011).**

Myelographic studies have demonstrated that ventro-flexion and linear traction of the neck can alleviate ventral spinal cord compression. Conversely, such compression can be worsened by neck dorsiflexion. These biomechanical characteristics were first described in the early 1980s, and can explain the dynamic element of CSM (Seim and

---

Withrow, 1982). This dynamic relationship between neck position, mechanical forces, and spinal cord compression, is one rationale for treating canine CSM with vertebral stabilisation (Jeffery, 1995).

### **2.2.3. Morphology of the Cervical Vertebrae and IVDs**

The selection of the optimal surgical approach for CSM treatment can be complex, with no universally recognised technique available. A deep analysis of the vertebrae morphology and their biomechanical characteristics may significantly contribute to developing more accurate and effective implants and instrumentation for this disease.

Diverse morphological studies have analysed different landmarks of the cervical vertebral column vertebrae and their respective IVDs of CSM-affected and non-CSM-affected dogs. Some of the landmarks encountered have been shown to be unrelated to DACSM. For instance, IVD width does not differ between Dobermans with and without DACSM (De Decker et al., 2012b). Additionally, Bonelli and colleagues found no significant differences in angle, shape or position (lateral distance) of the articular surfaces within the articular processes between non-affected Dobermans and CSM-affected Dobermans; and between non-affected Great Danes and CSM-affected Great Danes. Although some differences were found between different breeds, these landmarks did not have a primary pathological role of CSM as they do not differ within identical breed specimens (Bonelli et al., 2017).

Conversely, various studies have demonstrated how other landmarks differ from DACSM-affected and non-affected dogs, including vertebral canal height and vertebral body size. It was found that DACSM-affected Dobermans exhibit considerably shorter vertebral canal heights and smaller vertebral bodies than non-affected Dobermans. Additionally, the pathological characteristic of some degree of vertebral canal stenosis present in DACSM-affected Dobermans has been shown. Such canal stenosis exhibited a funnel shape at its caudal end across C7 to a greater degree than non-affected dogs. These studies were based on measurements with ratio-based parameters (De Decker et al., 2011b, De Decker et al., 2011c). By assessing the parameters that differ between

healthy and DACSM-affected samples, two-dimensional and 3-dimensional surface mapping parameters can be developed, which are necessary for the design stage of this project.

## **2.3. Management Options for CSM**

### **2.3.1. Medical Treatment**

Management options for CSM include conservative therapy and surgical treatment, which have evolved from the studies of all characteristics of CSM. The management's decision depends on every single case and varies not only from the dog's pathological signs and the nature of spinal cord compression (static or dynamic) but also from the owner's financial situation and post-operative expectations. Dogs with minimal-mild signs of ataxia or tetraparesis may often be treated medically by oral corticosteroids (da Costa, 2010, Newton and Nunamaker, 1985).

A study compared the outcomes and survival times of medically-treated and surgically-treated CSM-affected dogs but found no significant differences in outcome and survival times (da Costa et al., 2008). Although surgical treatment does not appear to bring longer survival times, it offers a slightly higher success rate and a greater chance of clinical improvement. By improving the implants and instrumentations available, and their conformation with the affected vertebrae/IVD using modern methods of manufacture, which offer greater design latitude, the success rate for surgical treatment may be significantly increased.

### **2.3.2. Surgical Treatment**

It is widely known that multiple surgical techniques exist for DACSM treatment in dogs, with ventral and dorsal approaches being the most significant techniques (da Costa, 2010, Fossum, 2018). The ventral technique generally involves a ventral slot (either partial or full) at the compression site, or multiple sites, in combination with a distraction-stabilisation technique, which can further involve bone grafts at these

---

site(s). On the other hand, a dorsal approach generally involves a dorsal laminectomy and is typically chosen for OACSM and some DACSM affecting multiple sites (Fossum, 2018). Advantages of a ventral approach over a dorsal approach include:

- A technically less demanding.
- A larger bone surface is available over the vertebral bodies for vertebrae stabilisation with screws/implants.
- Thicker bone stock is available compared to the articular processes available from a dorsal approach.
- Patients show shorter periods of recovery post-surgery.

However, some disadvantages are also present, including a higher chance of haemorrhage, and limited spinal cord and vertebral canal visibility, allowing for a narrower decompression (Fossum, 2018).

Factors for selecting the most appropriate surgical treatment for each CSM case include the nature (static or dynamic), location of the spinal cord compression, the number of affected sites, and any other concurrent non-neurologic disease that may aggravate the surgery or the long-term outcome (e.g. dilated cardiomyopathy) (da Costa, 2010, Birchard and Sherding, 2006). The choice of which surgical approach to use can be complex, with no universally recognised technique available.

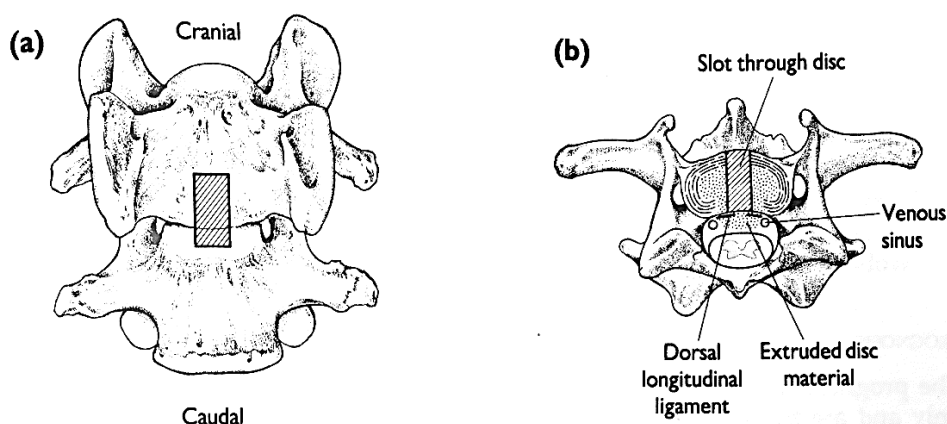
The various surgical approaches are classified into three main groups/categories according to their methodologies: direct decompression (with or without stabilisation), indirect decompression, and motion-preservation. Table 2-1 summarises the most reported surgical techniques based on the type of surgery. Within the surgical techniques, ventral slot, dorsal laminectomy and distraction-stabilisation are the most preferred techniques by veterinary surgeons and are described in Table 2-1 (Birchard and Sherding, 2006).

**Table 2-1. Surgical Techniques for CSM treatment (Birchard and Sherding, 2006).**

Surgery Category	Surgical Technique
Direct decompression without stabilisation	<ul style="list-style-type: none"> <li>• Ventral slot</li> <li>• Inverted cone slot</li> <li>• Dorsal laminectomy</li> <li>• Dorsal laminoplasty</li> </ul>
Indirect decompression	<ul style="list-style-type: none"> <li>• Distraction-stabilisation</li> </ul>
Motion-preservation	<ul style="list-style-type: none"> <li>• Artificial IVD replacement</li> <li>• Disc arthroplasty</li> </ul>

### Ventral Slot

This technique is typically utilised for static-single compressions. However, the outcome is similar when applied to dynamic compressions. In this surgical technique, the disc protrusion material should be entirely removed to decompress the spinal cord by making a ventral slot (Figure 2-5). The slot section will then promote osseointegration after 8-12 weeks post-surgery. The success rates are around 72%, with complication rates about around 15%. Complications include the possibility of compromising the respiratory system, spinal subluxations, bradycardia and haemorrhage caused by an injury to the vertebral venous plexus (da Costa, 2010, Jeffery, 1995).

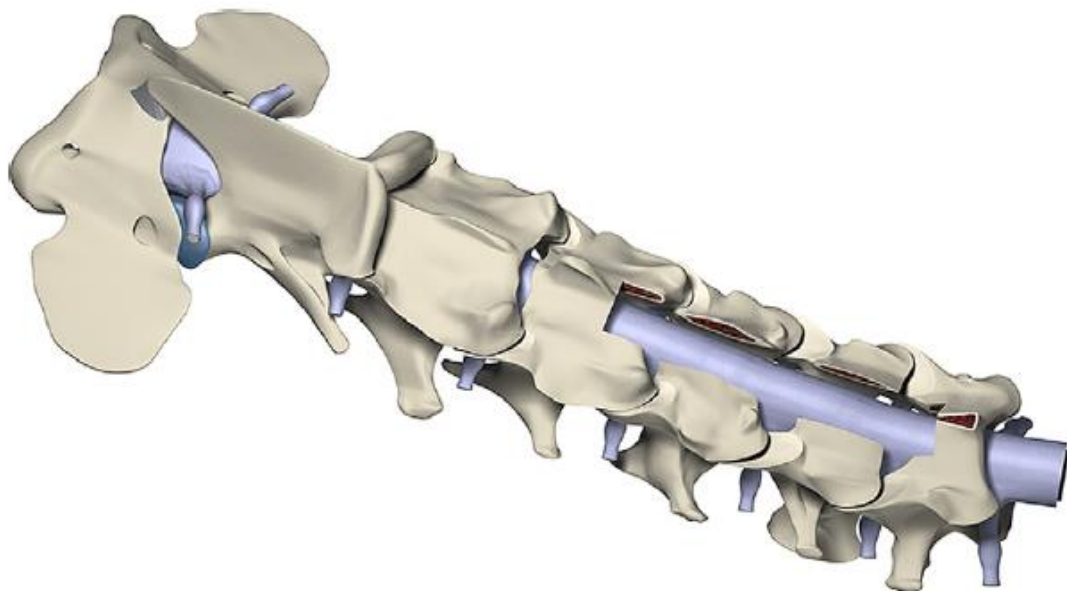


**Figure 2-5. (a) Position and size of slot on ventral aspect of vertebrae, (b) Diagram of slot size and relationships in conventional slot technique (Jeffery, 1995).**

## Dorsal Laminectomy

As the name indicates, this technique is mainly used for dorsal or dorsolateral compressions and multiple dorsal lesions caused by stenosis (at multiple levels), associated with lamina malformations, osteoarthritic malformations of the articular facets or hypertrophy of ligamentum flavum. Ventral approach results are less effective and show higher complication rates when lesions at multiple levels are involved (Jeffery, 1995, da Costa, 2010, Birchard and Sherding, 2006).

Dorsal laminectomy is routinely performed on the caudal cervical vertebral column from a dorsal approach. Surgical equipment required includes Gelpi self-retaining retractors to expose the laminae, a blade for fascia removal, a bur to perform the laminectomy and resorbable sutures to close the muscles (Birchard and Sherding, 2006). Figure 2-6 illustrates a dorsal laminectomy at multiple sites. Complications include aggravation of neurologic dysfunctions and a high risk of intraoperative haemorrhages (Jeffery, 1995). The success rates are above 78% (Lipsitz et al., 2001, De Risio et al., 2002, Lyman, 1989), but recurrence rates of neurologic dysfunctions are around 30% at three years post-operative (De Risio et al., 2002).



**Figure 2-6. Dorsal laminectomy from C4 to C5 (da Costa, 2010).**

---

## **Distraction-Stabilisation**

Over recent years, many surgeons have been utilising (1) distraction devices such as Poly methyl methacrylate (PMMA), PMMA-anchored implants, and interbody spacers/cages; in conjunction with (2) a fusion-promoting approach such as bone grafts; and (3) stabilisation systems such as screws+PMMA, pins+PMMA, locking plates, and screw+rods (Birchard and Sherding, 2006, Bergman et al., 2008, Trotter, 2009, Joffe et al., 2019). Distraction-stabilisation techniques are commonly performed on the caudal cervical vertebral column from a ventral approach (Birchard and Sherding, 2006).

The primary complications of distraction-stabilisation techniques include the risk of further stresses on adjacent IVDs, leading to compressions that affect such IVD's due to the stabilisation of vertebrae; implant penetration into the spinal cord; implant(s) failure causing a collapse of the IVD segment (Lorenz et al., 2011). Additionally, the metal implants utilised for vertebral body fixation may cause significant MRI artefacts, making performing post-operative follow-up by MRI challenging (da Costa, 2010).

It has been demonstrated that interbody cages that perfectly conform with adjacent endplates present a better biomechanical performance compared to generic interbody cages in humans; significantly lower interface stress in all directions of motion (flexion/extension, lateral bending and axial rotation), higher cervical stability in flexion/extension, and minimal implant subsidence (Zhang et al., 2016). Similar results have been reported in dogs (Joffe et al., 2019).

### *PMMA Plug*

For multiple ventral-dynamic compressions, a distraction-stabilisation procedure using an interbody PMMA plug is one of the most preferred distraction techniques when comparing the level of difficulty of the procedure with its consistent good-excellent results (Birchard and Sherding, 2006). Firstly, the annulus fibrosus is fenestrated ventrally to remove the nucleus pulposus with a small rongeur or

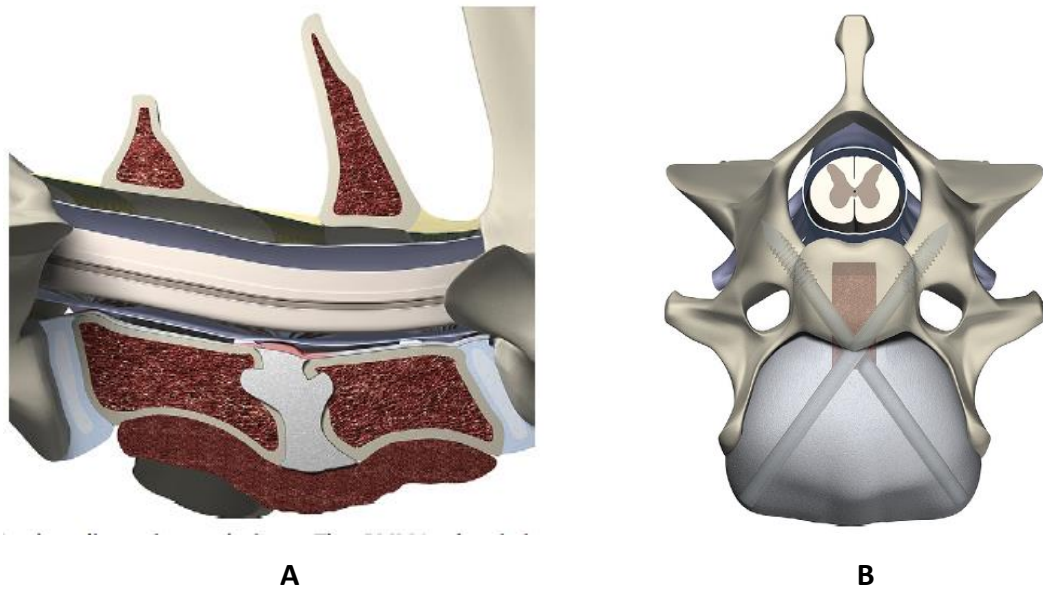
---

haemostat. Secondly, linear traction is applied, and the distraction is carried out by making two small ventral slots on both caudal and cranial vertebra bodies adjacent to the disc to place Gelpi retractors and distract the vertebrae (Birchard and Sherding, 2006, da Costa, 2010). Two holes are drilled in the cranial and caudal end plates to achieve a bone cement anchor. Finally, liquid PMMA is applied to the IVD and allowed to cure. Bone grafting from the greater tubercle is then applied at the ventral aspect of the vertebrae, as shown in Figure 2-7A (Birchard and Sherding, 2006, da Costa, 2010). The success rates are reported to be around 82%, with minimal complications noted (Dixon et al., 1996).

#### *Screw/Pins and PMMA*

For single ventral-dynamic compressions (or dorsal compression), a distraction-stabilisation procedure using pins and PMMA is another preferred distraction technique. Firstly, a ventral slot procedure is carried out, and the implants are inserted across the pedicles (e.g. Steinmann or threaded pins or bone screws) of adjacent vertebrae, which are commonly about 2mm in diameter for Dobermans. Insertion angles have been reported to be safe at 30°-35° for C5 and C6 and at 45° for C7 (Corlazzoli, 2008). Secondly, the pins are covered over with PMMA (Figure 2-7B), and linear traction is applied (if desired) whilst the PMMA is curing (Jeffery, 1995, da Costa, 2010). The success rates are reported to be above 72%. Complications include the risk of penetrating the vertebral or transverse foramens, and are reported to occur in 25%-57% of cases (Corlazzoli, 2008, Koehler et al., 2005).





**Figure 2-7. (A) Distraction-stabilisation with a PMMA plug (sagittal view). (B) Distraction-stabilisation with pins and PMMA combined with a partial ventral slot (cranial view) (da Costa, 2010).**

Pin-PMMA and screw-PMMA are among the most popular approaches for cervical distraction-stabilisation in dogs. Although such techniques are relatively easy to perform and utilise relatively economic materials, they have not had enough successful rates to become ‘of-the-shelf’ devices (Jeffery, 2010, McKee et al., 2016).

#### *Pedicle Screws + Rods*

When considering safe corridors for screw implantations, the pedicle areas withstand any other landmarks within the vertebrae, where the most extended screws can pass through (at both dorsoventrally and ventrodorsally approaches). The term ‘pedicle screw’ refers to a screw passing through a pedicle. On the human side, the gold standard over the last three decades for fixing the vertebral column is a combination of pedicle screws with fixation systems, namely rods, which has also gained popularity among its canine counterpart over the last years (Lewchalermwong et al., 2018). A recent ex-vivo biomechanical study concluded that a fixation system of screws and rods presents better biomechanical properties than those of screws fixed with PMMA;

---

namely bending yield load, bending stiffness and ultimate load (Lewchalermwong et al., 2018).

### *Interbody devices*

A combination of a distraction device, such as an interbody spacer with a plate fixation system, has been reported to increase the rate of vertebral fusion in humans (Kaiser et al., 2002). Interbody washers were one of the first devices used for the distraction of adjacent vertebrae, introduced in the late 1980s (McKee et al., 1989). However, this device struggled to gain popularity over the decades due to its non-conforming construct, low long-term success rate, high deterioration rate, and high recurrence of compression rates (Rusbridge et al., 1998, Jeffery and McKee, 2001). Over the last years, interbody spacers have gained popularity for distraction of adjacent vertebrae (leading to indirect spinal cord decompression) due to their relative ease to place compared to other approaches. However, there is no universally accepted interbody device to date. A review of some of the advantages and limitations of current interbody devices is described in section 2.3.3 (Reints Bok et al., 2019, Tuan et al., 2019, Solano et al., 2015, Rohner et al., 2019, Joffe et al., 2019).

### *Drill Guides*

Recent approaches also combine customised drill guides to accurately place pedicle screws in the vertebral column. They have been gaining popularity over recent years due to their fast manufacturing turnaround times; and also safeness and accuracy for placing cortical or pedicle screws (Hamilton-Bennett et al., 2018, Fujioka et al., 2019, Kamishina et al., 2019, Elford et al., 2019, Guevar et al., 2021, Mariani et al., 2020, Beer et al., 2020, Oxley and Behr, 2016, Toni et al., 2020).

### **2.3.3. Advancements in CSM Distraction-Stabilisation Devices**

Distraction-stabilisation techniques are preferred for dorsal-dynamic compression acting at one single site and ventral-dynamic compression acting at one or two sites.

Most surgically treated CSM-affected dogs are diagnosed with such compressions (Birchard and Sherding, 2006). Therefore, the stabilisation system proposed in this project is developed considering a distraction-stabilisation technique. A review of case study reports involving distraction-stabilisation devices is detailed in Table 2-2, concentrating on biomechanical performance, success rates, advantages, failure rates, and limitations (Reints Bok et al., 2019, Tuan et al., 2019, Solano et al., 2015, Rohner et al., 2019, Joffe et al., 2019, King et al., 2020).

Table 2-2. Review of advancements in orthopaedic devices for distraction-stabilisation techniques.

Surgical technique	Distraction-Fusion Devices:	Stabilisation Devices	Success Rates	Failure Rates	Advantages	Limitations	Reference
Ventral distraction-stabilisation	<ul style="list-style-type: none"> <li>* C-LOX cage (developed for dogs) (C-LOX; Rita Leibinger GmbH&amp;Co. KG, Muhlheim/Donau, Germany). Packed with bone graft as per surgeon discretion.</li> </ul>	<ul style="list-style-type: none"> <li>* The C-LOX cage includes a conventional screw fixation mechanism for two cranial and two caudal locking screws.</li> <li>* Locking self-drilling monocortical screws</li> </ul>	<ul style="list-style-type: none"> <li>* 70-76% of dogs showed improvement of neurological signs at 6-12 weeks post-operative</li> </ul>	<ul style="list-style-type: none"> <li>* 0-15% of dogs showed complete bone fusion by radiographic evidence at 6-12 week months post-operative</li> <li>* 60-66% of dogs presented implant complications, most commonly implant failure of the locking screws.</li> <li>* 45-50% of dogs presented implant subsidence.</li> </ul>	<ul style="list-style-type: none"> <li>* Decent rate of improvement of neurological status at 3 months post-operative</li> </ul>	<ul style="list-style-type: none"> <li>* High rate of implant failure and subsidence.</li> <li>* Low rate of bone fusion and bridging.</li> <li>* Being a stand-alone device, it limits the screw placement to only monocortical screws with little bone purchase, exposing them to high torsion forces, and leaving them prone to breakage.</li> <li>* The shape of the cage do not conform with the endplates and the shape of the cage ventral section does not conform with the ventral vertebra body either, which conflicts with the vertebrae biomechanics. This may be the reason for the high implant failure rates.</li> </ul>	(Rohrer et al., 2019; King et al., 2020)
Ventral distraction-stabilisation	<ul style="list-style-type: none"> <li>* SynCage-C Short (developed for humans), curved; DePuy Synthes. Packed with cancellous bone graft from proximal humerus.</li> </ul>	<ul style="list-style-type: none"> <li>* Two UniLock locking plates (developed for humans); DePuy Synthes.</li> </ul>	<ul style="list-style-type: none"> <li>* 100% radiographic evidence of bone fusion at 9 to 51 months</li> </ul>	<ul style="list-style-type: none"> <li>* 11% significant subsidence</li> <li>* 55% implant loosening or breakage of screws or plates</li> </ul>	<ul style="list-style-type: none"> <li>* Combination of an interbody device and double locking plates provided radiographic evidence of bone fusion in all dogs (9 to 51 months post-operative).</li> </ul>	<ul style="list-style-type: none"> <li>* The cage is developed for humans, and only the smallest size can be used for the largest breed dogs. The morphology of the endplates is different between humans and dogs.</li> </ul>	(Reints Bok et al., 2019)
Ventral distraction-stabilisation	<ul style="list-style-type: none"> <li>* FITS intervertebral titanium-threaded screw (developed for dogs) (FITS; FitBonics, Easing, Surrey, United Kingdom), ventrally coupled with harvested cancellous bone.</li> </ul>	<ul style="list-style-type: none"> <li>* Self-tapping 5-mm polyaxial spine screws coupled with a polyaxial head (developed for humans) (Smat Spine; Spatmetal, Eger, Hungary)</li> <li>* Two 5.5-mm stainless steel rods (developed for humans), intra-operative contoured.</li> </ul>	<ul style="list-style-type: none"> <li>* 60% of measurements had canal width increments at 27 months post-operative</li> <li>* 40% of measurements had cross sectional area increments at 27 months post-operative</li> <li>* 100% of sites revealed interbody fusion and ventral bone bridging</li> </ul>	<ul style="list-style-type: none"> <li>* 40% of measurements had canal width decrements at 27 months post-operative</li> <li>* 60% of measurements had cross sectional area decrements at 27 months post-operative</li> </ul>	<ul style="list-style-type: none"> <li>* Distraction at multiple sites resulted in improvement of neurological functions (10 days post-operative)</li> </ul>	<ul style="list-style-type: none"> <li>* The intervertebral screw provides limited endplate-implant contact to dissipate loads.</li> </ul>	(Tuan et al., 2019)
Ventral distraction-stabilisation	<ul style="list-style-type: none"> <li>* T16A14Y Customised intervertebral devices manufactured by Additive Manufacturing (developed for dogs).</li> <li>* Demineralised bone matrix (Canine DBM putty, Veterinary Tissue Bank, St Lucia Surgical Services, Brisbane, Australia) packed into the centre of the device.</li> </ul>	<ul style="list-style-type: none"> <li>* Cervical spinal plate (Trinica Select, Zimmer Biomet, Warsaw, Indiana, United States) (developed for humans), intra-operative contoured.</li> <li>* Monocortical screws (Titanium cortical screws, Kyon, Zurich, Switzerland) to secure the plate.</li> </ul>	<ul style="list-style-type: none"> <li>* 50% (1 of 2) of dogs showed complete bone fusion at 6 months post-operative.</li> <li>* 50% (1 of 2) of dogs showed progressive, but incomplete bone fusion at 6 months post-operative.</li> </ul>	<ul style="list-style-type: none"> <li>* 100% of dogs presented mild implant shifting at 2 month post-operative</li> </ul>	<ul style="list-style-type: none"> <li>* The customised interbody devices resulted in excellent endplate-spacer conformance, and showed bone fusion to some extent at 2 month post-operative</li> </ul>	<ul style="list-style-type: none"> <li>* The implants were designed from a CT traction and not at the intended fixation position, which constrains the position of the spine to a linear traction position. This might have been the reason for the mild ataxia presented in one of the dogs at 2 months post-operative.</li> <li>* Bone fusion was incomplete in one dog and slow in the other dog, possibly due to the solid construct of the implant.</li> </ul>	(Joffe et al., 2019)
Ventral distraction-stabilisation	<ul style="list-style-type: none"> <li>* FITS intervertebral titanium-threaded screw (developed for dogs) (FITS; FitBonics, Easing, Surrey, United Kingdom), ventrally coupled with harvested cancellous bone.</li> </ul>	<ul style="list-style-type: none"> <li>* SOP locking plate systems (Orthomed, Halifax, West York shire, UK) (developed for humans)</li> <li>* Cis-cortex only and 3.5 mm self-tapping stainless steel screws were placed monocortical (DePuy Synthes Vet).</li> </ul>	<ul style="list-style-type: none"> <li>* 93% of dogs presented some degree of improvement of neurologic status.</li> <li>* 62% of dogs showed radiographic evidence of bone bridging at 6 weeks post-operative.</li> </ul>	<ul style="list-style-type: none"> <li>* 73% of dogs presented minor complications by radiographic evidence at 6 week post-operative (53% of dogs presented minor implant subsidence. 13% of dogs presented implant loosening and 6% of dogs presented screw malpositioning).</li> </ul>	<ul style="list-style-type: none"> <li>* Some degree of indirect distraction was observed immediate post-operative</li> </ul>	<ul style="list-style-type: none"> <li>* No significant distraction levels were kept at 6 week post-operative.</li> <li>* The tapered feature and auto-distractor can lead to a non-desired extended fixation position as the distraction level is constrained by the size of the implant (cortic angle angulation), and size of the dog.</li> <li>* A pure solid interbody spacer reduces the room for intervertebral fusion and limits the amount of bone graft packing.</li> </ul>	(Solano et al., 2015)

---

## 2.4. Identification and Selection of Study Breed Dog

This section describes the process of identifying and selecting the study breed dog used for this project. Commencing with a revision of the breed dogs with a predisposition to CSM, their population size, and the identification of the Doberman as the study breed dog. Furthermore, the creation of a database was needed for in-silico modelling and implant development. Medical images of Dobermans, including Computed Tomography (CT) and Magnetic Resonance Imaging (MRI) scans, were collected and compiled for use in the following stages of the project.

### 2.4.1. Breed Predispositions to CSM

Breed predispositions to CSM have been identified: Great Dane and Doberman Pinschers being the most commonly affected breeds, and together account for 60-70% of all CSM-affected dog breeds (Alex et al., 2018, Mai, 2018). Breed predisposition has also been identified in horses, with Thoroughbreds being the most commonly affected breed (Lorenz et al., 2011). According to various studies, Dobermans are more likely to suffer CSM disease than other dog breeds, being at high risk to suffer from malformation of cervical vertebrae, and is more prone to occur on C5, C6 and C7 (da Costa, 2010, Alex et al., 2018), and with a maximum incidence in 4- to 8-year-old dogs (Lorenz et al., 2011). Of the breeds pre-disposed to CSM, the Doberman population is the largest in the UK, according to Kennel Club (1,462 dogs in the UK in 2018, Table 2-3). The Great Dane follows this with 903 dogs (The Kennel Club UK, 2018).

**Table 2-3. Most commonly affected breed dogs by CSM**

Breed	Size	Median Lifespan (O'Neill et al., 2013a, American Kennel Club, 2019)	Weight (American Kennel Club, 2019, Alex et al., 2018)	UK Population (The Kennel Club UK, 2018)	CSM Prevalence (da Costa, 2018)
Basset Hound	Medium	12.5	18.1-29.5	571	No data available
Bernese Mountain Dog	Large	8.5	36.3-52.2 (Male) 31.8-43 (Female)	501	No data available
Borzoi	Large	12	34-47.6 (Male) 27.2-38.5 (Female)	91	No data available
Doberman	Large	9.2	34-45.3 (Male) 27.2-40.8 (Female)	1462	5.5%
Great Dane	Large/ Giant	6	63.5-79.4 (Male) 49.9-63.5 (Female)	903	4.2%

## 2.5. Additive Manufacturing for Novel Veterinary Devices

Additive Manufacturing (AM) is a recent approach for transforming CAD models into actual three-dimensional elements. As previously mentioned, CAD files are converted to STL files in order to 3D-print out the models. The principal AM techniques include Stereolithography, Selective Laser Sintering/Melting (SLS/SLM), 3D printing, Fused Deposition Modelling (FDM), and Inkjet Printing (Gibson et al.). Initially, additive manufacturing processes were utilised to produce prototype models of the products under development to prove and visualise their characteristics in a real three-dimensional shape. Recently, various additive manufacturing techniques have been developed to produce pieces and parts suitable for end use, fabricating them in small quantities (Chua et al., 2009, Tuomi et al., 2014).

Over the last years, the biomedical industry has employed AM techniques for sophisticated applications. These applications range from standard prostheses to more innovative and complex approaches, such as the cardiac micro-physiological

---

device developed by Harvard University researchers in 2017 (Lind et al., 2017). Fused Deposition Modelling is commonly utilised for 3D-printing anatomical models such as bones, which results in a proper AM technique for manufacturing vertebrae models for this project's development. Furthermore, SLM is utilised to manufacture 3D metal-based components such as titanium devices. For example, an anatomical bone plate made of titanium (Ti6Al4V) can be manufactured by SLM, which can be utilised in real surgical implantations (Wang et al., 2017).

### **Selective Laser Sintering/Melting (SLS/SLM)**

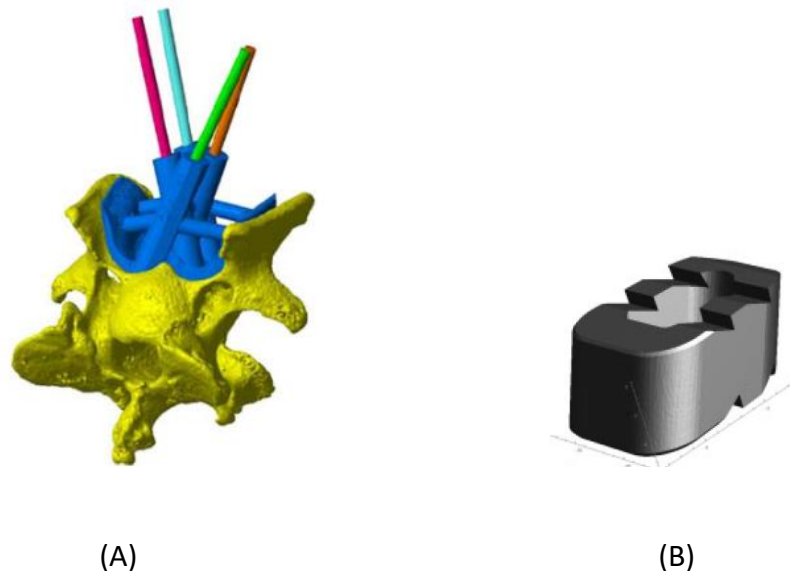
Selective Laser Sintering (SLS) and Selective Laser Melting (SLM) technologies are capable of producing parts with polymer powder materials for SLS and metal powder materials for SLM, which are sintered/melted by a Carbon Dioxide laser (Chua et al., 2009). Over the years, SLS has become a popular AM technique to create long-term products, including biomedical devices such as implants. SLS has achieved broad acceptance as an AM process because of the capability to fabricate parts of almost any kind of element. A high density (minimal internal porosity) is needed to manufacture metallic components or pieces to impart high strength and endurance properties to the component. This characteristic can be improved through powder-based systems such as SLM, with which bone plates could be manufactured (Kruth et al., 2004).

### **Manufacturing of Anatomical Plates**

Different prostheses can be fabricated with SLM based directly on a three-dimensional virtual model. For instance, Wang and colleagues (2017) recently developed a customised titanium (Ti6Al4V) plate for a fracture located in the pelvis manufactured using SLM (Wang et al., 2017). Moving into vertebral column approaches, various disc-associated diseases in humans have recently benefited from the use of AM techniques such as SLM and electron-beam melting (EBM). The use of AM techniques facilitates manufacturing complex and well-defined pieces such as intervertebral cages, commonly known as 'spacers'. Furthermore, porous structured surfaces with solid

inner bodies can be also manufactured by AM in biocompatible materials (e.g. titanium alloys), to facilitate osseointegration after implantation- a design feature which cannot be contemplated using traditional manufacturing techniques (Mullen, 2009, Mullen et al., 2009, Mullen et al., 2010, Zhang et al., 2013).

Similarly, veterinary medicine has also benefited from the use of AM techniques. Recent approaches include the development of customised implants for treating DACSM in dogs, namely drilling guides and intervertebral spacers, as shown in Figure 2-8 (Hamilton-Bennett et al., 2018, Joffe et al., 2019). For instance, the customised interbody device developed by Joffe and colleagues (reviewed in section 2.3.3) was manufactured by AM (Joffe et al., 2019).



**Figure 2-8. (A) Customised drilling guide manufactured by SLS (Hamilton-Bennett et al., 2018), (B) Customised interbody device manufactured by EBM (Joffe et al., 2019).**

### **Manufacturing of Surgical Guides**

Surgical drill guides can be manufactured by Stereolithography and have become widely used in veterinary orthopaedics over the last decade for various reasons: they can be designed to perfectly conform patient-specific bone morphology; they provide high accuracy for screw/pin placement; and their fast manufacturing turnaround times



(Hamilton-Bennett et al., 2018, Fujioka et al., 2019, Kamishina et al., 2019, Elford et al., 2019, Guevar et al., 2021, Mariani et al., 2020, Beer et al., 2020, Oxley and Behr, 2016, Toni et al., 2020).

## **2.6. Software for 3D-Modelling and Implant Designing**

### **Materialise Mimics Innovation Suite**

Mimics Innovation Suite (MIS) is a group of software developed by Materialise, which is principally focused on biomedical applications. This software package utilises medical image data as primary resource, which can be further processed for developing a wide range of engineering approaches. For instance, veterinary medicine has benefited from the use of software such as Mimics and 3-Matic for biometric analysis of the vertebral column (Materialise, 2014, Joffe et al., 2019, Reints Bok et al., 2019, Hamilton-Bennett et al., 2018).

### **CREO Parametric**

Computer-Aided Design (CAD) is a powerful engineering tool that has gained popularity over recent decades due to its potential for designing three-dimensional models (via software) for various applications. CAD allows engineers to design specific and complex models (e.g. anatomical implants) before manufacture. CAD also provides a valuable way to pre-assemble different components to analyse their fitting and interaction (Raja and Fernandes, 2008), for instance, bone-plate conformation. CREO Parametric is a CAD software commonly utilised in industry and research and includes a wide range of modelling tools. This software helps design 3D models, industrial designs, concept designs, computer-aided manufacturing and simulations. CREO Parametric allows users to export the models to STL files, which can be further 3D-printed by additive manufacturing techniques (PTC, 2017).

---

## 2.7. Proposition of Stabilisation System

Complete and quick bone fusion is the ultimate goal of any cervical stabilisation system. Distraction-stabilisation devices have demonstrated satisfactory rates of bone fusion (compared to other approaches) while increasing the stiffness of a distraction system, as described previously in this chapter. Therefore, a review of the current distraction-stabilisation devices was included in section 2.3.3.

Following the review of advancements in CSM distraction-stabilisation devices, the main positive features of current approaches are as follow:

- Interbody devices provide some degree of distraction and subsequent improvement of neurological functions.
- End-plate conforming interbody devices reduce flexion/extension and lateral bending range of motions.
- Ventral plating increases stability and reduces axial torsion.
- Patient-specific surgical drill guides allow for the insertion of pedicle screws and therefore provide higher bone purchase than monocortical screws.

Likewise, their main limitations are as follows:

- Vertebra morphology differs between humans and dogs; only a few interbody devices are specifically designed for dogs. In dogs, higher shear forces are present at the cervical vertebral column due to their natural lordotic stance, which increases the risk of implant subsidence.
- Most of the available interbody devices provide a limited bone-implant contact area, resulting in limited load distribution, and affecting the implant's stability.
- Monocortical screws are subjected to higher loads compared to pedicle screws.
- Current implant constructs lack a systematic distraction approach, leading to under/over-distraction results.

- Only a few devices have achieved complete fusion on post-operative follow-up. Micro-porous structures may help overcome this limitation (Mullen, 2009, Mullen et al., 2009, Mullen et al., 2010, Zhang et al., 2013).

The wide variety of implants utilised for cervical stabilisation reflects the lack of a universal or 'of-the-shelf' stabilisation system. Some of the current implants feature some positive features and limitations. Therefore, a sophisticated and subtle canine-specific system is then proposed to maximise and reduce limitations considering (1) a wide endplate-conforming interbody device with a micro-porous structure for osseointegration and pre-defined distraction levels, (2) an anatomical ventral locking-plate for stabilising the vertebrae site, coupled with drill guides for insertion of pedicle screws to maximize bone purchase and allow higher stabilisation rates.

## **3. Design and Development of Patient-Specific Implant Prototypes**

### **3.1. Introduction**

For a stabilisation system to be clinically released, it is necessary to carry out a pilot study. The first aim is to prove implant stability by developing patient-specific implants, as described in this chapter, that can be tested using in-silico models (as it will be described in Chapter 4), and second, to assess the implant performance in surgical cases (as it will be described in Chapter 5).

This chapter describes the creation of a database that was needed not only for implant development but also for in-silico modelling. As described in Chapter 2, Dobermans were identified as the study breed dog, therefore medical images of Dobermans, including Computed Tomography (CT) and Magnetic Resonance Imaging (MRI) scans, were collected and compiled for use in the multiple stages of the project.

This chapter also describes the process of generating 3D bone models of the cervical spine that can be used for morphology analysis and implant development using medical imaging software such as Mimics and 3-matic. The development of a vertebra orientation technique is described, along with intra- and inter- observer variability studies, to validate its reliability.

Due to time constraints, the development of the stabilisation system was split into two sections: (1) the development of end-plate conforming interbody spacers and (2) the development of anatomical ventral locking plates. This section describes the development and manufacture of custom spacers for large breed dogs with CSM at one or two sites (C5-C6 and/or C6-C7), and the development of initial anatomical ventral locking plates.

## 3.2. Collation and Assembly of a Library of Anatomic Images

### CSM-Affected Breeds

From the early stages of this research project, the search for and compilation of medical images commenced, namely X-rays and CT/MRI scans. Two potential clinics for collecting such data were identified; The Veterinary Clinic, University of Liverpool, Leahurst Campus, and Chestergates Referral Hospital, because of its solid and collaborative research relationship with the University of Liverpool. These two veterinary centres were the primary medical image providers for the current project. CT and MRI scans collected accounted for 41 CT and 12 MRI Doberman Scans; and 1 CT and 5 MRI Great Dane scans. The scans were used for in-silico modelling and implant designing.

All the CT scans were taken under slightly different scanning parameters, such as slice thickness and pixel dimension, which determine the quality of each CT scan. The quality of the CT scans is of paramount importance for designing accurate cervical implants. Additional details of the CT scans were provided by the source clinics, including diagnosis, age, and weight. With this information, the CT files were classified according to quality, size and whether the vertebrae are healthy or unhealthy (e.g. bone or disc-associated diseases). Eight Doberman CT scans comprised the CSM-affected group of samples. The medical images were anonymised to comply with ethical requirements and labelled as a number preceded by an S. (E.g. S0001, S0002, S0003) according to their addition order to the database.

### 3.3. Development of Endplate-conforming Interbody Spacers

#### 3.3.1. Identifying CT Scan Sample

The first implant prototype was developed using a CSM-affected CT scan sample from this research database (section 3.2). Sample S004 was identified for this purpose because it included the whole cervical and cranial-thoracic vertebral column. This sample had two DACSM-affected sites: C5-C6 and C6-C7.

#### 3.3.2. Generation of 3D-Bone Models

Firstly, the bone segments were isolated from the CT scan file with Mimics, with the aim of separating the desired bone segment from adjacent bones. The bone samples were carefully isolated according to the following methodology:

1. **Merging of Image Stacks.** A new project was created in Mimics with the “New project wizard” tool, selecting the DICOM folder (or all necessary files) where the desired vertebra was located. The length of the process for merging the image stacks depended on the number of files (slices) and slice thickness. Additionally, when parameterising the image stacks, “Lossless” was selected for compression in order to see all features of the files. Finally, the converted images appeared in three views: axial, coronal and sagittal. The main window showed these three views plus a 3D pane, where 3D models could be visualised, as shown in Figure 3-1.

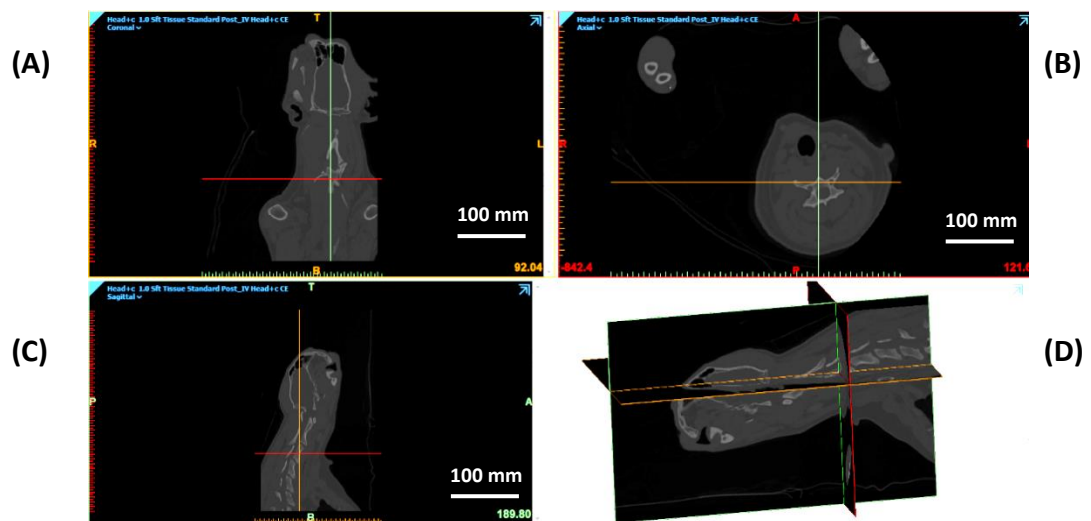


Figure 3-1. Merge of image stacks. (A) Coronal view, (B) Axial view, (C) Sagittal view, (D) 3D Pane.

- 3D Reconstruction (Thresholding).** The thresholding feature groups pixels according to their colour or mask. It includes preconfigured settings for segmenting specific biological matters such as bones (higher threshold value) and soft tissues (lower threshold value). In this case, a predefined threshold value for “bone (CT)” was selected (Figure 3-2A) for every sample, which was then slightly modified (up or down) to eliminate unnecessary pixels (Figure 3-2B) and facilitate segmentation.

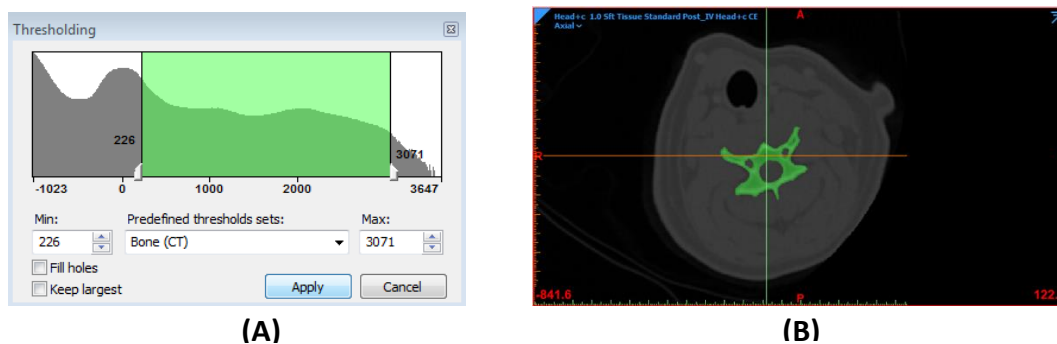
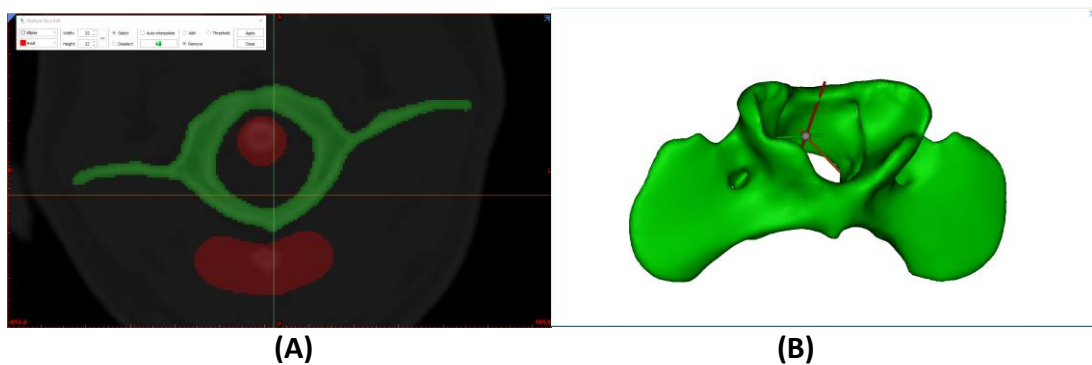


Figure 3-2. 3D Reconstruction (Thresholding). (A) Thresholding value for bones, (B) Selected thresholding pixels in green.

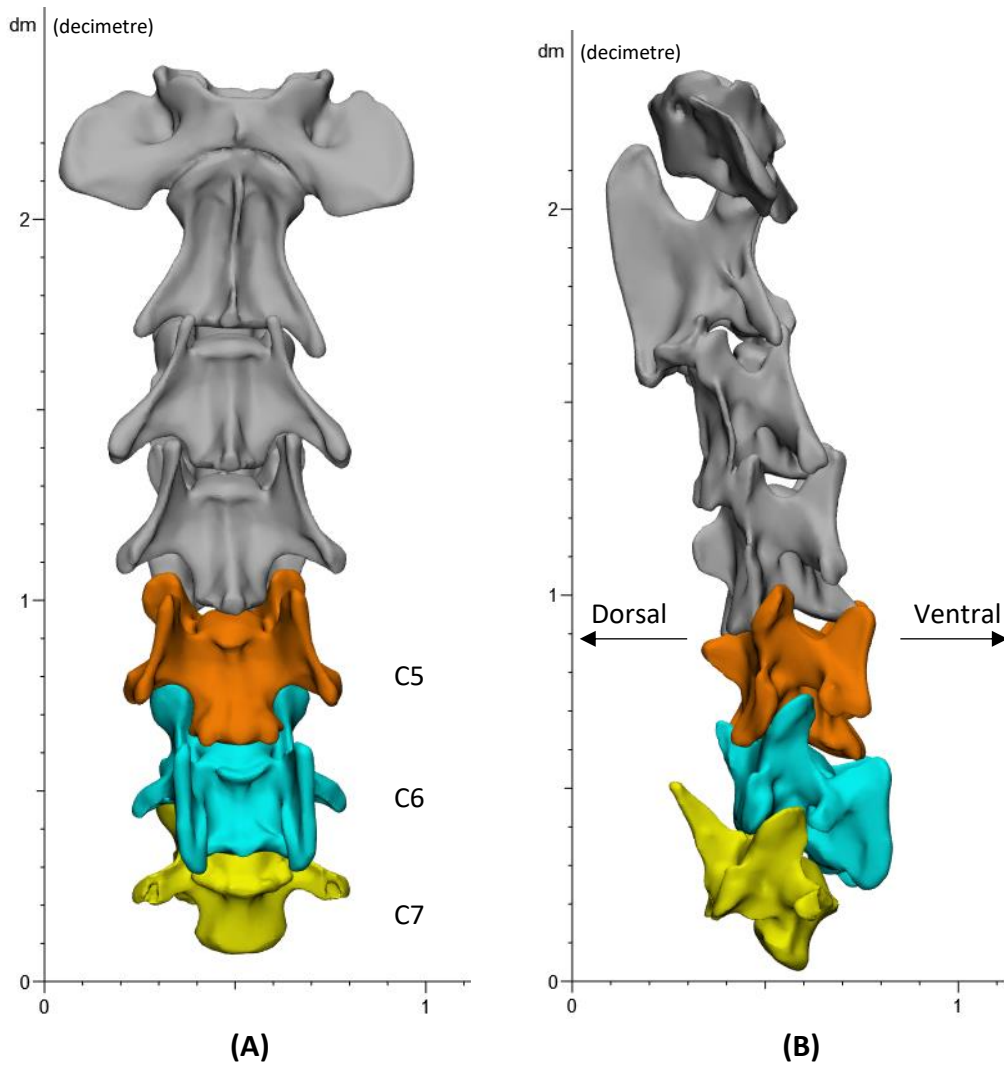
**3. Segmentation.** Each sample was then segmented (or isolated) by separating the grey values that correspond to the vertebra from those of adjacent bones in order to obtain a 3D model of every vertebra sample - the “multiple slice edit” function was utilised for this purpose. With the aid of a circular cursor, the pixels of the non-desired bones were erased on the slices from all the three different views. For example, a cervical vertebra (C1) in green and a non-cervical vertebral column section in red is shown in Figure 3-3A. The interpolate function helped skip various slices during the edition to save time. After this, a 3D model of each desired bone segment was generated using the ‘region growing’ tool (Figure 3-3B).



**Figure 3-3. Segmentation. (A) Multiple slice edit on transverse view, (B) 3D model of an isolated bone (Cervical vertebra 1).**

Following the described methodology, a 3D model of the cervical vertebral column for Sample S004 was generated in Mimics as follows: individual 3D-bone models of the affected vertebrae (C5, C6, and C7) and a single ‘fixed’ 3D-bone model of the remaining cervical vertebrae (C1-C2-C3-C4-) were generated (as shown in Figure 3-4). The 3D-bone models were then exported to 3-matic for further modelling.



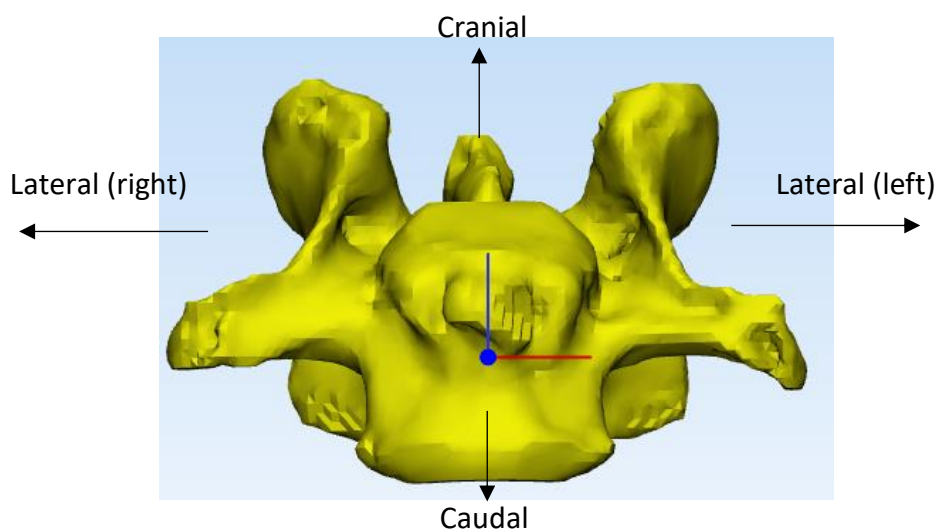


**Figure 3-4.** 3D model of a Doberman cervical vertebral column. (A) 3D model of an isolated cervical vertebral column (ventral view), (B) 3D model of an isolated cervical vertebral column (lateral view).

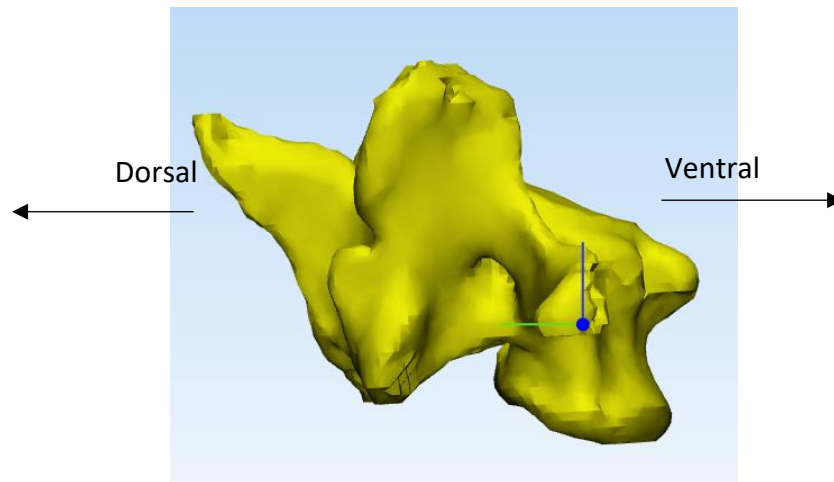
### 3.3.3. Development of Cervical Vertebrae Orientation Technique

Although some standards for vertebral orientation in humans indicate terminology of 3D anatomy and coordinate systems of a vertebra, they are quite general and based on landmark positioning, which makes the orientation subjective when locating the landmarks (ISB, 2002, Stokes, 1994, McDonald et al., 2010). Thus, such anatomical coordinate systems might serve for patient-specific matters but not for precise comparisons between different samples, which is crucial for the development of implant devices. Additionally, the morphology of a canine vertebra is different from its human counterpart, making its orientation even more subjective. Developing a vertebra orientation technique for this project was necessary to allow for vertebra comparisons across different samples and morphology analyses between healthy and CSM-affected samples.

The orientation technique was based on various landmarks and was carried out from cranial, lateral and ventral aspects. Figures 3-5 and 3-6 show the anatomical directions for 3D orientation on Mimics.

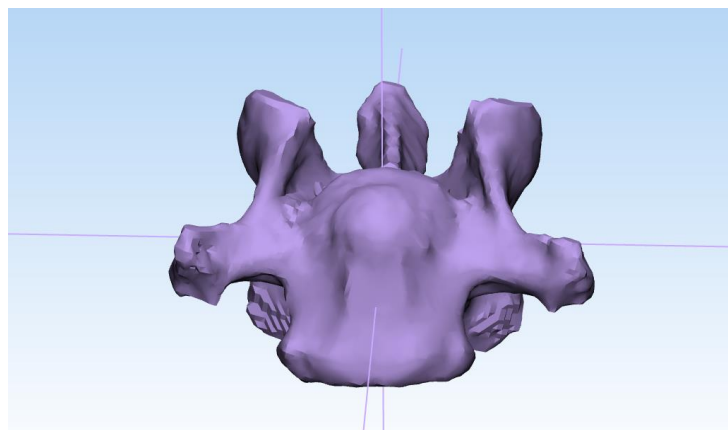


**Figure 3-5. Anatomical directions of cervical vertebrae for 3D orientation on Mimics.**

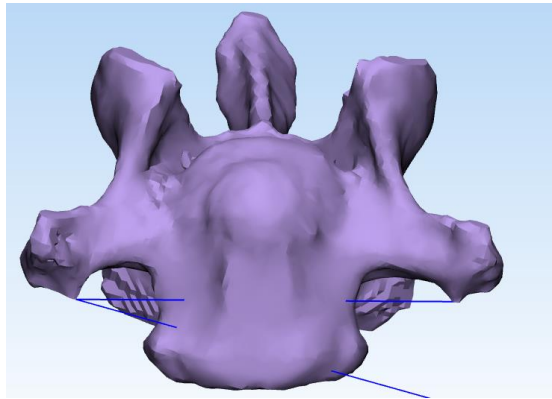


**Figure 3-6. Anatomical directions of cervical vertebrae for 3D orientation on Mimics.**

Different methods for obtaining the orientation references were considered. Firstly, the inertia axes were analysed; however, not all samples were fully symmetric, and therefore, the inertia axes did not necessarily correlate with the anatomical landmarks (Figure 3-7). Secondly, the most caudal points of the transverse processes were considered, but they were not symmetric in all samples and were different in size (Figure 3-8).



**Figure 3-7. Inertia axes of a cervical vertebra.**

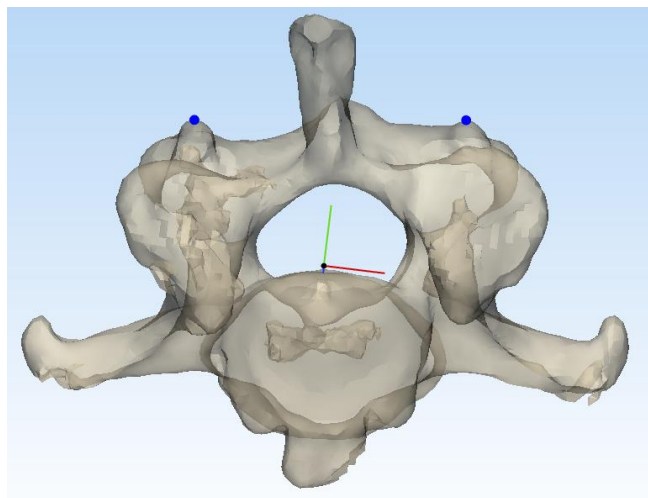


**Figure 3-8. Most caudal points of transverse processes.**

Therefore, a more detailed orientation technique -considering anatomical landmarks from all three different 3D views- was developed as follows:

#### **Pre-orientation**

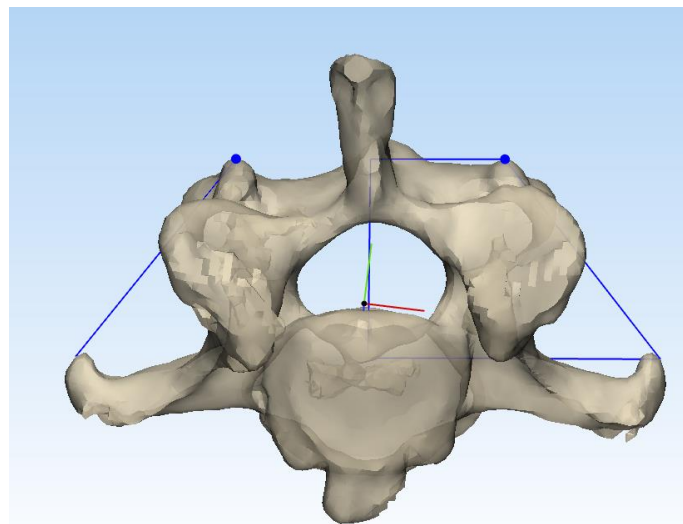
1. The vertebra was pre-orientated from a cranial view with the interactive rotate tool in Mimics. The dorsal aspect of both cranial and caudal endplates of the vertebral body was oriented to follow a vertical cranial-caudal direction; and the transverse processes were aligned parallel to the transverse and dorsal planes (Figure 3-9).



**Figure 3-9. Vertebra orientation: Pre-orientation.**

### Cranial (Top) Orientation

1. The most-dorsal points of the laminae were located and a tangent line from these points to the most-lateral points of the respective left/right transverse process was created.
2. A trapezium was then formed, connecting such lines. A bisector line was plotted between the mid-points of the dorsal and ventral lines and then used for cranial orientation. The XY angle of the bisector line was measured in reference to the Y axis. The vertebra was then rotated by this angle along Z axis to make the middle line and the Y axis collinear (Figure 3-10).

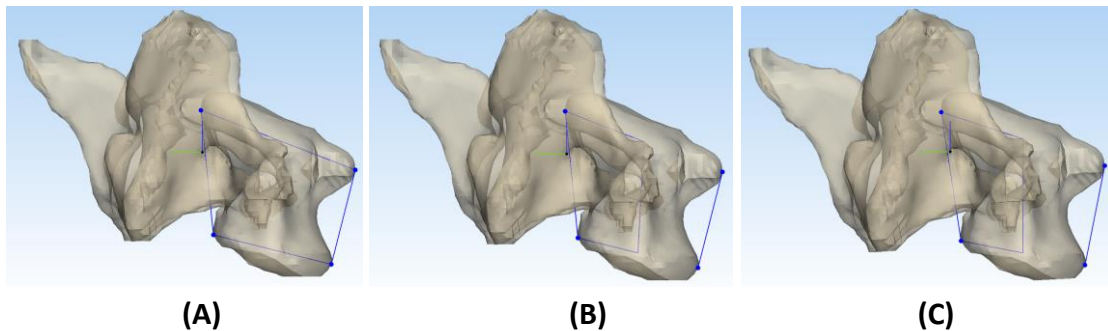


**Figure 3-10. Vertebra orientation: Cranial orientation.**

### Lateral Orientation

1. With the aid of a translucid analysis, the ventral and dorsal tangents of the vertebral body were located from a lateral view.
2. A trapezium was then formed, connecting such lines (Figure 3-11A). A bisector line was plotted between the mid-points of the cranial and caudal lines and then used for lateral orientation (Figure 3-11B). The YZ angle of the bisector line was measured in reference to the Z axis. The vertebra was then rotated by

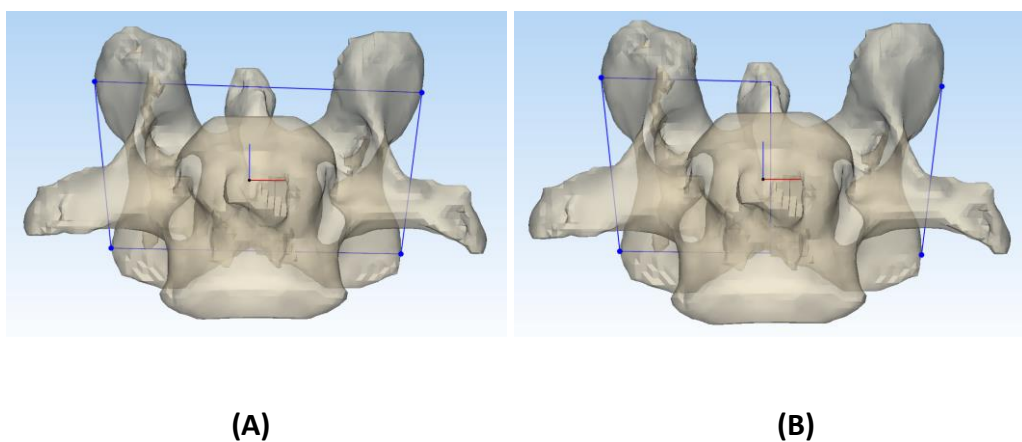
this angle along X axis to make the middle line and the Z axis collinear (Figure 3-11C).



**Figure 3-11. Vertebra orientation: Lateral orientation.**

### Ventral (Front) Orientation

1. The lateral tangents between the cranial and caudal articular surfaces of the vertebra's left and right sides were located from a ventral view.
2. A trapezium was then formed, connecting such lines (Figure 3-12A). A bisector line was plotted between the mid-points of the left lateral and right lateral lines and then used for ventral orientation. The XZ angle of the bisector line was measured in reference to the Z axis. The vertebra was then rotated by this angle along Y axis to make the middle line and the Z axis collinear (Figure 3-12B).



**Figure 3-12. Vertebra orientation: Ventral orientation.**

A coordinate system was then created by using the X, Y and Z axes from the orientation technique and their intersection of them (at the centre of the vertebral body) as a centre point.

### **3.3.3.1. Intra- and Inter- Observer Variability**

In order to assess the reliability of this orientation technique, intra-observer and inter-observer variability studies were designed. The aim was to carry out statistic analysis and obtain the intraclass correlation coefficient (ICC) (two-way mixed model, absolute agreement type) with SPSS software (<https://www.ibm.com/products/spss-statistics>). The ICC measures the level of agreement between measurements; an ICC value of over 0.9 is considered to be excellent reliability (Koo and Li, 2016). Three repetitions were considered for the intra-observer variability study. Similarly, three observers were considered for the inter-observer variability study, including the author of this thesis. Two other observers of similar experience levels with Mimics were involved in the study.

Seven different measurements were then defined for both the intra- and inter-observer variability studies: ventral width, ventral vertebral body height, ventrodorsal vertebral body length, vertebral foramen width, cranial radius, lateral width and caudoventral to craniodorsal length (Figure 3-13). All measurements were taken via software (3-matic) with an accuracy of +/- 0.0001 mm. Table 3-1 shows an example of measurements from sample S0004, vertebra C7.

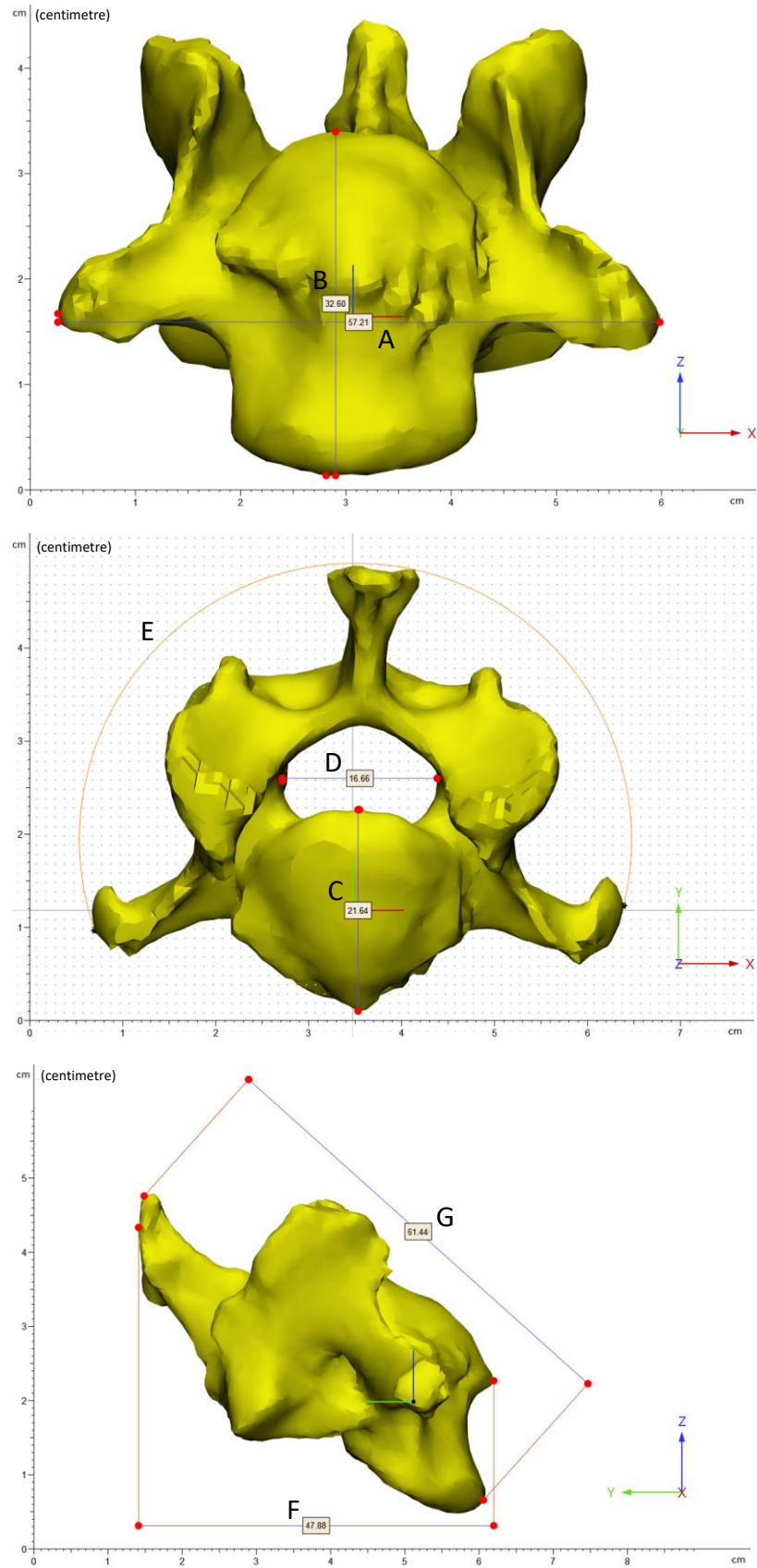


Figure 3-13. Vertebra measurements for intra- and inter-observer variability.



**Table 3-1. Vertebra measurements for intra- and inter-observer variability.**

Reference	Landmark (s)	Measurement (mm)
<b>A</b>	Ventral width	<b>57.21</b>
<b>B</b>	Cranial caudal vertebral body length	<b>32.60</b>
<b>C</b>	Ventrodorsal vertebral body length	<b>21.64</b>
<b>D</b>	Vertebral foramen width	<b>16.66</b>
<b>E</b>	Cranial external radius	<b>29.70</b>
<b>F</b>	Lateral (ventrodorsal) width	<b>47.88</b>
<b>G</b>	Caudoventral to craniodorsal length	<b>61.44</b>

The intra- and inter-observer variability measurements are shown in table 3-2 and 3-3 respectively.

**Table 3-2. Intra-observer variability. Same sample (S0001-C7), same observer, three repetitions.**

Reference	Measurement	1	2	3	SD
<b>A</b>	Ventral Width	55.738	55.7488	55.7489	0.006264
<b>B</b>	Ventral Vertebral Body Height	24.4807	24.6262	24.6162	0.081272
<b>C</b>	Ventro-dorsal vertebral body length	21.3142	21.3114	21.3143	0.001646
<b>D</b>	Vertebral Foramen width	13.7828	13.8128	13.811	0.016825
<b>E</b>	Cranial Radius	28.3942	28.4012	28.4032	0.004726
<b>F</b>	Lateral Width	46.4503	46.4402	46.4505	0.00589
<b>G</b>	Caudal ventral to cranial dorsal length	52.1264	52.1264	52.1254	0.000577

**Table 3-3. Inter-observer variability. Same sample (S0004-C7), three different observers.**

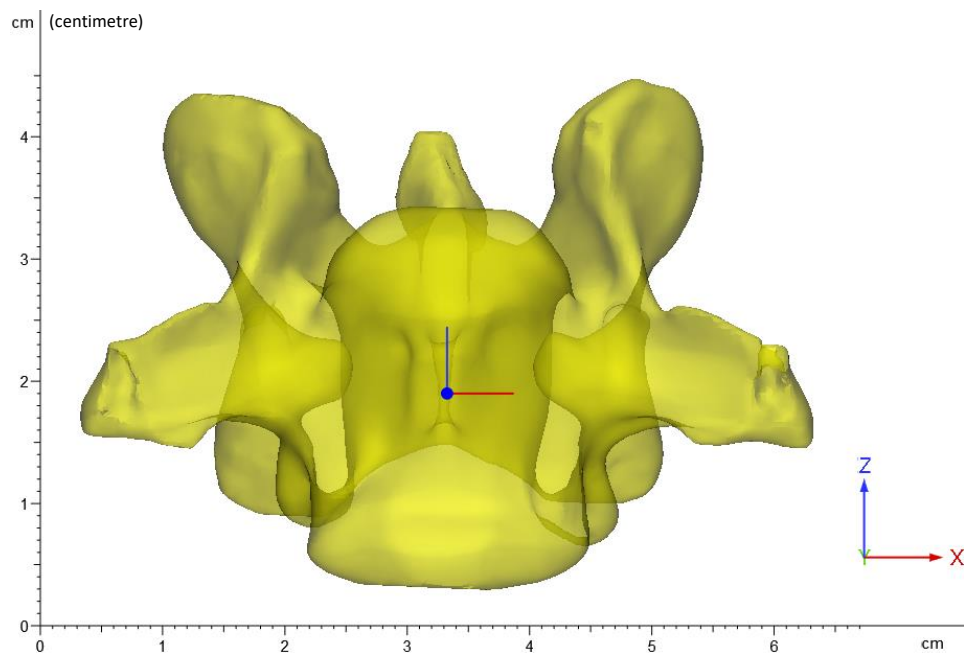
Reference	Measurement	Observer 1	Observer 2	Observer 3	SD
<b>A</b>	Ventral Width	57.2129	57.1983	57.2078	0.00741
<b>B</b>	Ventral Vertebral Body Height	32.601	32.6141	32.5997	0.007965
<b>C</b>	Ventro-dorsal vertebral body length	21.6396	21.6307	21.6392	0.005027
<b>D</b>	Vertebral Foramen width	16.6561	16.6486	16.4976	0.089424
<b>E</b>	Cranial Radius	29.7029	29.7035	29.582	0.069975
<b>F</b>	Lateral Width	47.8809	47.8541	47.8979	0.022082
<b>G</b>	Caudal ventral to cranial dorsal length	61.4405	61.5599	61.5445	0.064948

### 3.3.4. Virtual Orientation of Cervical Vertebrae

The implant development was started following the vertebra orientation technique previously described in section 3.3.3. The orientation process commenced by orientating the most caudal affected vertebra (C7), followed by subsequent cranial vertebrae one by one (i.e. firstly C7, secondly C6, thirdly C5, and lastly segment C1-C2-C3-C4). Only the most caudal affected vertebra (C7) was ‘fully’ oriented from the cranial (top), lateral, and ventral (frontal) aspects. The remaining vertebrae were only orientated from the cranial and ventral aspects to keep the intended fixation position from the CT scan (i.e. modifying the lateral orientation of all vertebrae will alter the final fixation position of the vertebral column). Ideally, the intended fixation position would be driven by the CT-scanned position of the patient.

In order to prepare the samples for systematic implant development and correlation analysis between samples, it was essential to define a global coordinate system by

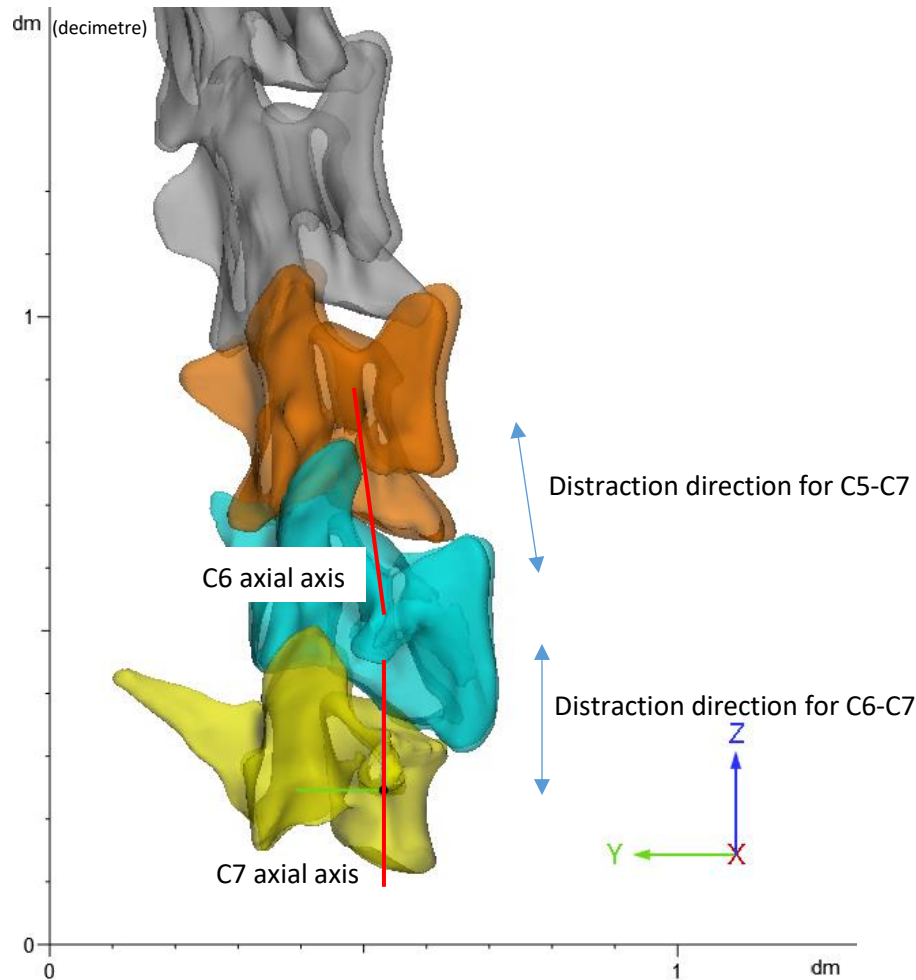
defining an origin point (0, 0, 0). The X, Y, and Z coordinates for the origin point were derived from the corresponding reference orientation axes of C7 (Figure 3-14).



**Figure 3-14. Fully-oriented C7, featuring the origin point at the centre of the vertebral body (in blue).**

### 3.3.5. Development of Virtual Distraction Technique

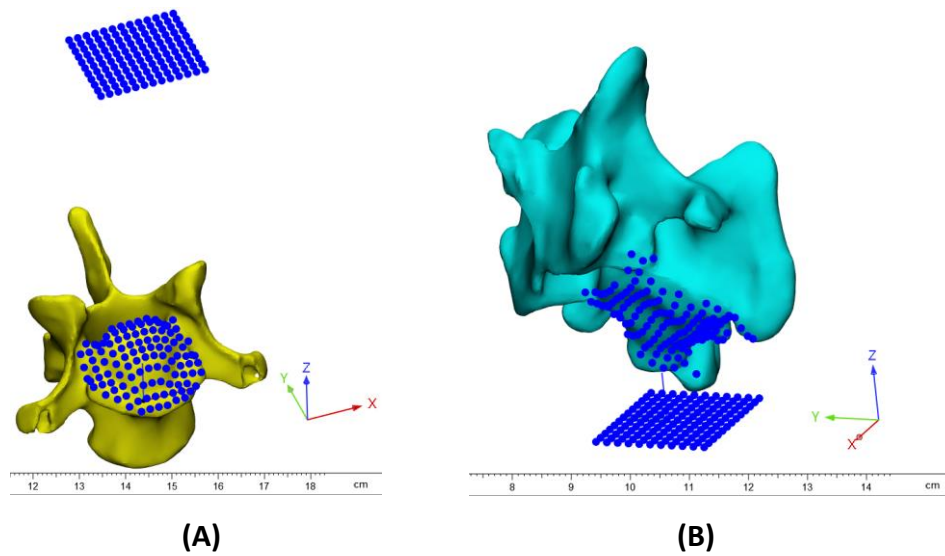
As previously discussed, current distraction-stabilisation devices lack a systematic approach for defining the distraction level of the affected sites. A virtual distraction technique was then developed to analyse distraction levels based on the IVD distances of the healthy and affected sites. After the virtual orientation of the cervical vertebrae, the IVD distances were measured with 3-matic using as a reference the axial axis of the corresponding caudal vertebra per IVD. The average value of the healthy IVD distances was calculated and defined as the ‘healthy’ reference distance (i.e. distraction level 0%). The affected segments were then virtually distracted using as a reference the axial axis of the corresponding caudal vertebra per IVD (Figure 3-15).



**Figure 3-15. Virtual distraction using as a reference the axial axis of the corresponding caudal vertebra per IVD.**

### 3.3.6. Mapping of Endplate Morphology

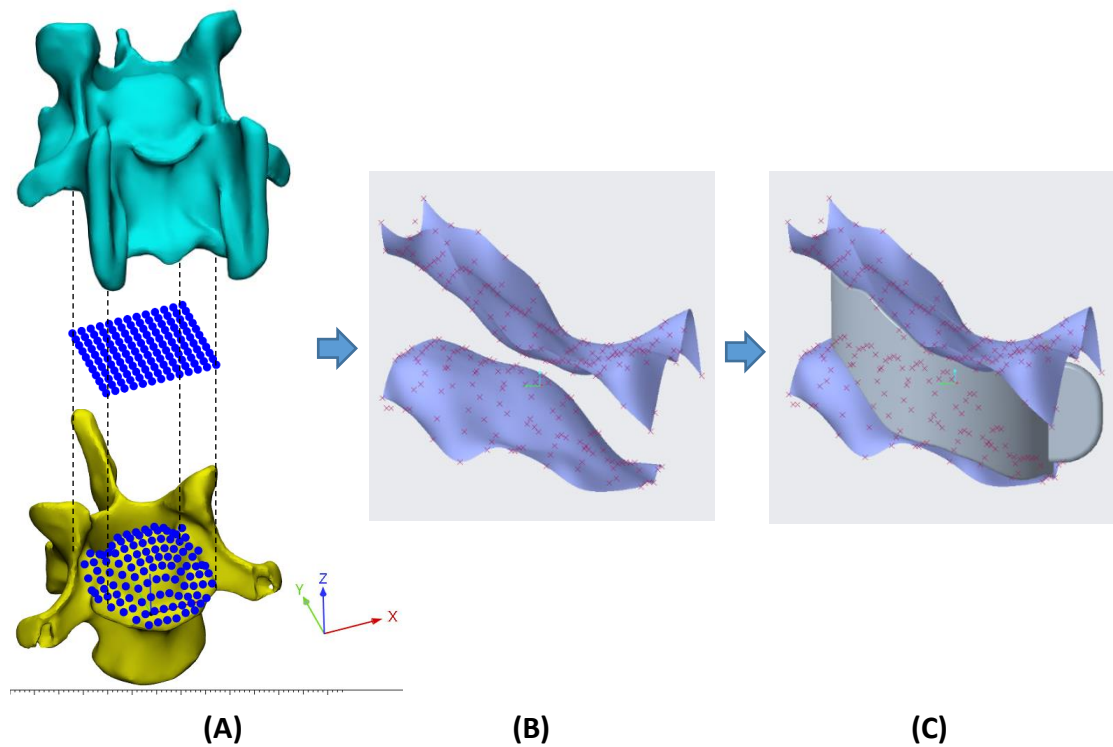
Once the cervical vertebral column was distracted at the intended fixation position, the morphology of the endplates was necessary for implant development. A two-dimensional grid of 10x10 points was defined per IVD segment based on the cranial endplate size of the corresponding caudal vertebra as follows: 10 reference points were set as a ratio of the ventral width over the X axis, and 10 reference points as a ratio of the ventrodorsal width over the Y axis. All points were then projected on the corresponding IVD cranial and caudal vertebrae to generate endplate morphology data (Figure 3-16). The point data set was then exported to Creo Parametric for implant designing.



**Figure 3-16. Mapping of vertebral endplate morphology data. A) Mapping of C7 cranial endplate morphology, B) Mapping of C6 caudal endplate morphology.**

### 3.3.7. CAD Profile Modelling

The endplate morphology data set was then processed with Creo. This point data set represents the bone-implant interfaces which were used for modelling endplate-conforming interbody spacers. 3D surfaces were blended to generate the cranial and caudal ends of the implant (Figure 3-17B). A solid profile was then generated based on these surfaces and further engineered to generate the final devices (Figure 3-17C).




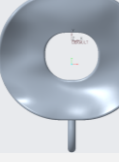

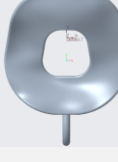


**Figure 3-17. A) Mapping of endplate morphology data, B) CAD of endplate surfaces, C) Endplate-conforming interbody spacer.**

### 3.3.8. Analysis of Spacer Dimensions and Shapes

Different spacer profiles were generated using percentages of lateral and ventrodorsal widths of the vertebral body from the caudal vertebra of the affected site. Initially, a wide range of trial spacer sizes and distraction levels was considered. In order to accomplish this, three different sizes (varying width and length) were designed for each affected segment, making 6 in total (Table 3-4).

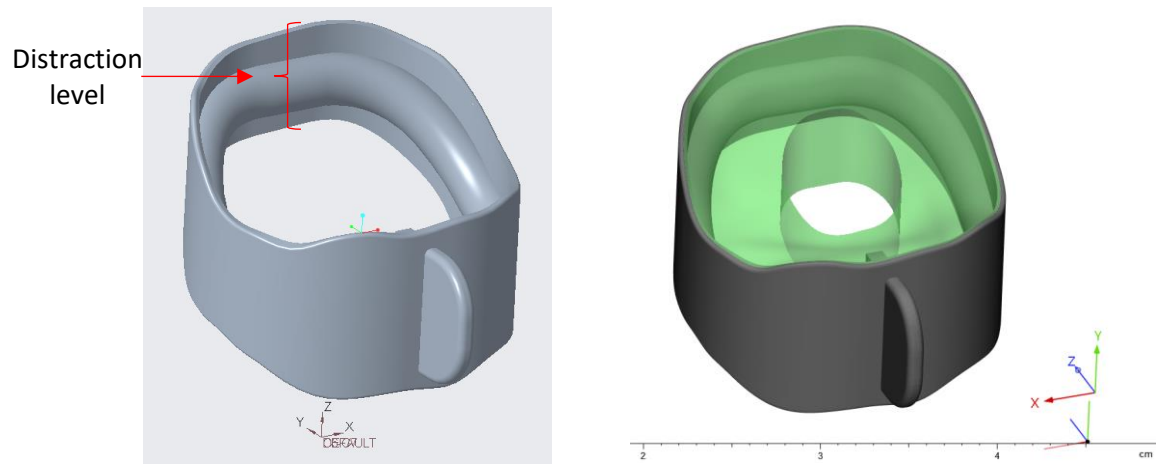
**Table 3-4. Dimensions and shapes of spacer profiles.**

Design	C5-C6 Standard	C5-C6 Narrow	C5-C6 Wedged	C6-C7 Standard	C6-C7 Narrow	C6-C7 Wedged
Lateral Width	70%	50%	70%cr- 50%cd	70%	50%	70%cr- 50%cd
Ventrodorsal Width	80%	80%	80%	80%	80%	80%
Profile						

### 3.3.9. Distraction Level and Implant Construct

Three different shapes were designed for each spacer with different sizes of implant-endplate footprint. Additionally, the implants were manufactured at four distraction levels (or implant height as seen in figure 3-18A) based on the mean distance of the healthy intervertebral segments taken from the respective CT scan: 0%, +10%, +17, and +25% distraction level. For the first custom case, the average IVD distance of the healthy segments C2-C3, C3-C4, and C4-C5 was 4.04 mm. Hence, a distraction level of +10% made the IVD distance 4.44 mm, +17% made it 4.72 mm, and +25% made it 5.05 mm.

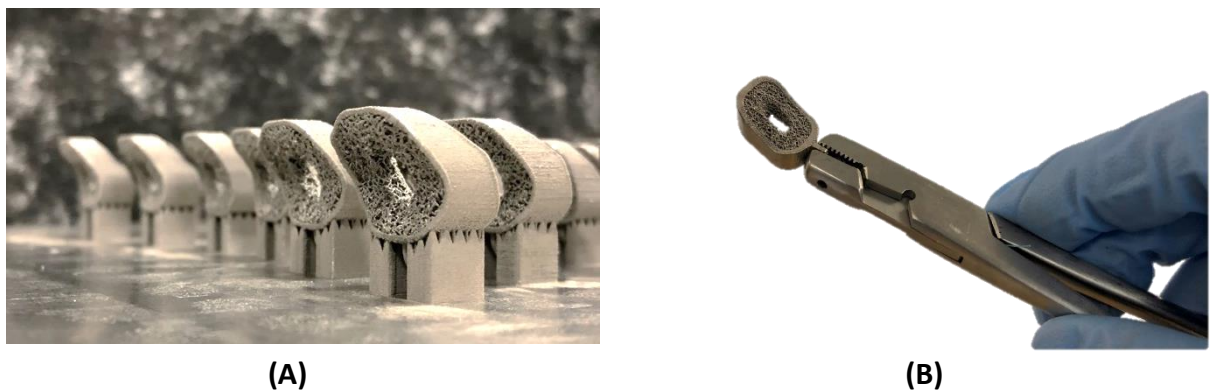
As previously described, by combining an endplate-conforming spacer with an internal porous structure, the endplate-conforming feature can promote stabilisation while the porous structure promotes osseointegration. A porous structure file was generated and incorporated into each design (Figure 3-18B) with technology previously reported for optimal bone in-growth (Mullen, 2009, Mullen et al., 2009, Mullen et al., 2010, Zhang et al., 2013). Each implant featured a solid outer wall and inner ring for protecting its structure, an inner porous structure with a central hole for bone graft packing, and a frontal fin to facilitate implant placement.



**Figure 3-18. Ventrolateral view of spacer. A) Solid section of spacer, B) Solid part of spacer (in grey) and porous part of spacer (in green).**

### 3.3.10. Manufacturing by Selective Laser Melting

The interbody spacers were manufactured in titanium alloy (Ti6Al4V) using a selective laser melting system RenAM 500Q (Reinshaw plc; Wotton-under-Edge, UK) (Figure 3-19). The outer lateral and ventro-dorsal sections of the spacers were gently polished for a better surface finish. Bone-implant conformance occurs on the cranial and caudal sections of the spacers, which was therefore not compromised by the polishing. All individual implants were heat-treated, ultrasonically cleaned in distilled water (40 minutes), dried (120 °C for 4 hours), and stored prior to sterilisation and implantation.



**Figure 3-19. CpTi interbody spacers. A) SLM build plate, B) Patient-specific spacer.**



### 3.4. Development of Ventral Anatomical Plate

The development of a patient-specific anatomical ventral locking plate was started based on the virtual models of the same CT scan sample identified in section 3.3.1.

#### 3.4.1. Mapping of Ventral Vertebra Bodies

The 3-matic file containing the vertebral column model that was oriented and set to the intended fixation position (i.e. virtually distracted) described in section 3.3.4, was used for plate designing. A two-dimensional grid of 11x11 points was defined per IVD segment based on the same cranial endplate size of the corresponding caudal vertebra (to keep consistency across designs) as follows: 11 reference points were set as a ratio of the ventral width over the X axis, and 11 reference points as a ratio of the ventro-dorsal width over the Z axis. All points were then projected on the corresponding ventral vertebral bodies to generate their morphology data (Figure 3-20). The point data set was then exported to Creo Parametric for implant designing.

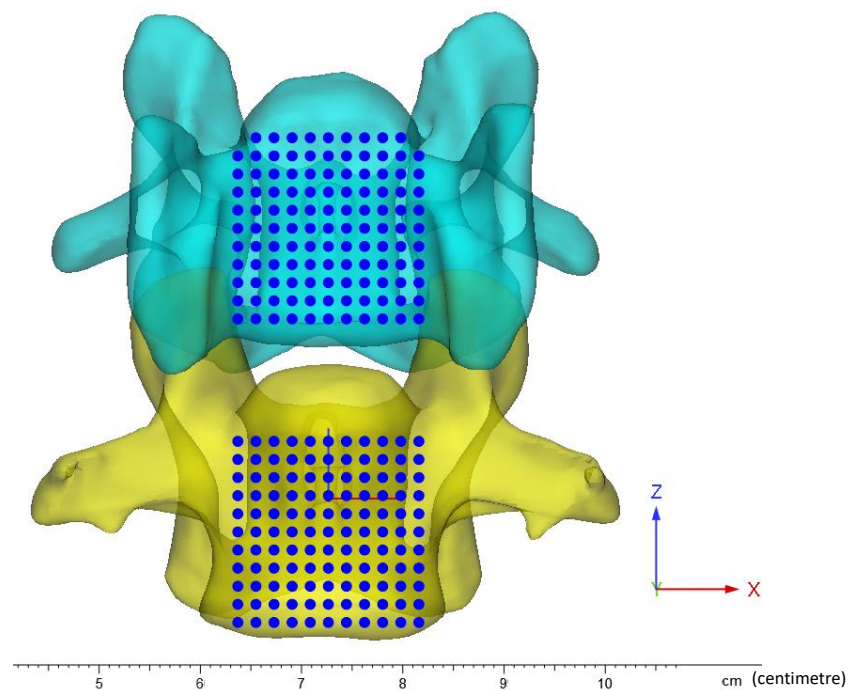


Figure 3-20. Mapping of ventral vertebra body morphology data.

### 3.4.2. CAD Profile Modelling

The vertebra body morphology data set was then processed with Creo. This point data set represents the bone-implant interface which was used for modelling ventral-conforming anatomical plates (Figure 3-21A). A 3D surface was blended to generate the shape of the plate (Figure 3-21B). A solid profile was then generated based on this surface and further engineered to generate the final device.

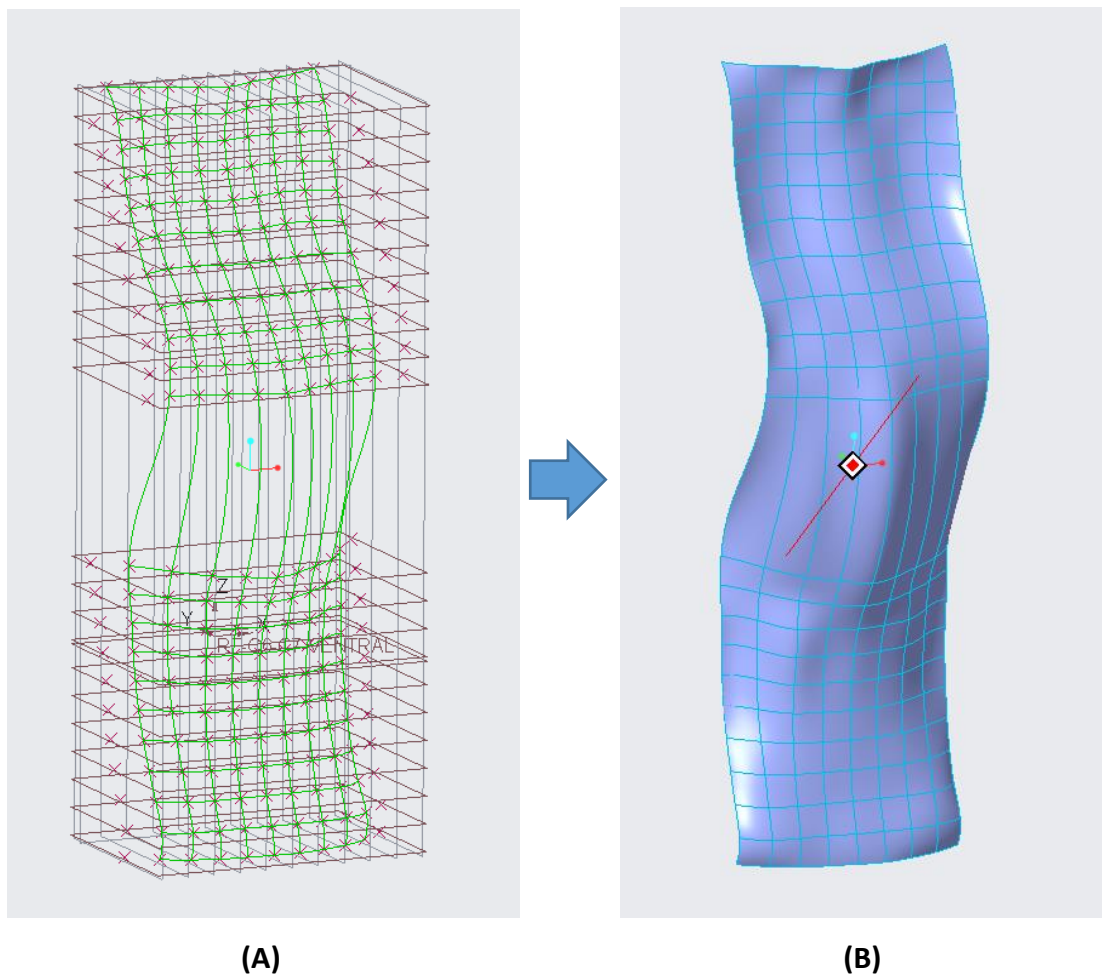
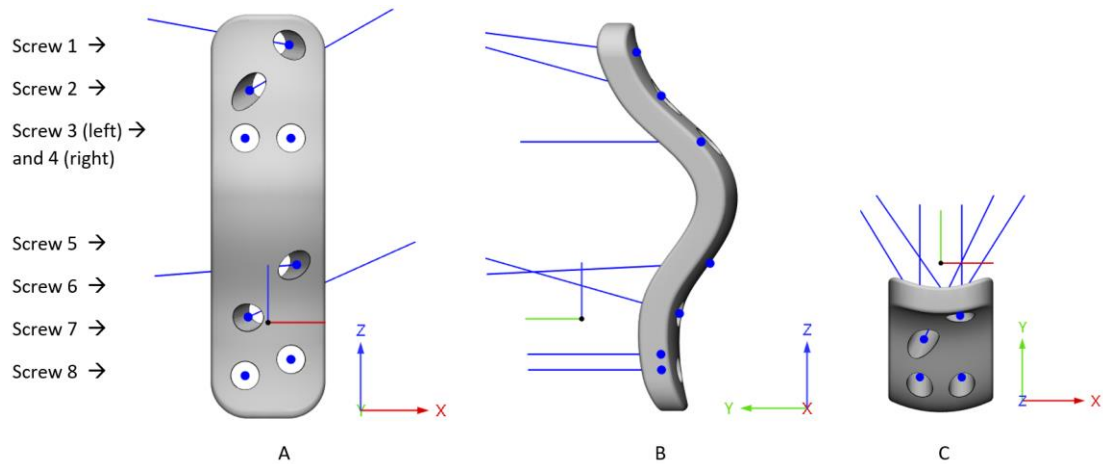


Figure 3-21. A) CAD of ventral surfaces, C) Ventral-conforming anatomical plate.

### 3.4.3. Identification of Screw Trajectories

Once the solid CAD profile was designed, optimal pedicle screw trajectories were identified in 3-Matic. Figure 3-22 depicts the patient-specific anatomical plate with identified pedicle screw trajectories. Table 3-5 lists the screw directions (position and angles).



**Figure 3-22. Custom plate and screw trajectories, (A) Front view, (B) Lateral view, (C) Top view.**

**Table 3-5. Screw positions and angles for custom plate.**

Screw	Screw Position			XY Angle	YZ Angle
	X	Y	Z		
1	2.5772	-6.9939	33.8945	124.94	7.26
2	-2.2508	-10.1444	28.3385	64.06	15.41
3	-2.8000	-15.1906	22.5000	0	0
4	2.8000	-15.2121	22.5000	0	0
5	3.5004	-16.3470	7.0550	124.38	-2.78
6	-2.4245	-12.4620	0.6761	57.65	15.86
7	2.8000	-10.0895	-4.5000	0	0
8	-2.8000	-10.1689	-6.4860	0	0

### 3.5. Results

In terms of orientation technique, the ICC measured was 1 for both intra- and inter-observer validations, which means the reliability level of the orientation technique is considered to be excellent with minimal error. With this result, the orientation technique can serve as a basis for developing a systematic approach for implant development, namely interbody spacers or anatomical plates.

This novel orientation technique for canine cervical vertebrae provided valuable guidelines for the development of canine vertebral column implants, such as patient-specific custom-designed titanium interbody devices and ventral anatomical plates). Although this technique was developed explicitly for the orientation of canine cervical vertebrae, transferring it to the thoracic and lumbar vertebrae could be considered.

The spacer designs resulted in excellent in silico conformity; they are wide enough to maximise bone-implant interface without compromising implant placement. This maximization of the bone-implant interface extends quite far ventrally, for which a ventral plate would be recommended in addition to the fixation system to prevent gross ventral migration. Additionally, the spacer design could facilitate CT-determined bone in-growth and subsidence for surgical applications.

An important matter when developing the endplate-conforming interbody spacers would be to scan patients at the intended fixation position to minimise implant subsidence. Additionally, getting more stability with a ventral (preferably patient-specific) plate in the first few post-operative days would enhance the overall vertebra stabilisation. Due to time constraints and manufacturing turnaround times, custom plates remained under development. However, development guideless were set in the last section of this chapter for future applications.

The use of endplate-conforming interbody spacers and the incorporation of 3D-printed bone models for surgical rehearsal and plate pre-contouring could also increase the ease of the surgery. A semi-standardised surgery protocol using the

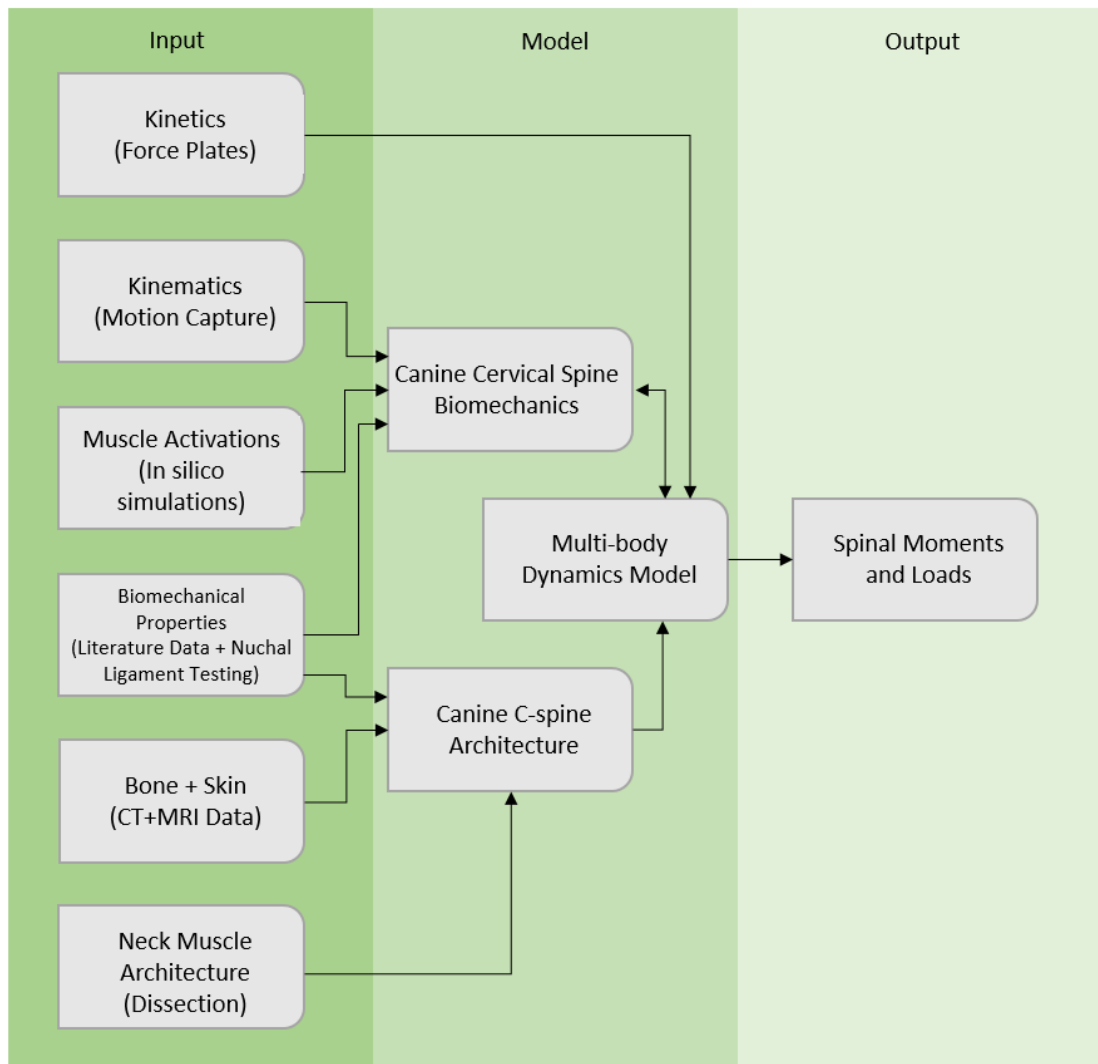
spacer designs described in this chapter could be followed with minimal implantation error due to the broader implant-endplate conformance. This in turn could allow the implants to be used by different surgeons across different institutions, leading the way towards the wider neurosurgery/orthopaedics community.

## **4. In-silico Modelling of the Kinematics and Kinetics of a Native Canine Cervical Vertebral Column**

### **4.1. Introduction**

This chapter presents the process of developing an in-silico model of the kinematics and kinetics of a native canine cervical vertebral column to understand how distraction-stabilisation impacts these. Data from healthy dogs was used for developing the model, which can be used as a reference model to compare with data from CSM-affected dogs. This in turn can help to optimise the development of distraction-stabilisation devices, including interbody spacers.

For the development of a Doberman multi-body dynamics model, advanced animal and vertebral column modelling concepts are used in this project (Alziadeh et al 2017; Foss et al., 2013a, Foss et al., 2013b; Charles, et. al, 2016). Diverse experimental parameters are then considered as 'inputs' towards predicting 'output' neck moments and vertebral column forces, focusing on the neck region. A schematic of this modelling approach is shown in Figure 4-1. The stages of the development of the multi-body dynamics model are described over the different sections of this chapter.



**Figure 4-1. Multi-body dynamics modelling approach.**

---

## 4.2. Non-invasive Gait Analysis of Neck Movements in a Normal Dog

A crucial aspect of this project is to analyse the kinematics and kinetics of a native canine cervical and cranial-thoracic vertebral column. Demonstrating feasibility through pilot data is, therefore, the aim of this section. It is proposed to apply the novel aspects of this workflow to three healthy Doberman dogs. Dobermans were chosen because of their predisposition to CSM and relatively large body size.

Various studies (Alizadeh et al., 2017, Foss et al., 2013a, Foss et al., 2013b) have shown that different biomechanical parameters of the canine neck can be obtained through gait analysis using force plates, EMG sensors and reflective markers. The biomechanical parameters determined lead to a better understanding of the CSM behaviour not only across the neck but also over the whole body of the dog. These methods are then combined into a single – non-invasive gait analysis – study for this research project, with data correlated from each Doberman to gain a comprehensive gait analysis.

### 4.2.1. Subject Recruitment

As discussed earlier, it was proposed to apply the novel aspects of this workflow to three healthy Doberman dogs. Dobermans were chosen because of their predisposition to CSM and their relatively large body size. Three healthy (non-geriatric) Doberman dogs were then recruited for a non-invasive gait lab analysis.

This study was wholly non-invasive and did not result in any harm or discomfort to the animals. It simply involved attaching small markers and sensors to the body and limbs of the dogs (using double-sided sticky tape) to record data while they walked normally through a large room (gait lab). The University of Liverpool Committee granted ethical approval on Research Ethics (VREC665) for the recruitment of three Dobermans (Table 4-1).



**Table 4-1. Non-Invasive Gait Analysis: Subject Information**

<b>Data</b>	<b>Subject 1</b>	<b>Subject 2</b>	<b>Subject 3</b>
Date	13/08/2018	20/08/2018	03/09/2018
Age	4y 4m	2y 3m	5y 6m
Gender	Female	Male	Female
Weight	30.4 Kg	45.4 kg	33 kg
Height	62 cm	72 cm	66 cm

#### 4.2.2. Quantification of Gait Kinematics and Kinetics

The kinematics (motion) and kinetics (forces) of three healthy Dobermann dogs using non-invasive approaches during a range of normal "everyday" activities (walking, trotting, neck movements [e.g. drinking from a water bowl]) were quantified as follows. Kinematic analysis of these neck movements were carried out using a standard surface marker (infra-red) motion capture system in a gait lab within the William Henry Duncan Building at the University of Liverpool.

The activity (e.g. activation/deactivation) of key neck muscles was intended to be recorded by surface electromyography (EMG) using existing Delsys trigno sensors. However, during the first study, most EMG sensors recorded little or null signal. This was most likely caused because of the hair-sensor interface- since the EMG sensors are not directly in contact with the skin, they can hardly detect muscle activities. This became a limitation in data acquisition, as according to the ethics approval, the hair of the dogs could not be trimmed at all. An alternative approach was considered and will be detailed in later sections of this chapter, comprising an in-silico musculoskeletal approach for simulating neck muscle movements.

#### Gait Study Protocol

The general procedure for the gait study commences by letting the subject dog walk around the gait lab to become familiarised with the facilities and walk with minimum-

zero stress. The participant was then weighed on veterinary quadrupedal scales (accuracy +/- 0.1kg).

For walking and trotting trials, the dogs were walked at self-selected speeds (with encouragement from their owners) along a defined straight path (using traffic cones) that includes three active Kistler force plates to measure 3D ground reaction forces (GRF) (Figure 4-2).



**Figure 4-2. Walking path with Kistler force plates.**

The gait lab setup for the study included an optical motion capture system (Göteborg, Sweden) with 12 Qualisys Oqus infrared cameras (7+ series) to capture and record reflective marker (RM) locations during the trials through Qualisys Track Manager (QTM) software. The study itself consisted of two parts: (1) leading the dog for multiple walks (preferably without a lead cord) and (2) performing neck movements (flexion/extension and lateral bending).

The marker data served as an input for recreating a three-dimensional motion model of the dog for inverse kinematics determination. Similarly, the forces measured served as an input for finite element analysis (FEA) to validate the in-silico model parameters. These simulations will help to understand the biomechanics of the limbs and neck and simulate bone-implant interactions via FEA to analyse their performance.

---

**Data Acquisition**

Forty-seven retro-reflective markers (B&L Engineering, California, USA) were attached over the body of the dogs (Table 4-2) using double-sided tape by a veterinary orthopaedic surgeon, Mr Ben Walton, thereby ensuring optimal positioning. These markers were placed strategically on known anatomical landmarks such as joints and mid-point of bones to facilitate correlation analysis. Three reflective markers were attached to the head: (RM1) Occipital Crest, (RM46) left frontal lobe, and (RM47) right frontal lobe. Six more markers were attached to the neck section: (RM2) left atlas transverse process, (RM3) right atlas transverse process, (RM4, RM5, RM6, and RM7). The neck was split into three lengthwise sections from the occipital crest (RM1) to the first palpable vertebra (RM7), and the markers were attached to the mid-point of these segments (Figure 4-3). Figure 4-4 shows the layout of the retro-reflective markers placed on the dog.

As Dobermanns are short-haired breeds, no trimming of hair/fur was required. Ten successful trials (defined as the dog carrying out the activity in the desired way) were collected per dog for each activity.

**Table 4-2. Position of Reflective Markers**

Reflective Marker	Segment	Landmark
46/47 (L/R)	Head	Frontal Lobe
1	Head	Occipital Crest
2/3 (L/R)	Neck	L/R Atlas Transverse Process
4	Neck	Split neck into three lengthwise from occipital crest to first palpable vertebra. Place markers at the mid-point of each segment (Figure 4-3).
5	Neck	
6	Neck	
7	Neck	First palpable vertebra
8/9 (L/R)	Forelimbs	Top of scapula
10/11 (L/R)	Forelimbs	Acromion
12/13 (L/R)	Forelimbs	Lateral epicondyle
14/15 (L/R)	Forelimbs	Medial epicondyle
16/17 (L/R)	Forelimbs	Mid-humerus
18/19 (L/R)	Forelimbs	Ulna styloid
20/21 (L/R)	Forelimbs	Metacarpophalangeal Joints (MCPJs)
22/23 (L/R)	Forelimbs	Toe
24	Vertebral Column	T13
25	Vertebral Column	L7
26/27 (L/R)	Hindlimbs	Wing of ilium
28/29 (L/R)	Hindlimbs	Ischial tuberosity
30/31 (L/R)	Hindlimbs	GT
32/33 (L/R)	Hindlimbs	Lateral epicondyle
34/35 (L/R)	Hindlimbs	Medial epicondyle
36/37 (L/R)	Hindlimbs	Lateral stifle
38/39 (L/R)	Hindlimbs	Lateral malleolus
40/41 (L/R)	Hindlimbs	Lateral Metatarsophalangeal Joints (MTPJs)
42/43 (L/R)	Hindlimbs	Toe
44/45 (L/R)	Hindlimbs	Femur

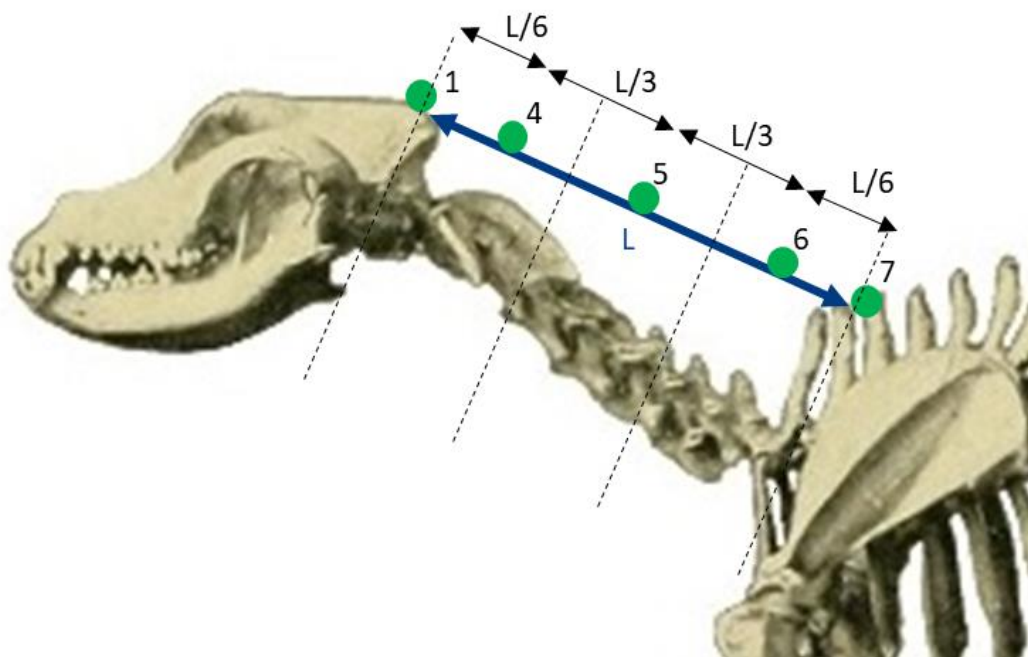


Figure 4-3. Neck Markers.

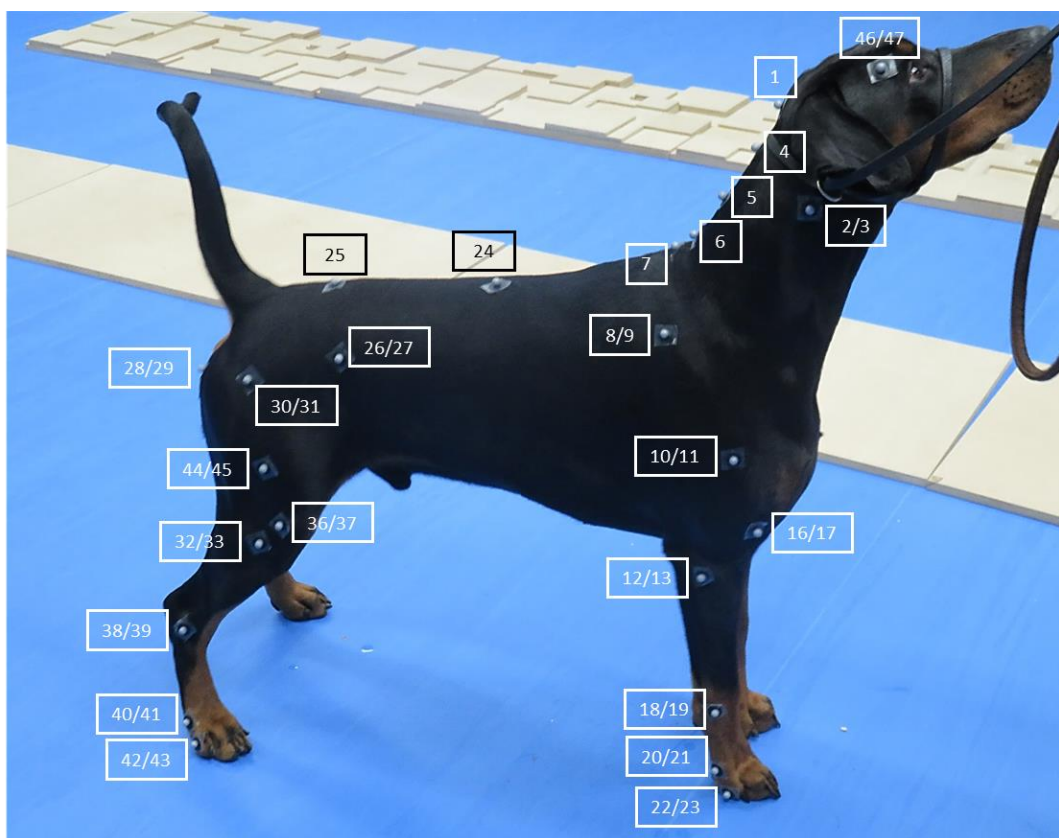
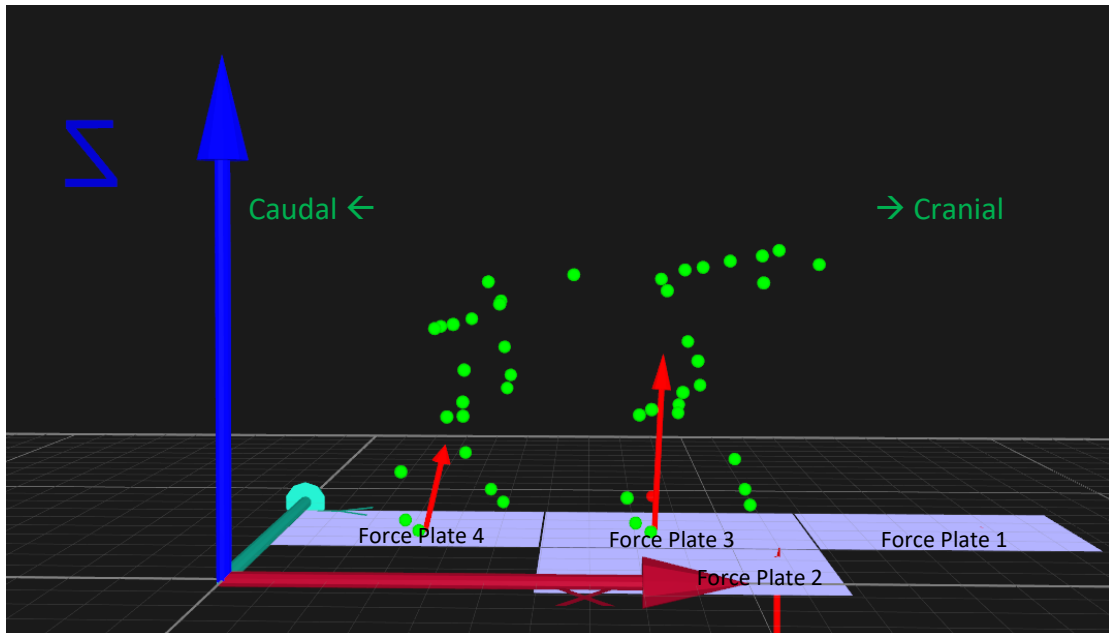


Figure 4-4. Reflective Markers: Whole Body Arrangement

The activity of the reflective markers (infrared reflection) was recorded during each trial by the Oqus cameras for calculating kinematics. The ground reaction forces were recorded at the same time by the Kistler force plates during the experiments. Both kinematics and kinetics are recorded and processed via QTM software (Figure 4-5).



**Figure 4-5. Data acquisition of reflective markers with Qualisys Track Manager. The green dots represent the recorded reflective markers (kinematics data), and the vertical red arrows represent the ground reaction forces from the limbs (kinetics data).**

#### 4.2.3. Quantification of Gross Body Proportions

The gross body proportions (body and limb circumferences) and body mass of the three healthy Doberman dogs that participated in the non-invasive gait analysis (section 4.2.2 of this thesis) were recorded as follows.

The dogs were previously weighed as described in section 4.2.2. A suite of body proportion measurements was developed using a tape measure in order to capture the lengths and circumferences of key 'body segments' (e.g. head, neck, thorax, thigh, shank etc.), so that a virtual model of a Doberman can be produced in a computer-

aided design package and scaled based on these measurements. This virtual volumetric model will be given segment-specific densities based on published mammalian data and thus will provide the body segment mass/inertial properties of each dog required for developing the multi-body dynamics model in (e.g. up/down scaling parameters).

Most of the measurements were taken using the reflective markers as reference points. E.g. transverse circumferences and distances between key reflective markers. The complete list of measurements is included in Appendix A. Each measurement was repeated three times (N1, N2, and N3), and the average was calculated (Appendix B).

#### **4.2.4. Identification of Reference Gait Cycle**

A QTM gait data set was recorded from each of the three subjects. Ten trial sets of 20 seconds (4000 marker frames) were recorded for each subject. Each trial set included 2-4 walk trials (gait cycles). A gait cycle was identified as a reference for the final musculoskeletal model, which comprises two main characteristics: (1) complete tracking of all reflective markers throughout (100% activity recorded during the gait cycle) and (2) at least one forelimb and hindlimb 'clean strike' were recorded by the force plates (e.g. a paw/foot alone hitting a single force plate at one moment of time) meaning only 'clean' ground reaction forces are recorded. Hence, each gait cycle was analysed individually in order to identify an appropriate cycle based on these criteria. Subject 1, trial set 5, walk trial 1 recorded at 2.5-4.49 seconds (500-900 marker frame) was identified as the gait cycle to be used for further musculoskeletal modelling (described in section 4.6.1). The identified gait cycle was exported as a .c3d file.

As a gait cycle from subject 1 was identified as a reference cycle, all additional gait cycles with 'clean strikes' from subject 1 were also recorded for further analysis of ground reaction forces. Appendix C lists these additional cycles.

---

### 4.3. Analysis of Muscle Architecture: Neck Dissection

Very few studies in the literature describe the muscular architecture of the canine neck, and those that are reported consider only mixed-breed dogs and small to medium-breed dogs. None of the dog breeds reported is similar in size to a Doberman. Sharir and colleagues dissected six mixed-breed dogs from 19-28 kg in weight (mean weight 23.8 Kg) and described in detail 52 epaxial muscles (Sharir et al., 2006). Webster et al. conducted a neck dissection on 9 Greyhounds and 6 Staffordshire Bull Terriers, reporting 14 neck muscles but featuring only seven cervical muscles (Webster et al., 2014). Bostrom et al. dissected 13 epaxial muscles from small breed dogs – 17 Dachshunds and 7 Border Terriers (Bostrom et al., 2019). None of the studies reported data from all neck muscles; therefore, this dissection study in this thesis aims to provide quantitative data on the muscular architecture (mass, length, fibre lengths, and pennation angles) of all neck muscles from a Doberman-like dog. This information will be used to develop a more accurate in-silico model of a Doberman dog, focusing on the muscles involved around the CSM-affected segments of the neck.

#### 4.3.1 Sample Acquisition

Ideally, a Doberman specimen was intended to be dissected, unfortunately, it was not possible to obtain a specimen, and it was decided to carry out the neck dissection on the most similar breed to a Doberman neck available at the Veterinary Teaching Suite (VTS) due to the importance of proceeding further with a musculoskeletal model for future analyses. This muscle data will work as initial muscle references, which can also be compared to data from other breeds in the literature. The specimen was a 16 Kg female hound that died of unknown reasons and was donated for research. This cadaver was kept in the freezer at -20 °C from when it arrived at the VTS.

#### 4.3.2. Dissection Protocol and Muscle Architecture

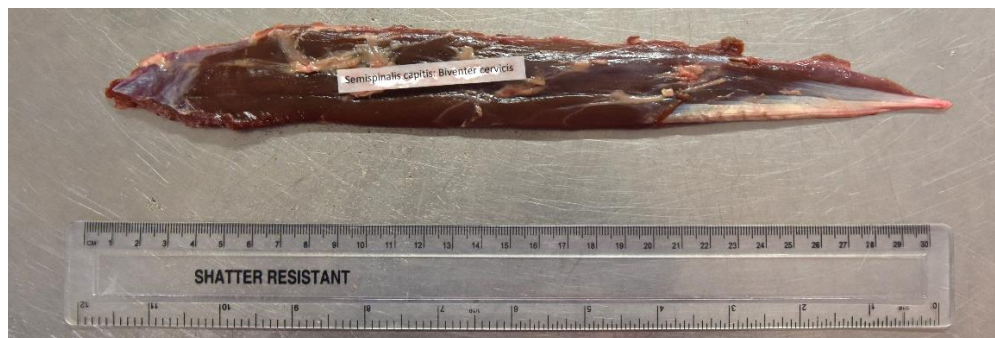
This dissection study was approved by the University Committee on Research Ethics (Reference number VREC665). The cadaver was thawed for 72 hours at 0-4 °C prior to



the dissection. The dissection was carried out at the VTS with help from Dr Sophie Macaulay- a research assistant from the Institute of Life Course and Medical Sciences, University of Liverpool. The dissection was done following well-documented guidance for muscle attachments and paths (Evans and DeLahunta, 2017).

Only the muscles from the left side of the neck were extracted because the neck muscles are paired. All muscles were extracted in one day, refrigerated overnight at 0-4 °C and measured the following day. This procedure was necessary due to the time taken for muscle dissection. All muscles from the cervical region were dissected and analysed, accounting for 16 muscles in total (Appendix D).

Muscle belly and muscle-tendon unit length were measured from origin to insertion points (including tendon length where applicable) using a flexible plastic ruler (to accuracy +/- 1 mm) and photographed. For fan-shaped muscles with multiple insertion points, this measurement was carried out according to the longest origin-insertion distance, ensuring that these measurements reflect each muscle's complete line of action. The muscle-tendon mass was measured using an electronic balance (to accuracy +/- 0.1g) (A&D, Tokyo, Japan). The tendon was subsequently cut, and both muscle and tendon were weighed separately (to accuracy +/- 0.1 g). Then, the length of five fibres was measured from each muscle. Finally, three pennation angles were measured with a plastic protractor (to accuracy +/- 1 degree) from each muscle. Each muscle's total mass, length, fibre lengths and pennation angles are listed in Appendix E. Muscle volumes were calculated by dividing muscle mass by muscle density of 1060  $\text{Kg}\cdot\text{m}^{-3}$  (Mendez, 1960). Additionally, the nuchal ligament was extracted for tensile testing (Section 4.4) to obtain data when building the musculoskeletal model.



**Figure 4-6. Muscle length measurement.**

---

## 4.4. Ex-vivo Nuchal Ligament Test– Tensile Strength

### 4.4.1. Experimental Design

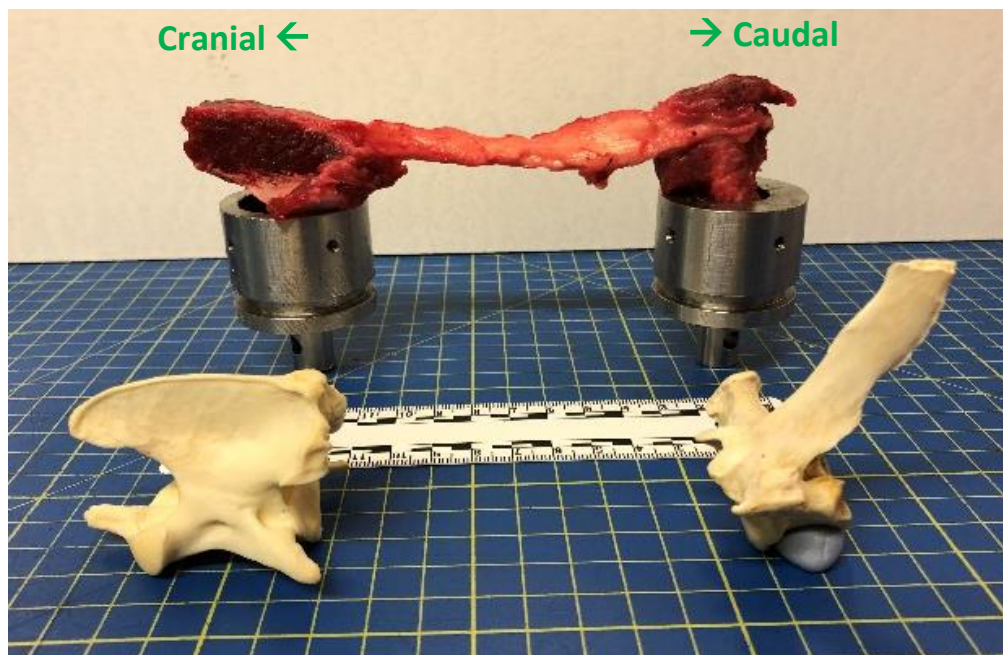
The nuchal ligament (NL) is a robust fibro-elastic tissue which plays a vital role in stabilising the head of the dogs. It complements the epaxial muscles by supporting the head's weight with no need for active exertion of such muscles (Wang et al., 2008). The nuchal ligament is the extension of the dorsal spinous ligament which extends from the dorsal spinous process of the first thoracic vertebra (T1) to the dorsal spinous process (apex) of the second cervical vertebra (C2; Axis) (Evans and DeLahunta, 2017). Unfortunately, no factual data are available in the literature regarding dogs' tensile properties of the nuchal ligament. The aim of this study is to determine the tensile strength of the nuchal ligament of different breed dogs to analyse their correlation. The analysis of this correlation will provide meaningful information on mechanical strength around the cervical region and complement the in-silico model.

### 4.4.2. Sample Acquisition and Dissection of the Nuchal Ligament

Frozen canine cadaveric specimens were obtained through the Veterinary Teaching Suite (University of Liverpool) with unknown reasons of death. Ethical approval was granted by the University Committee on Research Ethics (VREC665) for the use of this canine cadaveric material. Nuchal ligaments from three mixed-breed hounds (16 Kg, 24 Kg, and 44 Kg), labelled as 'nuchal ligament 1', '2', and '3' respectively, were analysed. Briefly, following the thawing of cadavers to 4°C for 48hrs, the skin and epaxial muscles of entire neck region were removed to expose the NL (Figure 4-7). These include the lateral *longissimus* group, and the very medial *transversospinalis* group muscles (Evans and DeLahunta, 2017). Entire NL specimens were carefully dissected between point of attachments (i.e. second cervical vertebrae (C1; axis) to the first thoracic vertebra (T1)). The extracted samples were then frozen at -20 °C for use at a later date. When required, they were thawed for 24-48 hours at 4 °C before the tensile testing. Ligament length was measured at relaxation and linear traction from each sample.



(A)



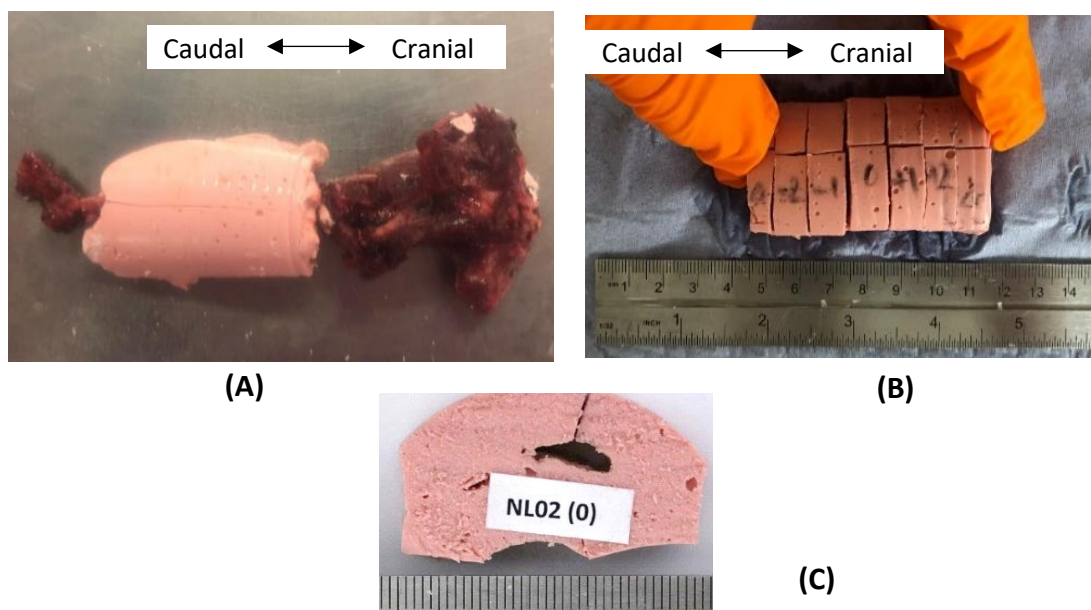
(B)

**Figure 4-7. Dissection and exposure of the Nuchal ligament (NL) for analysis. A) NL is exposed after removal of superficial Epaxial muscles (trapezius, rhomboideus, splenius, serratus dorsalis cranialis, Spinalis et semispinalis, longissimus cervicis, longissimus capitis and the cranial part of the longissimus thoracis, multifidus cervicis). B) Attachment of NL between the cervical vertebrae.**

#### 4.4.3. Measurement of Cross-Sectional Areas

Transverse cross-sections were obtained from each nuchal ligament using alginate dental impression material (UnoDent, Essex, England) as outlined by Goodship et al. (Goodship and Birch, 2005). Each ligament was placed into a plastic container and wrapped with the alginate paste, leaving the ligament origin and insertion points uncovered, allowing two minutes for the paste to set. A slit was cut with a scalpel along the mould to remove the ligament (Figure 4-8A). Each sample was then cut in transverse sections at 10mm intervals from the craniocaudal centre of the mould, thereby obtaining five different transverse sections (Figure 4-8B). Each transverse cross-section was photographed cranially (Figure 4-8C) for analysis of CSA with ImageJ (NIH, 2013). CSA's were used to calculate stress-strain curves. The five different sections per sample were labelled as follows:

- NL## +2 Most cranial section of mould paste (middle section +20 mm cranial)
- NL## +1 Middle section +10 mm cranial
- NL## 0 Middle section of mould paste
- NL## -1 Middle section +10 mm caudal
- NL## -2 Most caudal section of mould paste (middle section +20 mm caudal)



**Figure 4-8. (A) Photograph of NL embedded within alginate paste, (B) Mould transverse sections, (C) Cranial photograph of transverse cross-sectional area.**

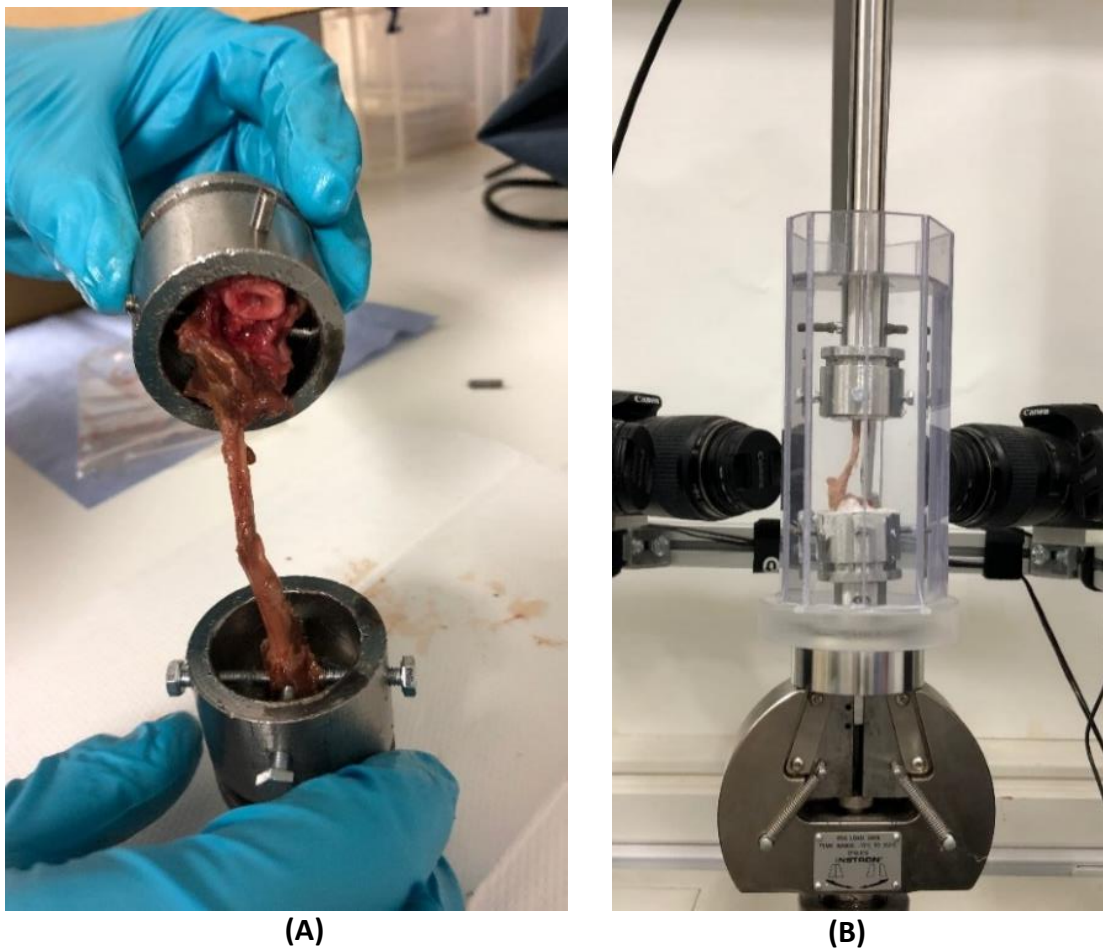
Cross-sectional areas of nuchal ligament 1, 2 and 3 are listed in table 4-3. Different material properties will be calculated from the tensile strength data and CSAs such as linear force, linear strain, linear stress and Young's modulus. These material properties will then be used for inverse dynamics and generating FEA models.

**Table 4-3. Cross-sectional areas of nuchal ligaments.**

Section	Nuchal Ligament 1 - CSA ( $mm^2$ )	Nuchal Ligament 2 - CSA ( $mm^2$ )	Nuchal Ligament 3 - CSA ( $mm^2$ )
NL (+2)	15.28	27.05	27.19
NL (+1)	22.49	20.52	27.86
NL (0)	21.49	19.03	28.03
NL (-1)	20.91	17.02	26.63
NL (-2)	19.26	15.56	26.42
Mean	19.89	19.84	27.22

#### 4.4.4. Sample Preparation

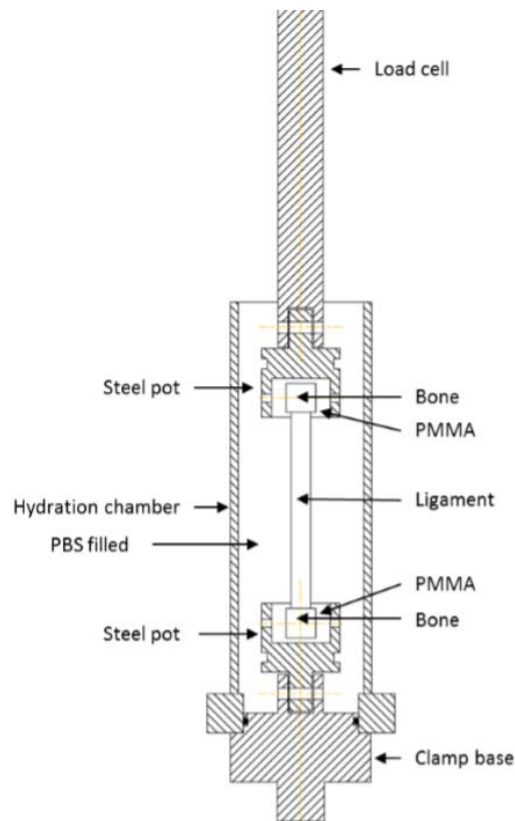
The tip of the spinous process of T1 (where the nuchal ligament originates) and the broad caudal end of the spinous process of C2 (where the nuchal ligament inserts) were cut from each sample with a saw blade in order to fit into the steel pots, leaving the nuchal ligament as a free 'string'. The bone samples were potted and secured in place with screws so that the origin and insertion points of the ligament were located at the centre of the pots, having the nuchal ligament perpendicular to the direction of tension (Figure 4-9A). The pots were then filled with polymethyl-methacrylate (PMMA) just below the ligament origin/insertion and cured for 10 minutes. The pots were put into an acrylic construct, clamped on the Instron mechanism, and filled up with phosphate-buffered saline (PBS) to keep the ligament hydrated (Figure 4-9B).



**Figure 4-9. (A) Potted C1-NL-T1 sample. (B) Rig setup for tensile testing of nuchal ligament.**

#### **4.4.5. Tensile Strength – Testing Protocol**

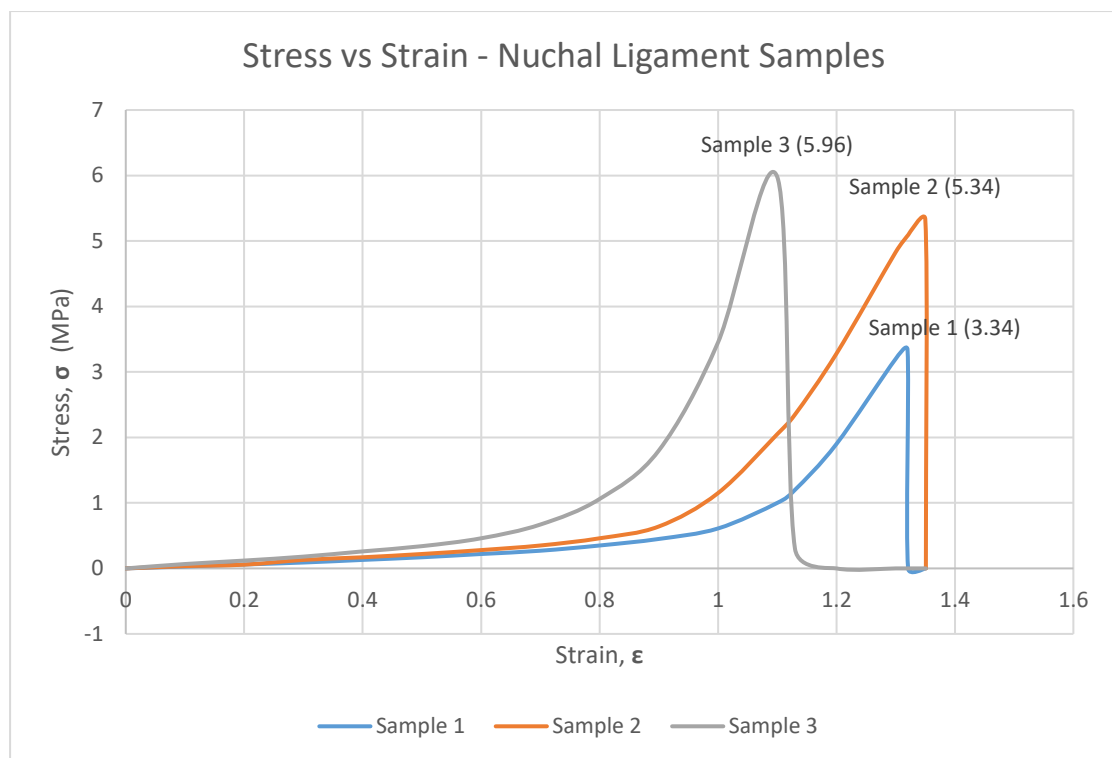
A uniaxial tensile system (Instron 3366, Buckinghamshire, UK) with 5 KN load force capacity was used. The Instron setup was similar to a previous study (Figure 4-10) (Peters et al., 2022). Each ligament was preloaded to a point where the extension/load rate curve became stable, set at 15N from the first ligament tested. Thus, each ligament was first subjected to 3 preconditioning cycles at 2.5, 3 at 25 mm/min, and 3 at 250 mm/min, all loaded from 1N to 15N. Secondly, each ligament was brought back to a 0 N relaxed position for 5 minutes before being loaded to failure at a strain rate of 250 mm/min.



**Figure 4-10. Schematic representation of the rig for the tensile testing of the nuchal ligament (Peters et al., 2022).**

#### 4.4.6. Nuchal Ligament Properties

Three ligament samples were tested. The stress-strain curves (Figure 4-11) were obtained using the linear force/displacement graphs from the Instron and the cross-sectional areas. Their tensile strength and stiffness were also calculated as in previous literature (Peters et al., 2022). A detailed listing of the nuchal ligament properties is shown in Table 4-4. This data will help to calculate the corresponding tensile strength and elastic properties of the in-silico model and generation of FEA models. The values will be used to calculate ligament properties for the musculoskeletal model.



**Figure 4-11. Stress vs Strain graph from nuchal ligaments 1, 2, and 3. A similar elasticity behaviour is noticed between samples.**

The long toe region of the curves (strain 0-1) are associated with the physiological region of the ligaments. The elastic behaviour was similar among samples, where the physiological region of the curves (long toe region). This highly extensible behaviour of the ligaments represents a large content of elastin fibres, which play an important role in the biomechanics of the ligaments (Kielty, 2006). Additionally, increasing body mass resulted in higher tensile strength.

**Table 4-4. Tensile properties of the nuchal ligaments.**

Test	Breed	Body Mass (Kg)	Ligament Length (mm)	Peak Tension Force (N)	CSA ( $mm^2$ )	Tensile Strength (MPa)
Sample 1	Hound	18	93	66.42	19.89	3.34
Sample 2	Hound	24	97	105.88	19.84	5.34
Sample 3	Hound	44	110	144.44	27.22	5.96



---

## 4.5. Generation of 3D-Reconstructed Skin-Bone Model

### 4.5.1. In-Silico Mesh Models

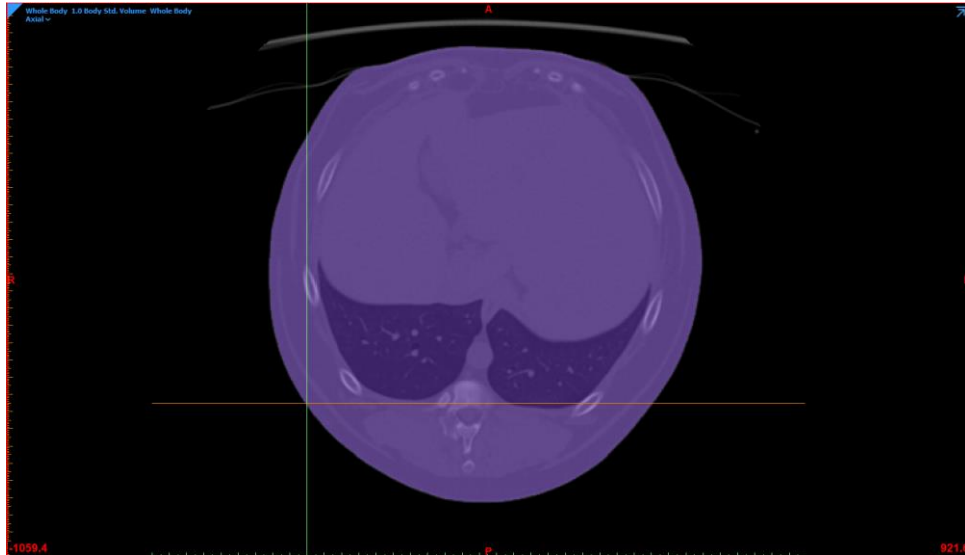
A whole-body Doberman CT scan was intended to be used as a basis for the multi-body dynamics model. However, because of the size of a Doberman breed dog, it is difficult to scan the whole body of a Doberman, along with the fact that routinely only one section of the dog's body is CT-scanned for veterinary diagnosis. Therefore, a 3D-reconstructed model was aimed to be reconstructed from as few CT scans of similar size and body weight as possible. 41 Doberman CT scans were analysed for 3D reconstruction with Mimics software, using the scans collected detailed in section 3.2 of this thesis. Three scans were selected for developing the whole-body model. Surface meshes of the skeleton and skin were generated as described below.

#### *Skeletal Mesh*

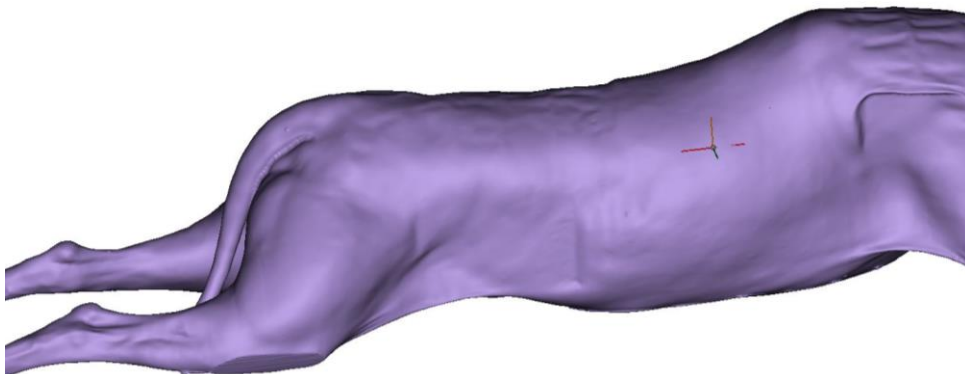
The methodology used to generate skeletal meshes for this chapter was the same as described in section 3.3.2.

#### *Skin Mesh*

The skin segments were isolated from the CT scans using Mimics software following the same methodology as the skeletal meshes. However, the skin was isolated as one single geometry per scan. The 'smart fill' tool on Mimics was used to ensure every image/layer was fully filled, as shown in Figure 4-15, to generate a fully dense skin body (Figure 4-16).



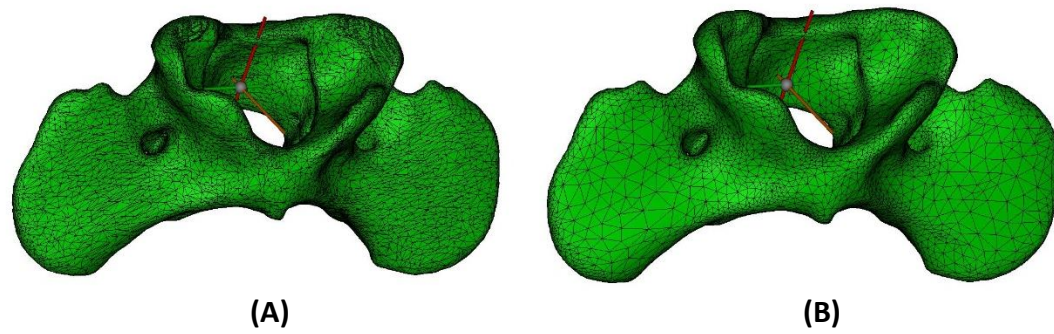
**Figure 4-15. Segmentation of skin geometries in Mimics (transverse view) for the generation of a fully dense skin body.**



**Figure 4-16. 3D mesh of a fully dense skin body.**

### *Final Meshes*

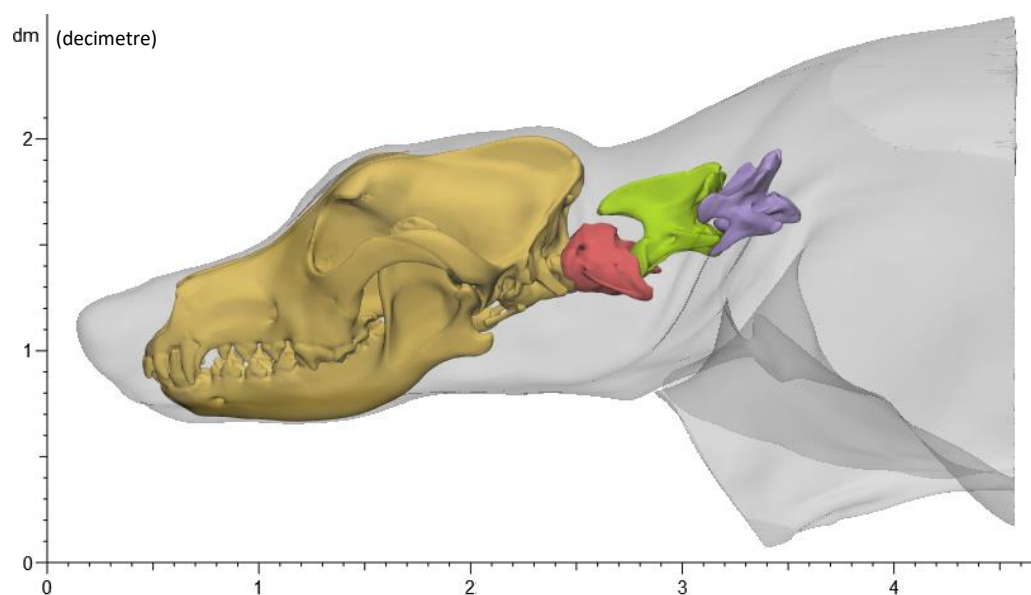
The bone and skin meshes were then smoothed and wrapped to reduce imperfections and generate better-quality meshes (Figure 4-17). The geometries were then exported to 3-matic for further processing.



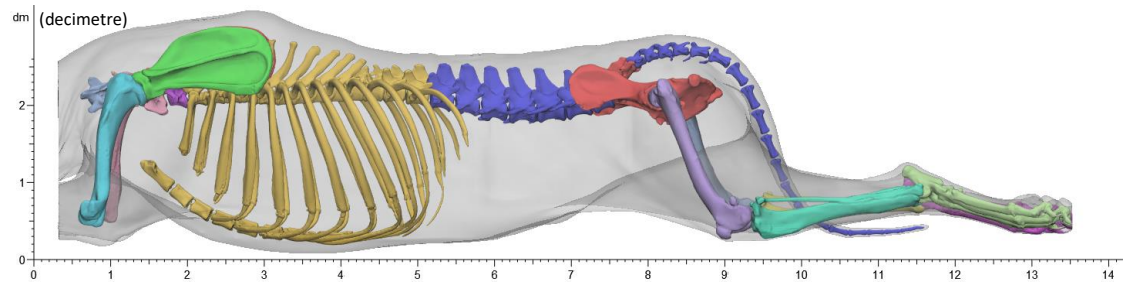
**Figure 4-17. (A) Bone mesh prior to smooth and wrap, (B) Bone mesh after smooth and wrap process.**

#### **4.5.2. Generation of 3D-Reconstructed Skin-Bone Model**

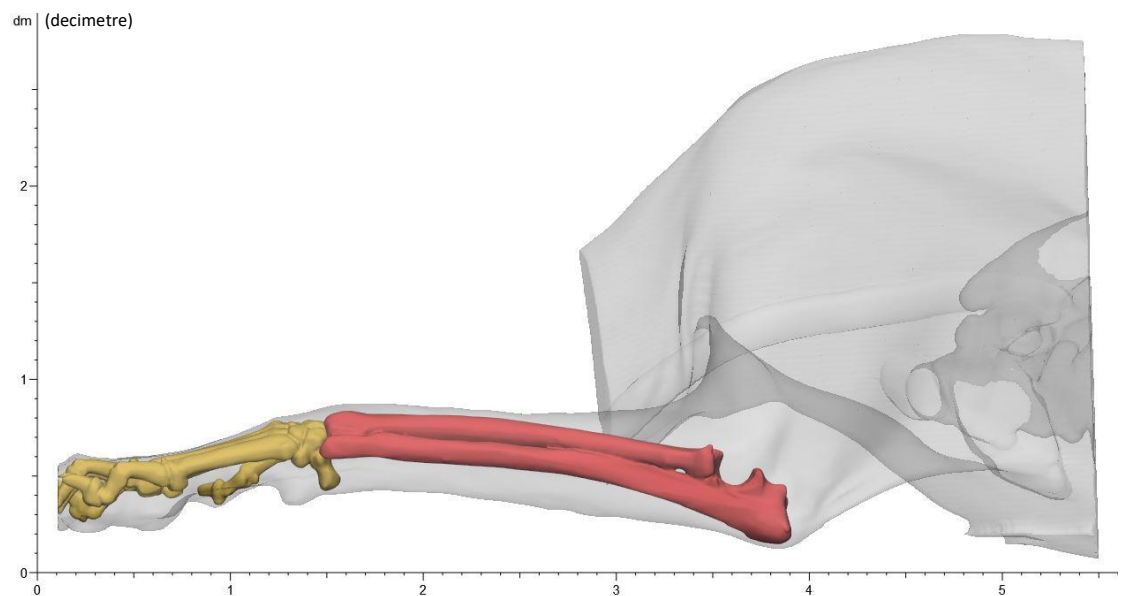
As mentioned above, bone and skin meshes from three scans were used for the generation of the 3D-reconstructed skin-bone model. 3-matic was used for developing this model, which included the segmentation of each cervical vertebra since the neck is the main section of interest for this study. The skull and cranial cervical vertebral column were taken from sample S0017 (Figure 4-18); the caudal cervical vertebral column, thorax, and hind limbs were taken from sample S0023 (Figure 4-19); and the forelimbs were taken from sample S0037 (Figure 4-20).



**Figure 4-18. Bone-skin meshes generated from S0017 (skull, vertebra C1, C2, and C3).**



**Figure 4-19. Bone-skin meshes generated from S0023 (vertebra C4, C5, C6, C7, thorax, lumbar vertebral column, pelvis, L/R humerus, L/R femur, L/R tibia, L/R foot).**



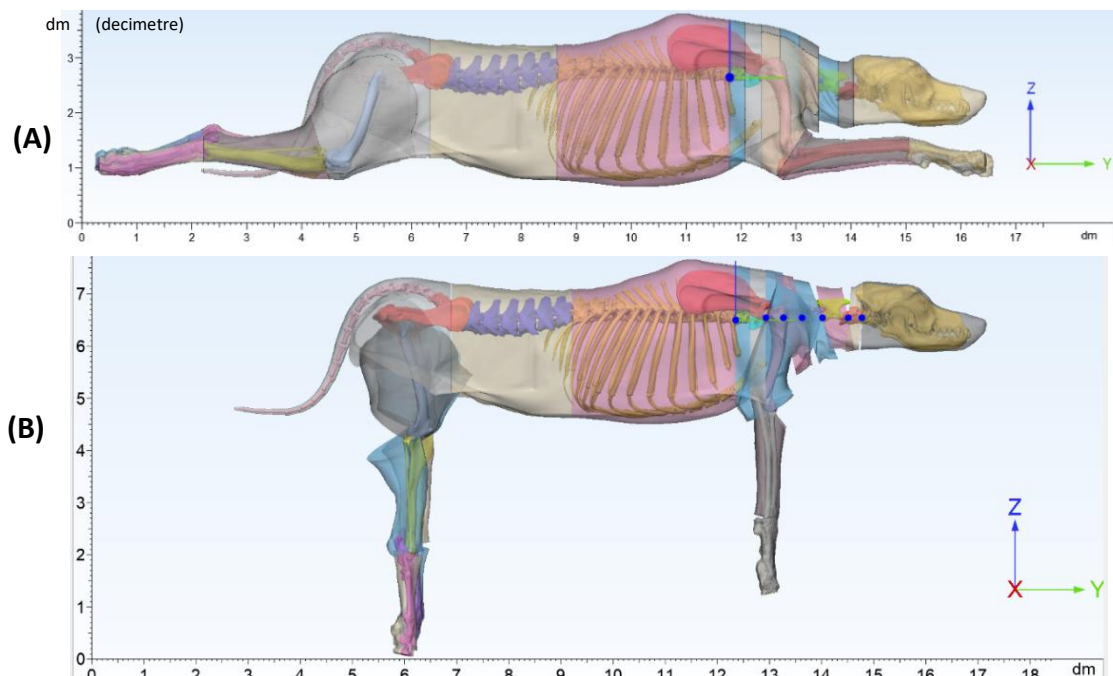
**Figure 4-20. Bone-skin meshes generated from S0037 (L/R radius-ulna, L/R paw).**

A scale factor was then used to merge the three different samples and create a uniform-size model. This scaling factor was based on humerus length since this bone was present in all three samples. S0023 was used as a reference for scaling (scale factor 1) because this scan included the majority of the body segments. Table 4-5 describes the scale factors used for each sample.

**Table 4-5. Description of samples used for the 3D-reconstructed model.**

Sample	Bone	Length (mm)	Scale Factor (based on length)
S0023	Left humerus	210.55	1.00
S0017	Left humerus	205.89	1.02
S0037	Left humerus	211.48	0.99

The 3D-reconstructed model was further sectioned into 23 functional segments: skull, C1, C2, C3, C4, C5, C6, C7, thorax, lumbar vertebral column, pelvis, L/R humerus, L/R radius-ulna, L/R paw, L/R femur, L/R tibia, and L/R foot. Figure 4-21A illustrates the final merged skeleton-skin model. This model was then realigned to a neutral position (as shown in Figure 4-21B) to serve as a basis for locating the joint centre positions (JCPs) and for defining virtual muscle-tendon units as in previous studies (Bates and Schachner, 2012, Bates et al., 2012a, Bates et al., 2012b, Maidment et al., 2014). The X, Y, and Z coordinates from the JCPs were then located and recorded to be used in the next stage of the modelling.



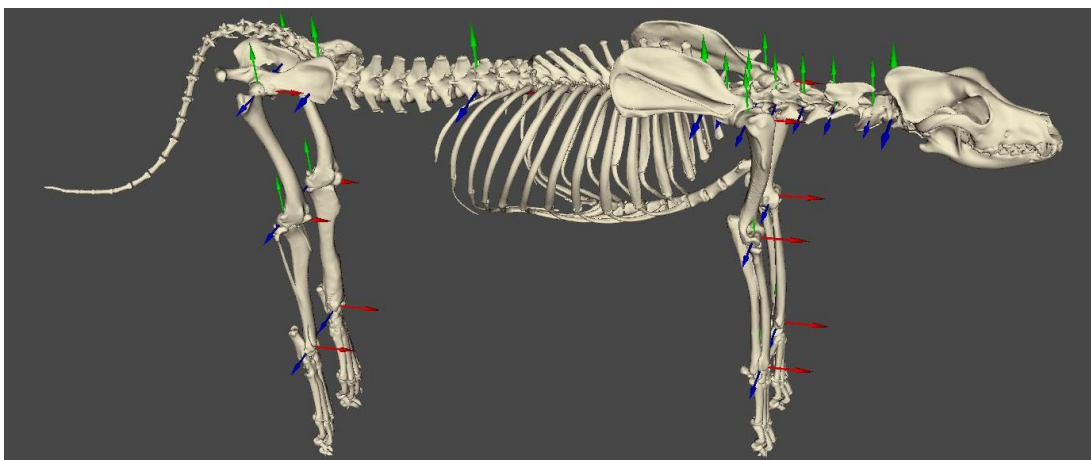
**Figure 4-21. 3D-reconstructed model from 3 different samples. (A) Skin and body segmentation, (B) Alignment.**

## 4.6. Results: Multi-Body Dynamics Model

The ultimate goal of this chapter was to generate a 3D musculoskeletal model that can be used to perform inverse kinematics and inverse dynamics by merging it with gait data obtained previously in this chapter. This model was developed based on data and files from the previous modelling stages in this chapter. The final 3D model will allow for FEA model validations, which will help understand the forces involved across the CSM-affected segments for implant testing.

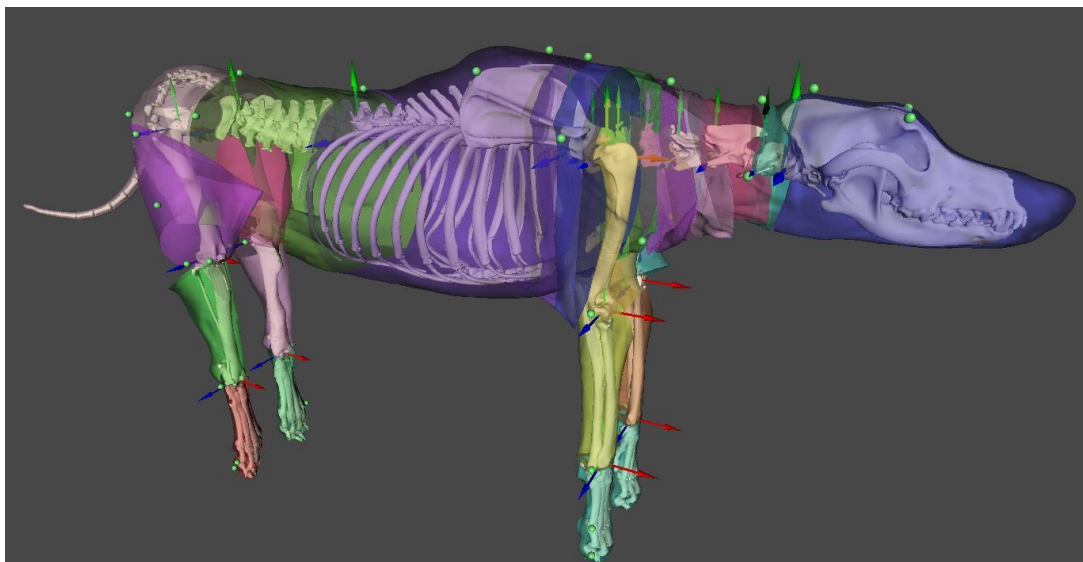
### 4.6.1. Musculoskeletal Model

The virtual representation of the muscle architecture (origin/insertion points and action paths) and their force generation properties were necessary to develop a 3D musculoskeletal model. To generate the musculoskeletal model, binary STL files were generated for each bone and skin mesh from the final 3D-reconstructed model in 3-matic. These STLs were then processed in MeshLab software (<https://www.meshlab.net/>) to reduce their file size by 70%. The size-reduced STL files were subsequently imported into nmsBuilder software (<http://www.nmsbuilder.org/>) where they were they kept their previous orientation from 3-matic. Reference coordinate systems were created for each of the functional segments based on the JCP coordinates from the 3D-reconstructed 3-matic model, as shown in Figure 4-22.



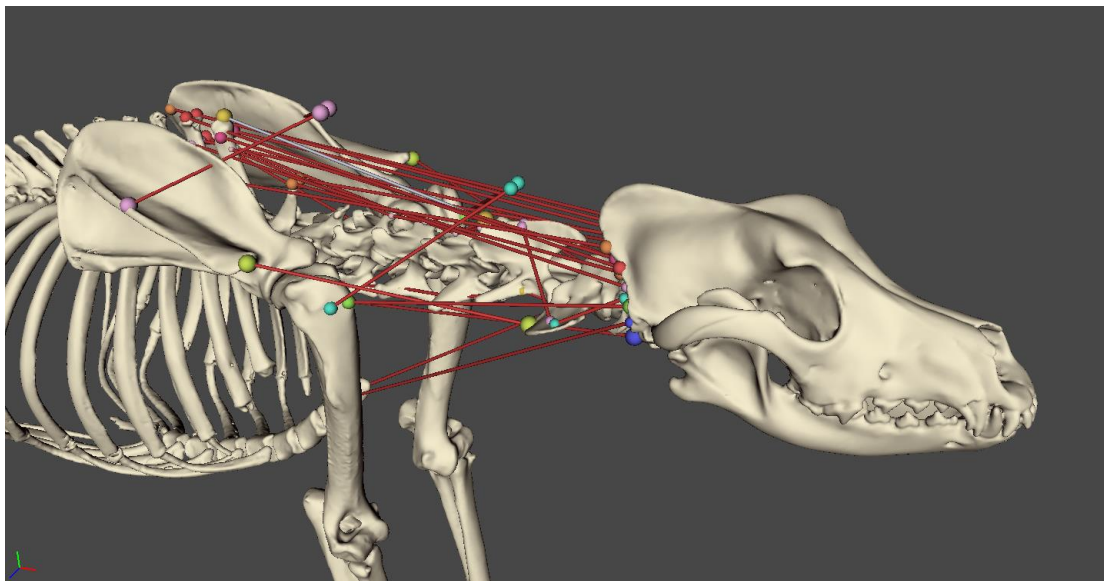
**Figure 4-22. Initial musculoskeletal model in nmsBuilder. Reference coordinate systems are set for each functional segment based on their JCP coordinates.**

Mass properties for the skin and bone meshes are calculated by the software based on the volume of the meshes and user-defined density values. A density value of  $1.06 \times 10^{-6} \text{ Kg/mm}^3$  was set for the skin meshes and  $1.9 \times 10^{-6} \text{ Kg/mm}^3$  for the bones as per literature (Cameron, 1999). All functional segments were manually configured in nmsBuilder to allow articulation of the virtual anatomical joints by linking the JCPs to their appropriate adjacent segments. 22 joints were created as follows: skull-C1, C1-C2, C2-C3, C3-C4, C4-C5, C5-C6, C6-C7, C7-thorax, thorax-lumbar, L/R shoulder, L/R elbow, L/R wrist, lumbar-pelvis, L/R hips, L/R stifles, and L/R ankle. As the main area of interest in this study is the neck, all JCPs of the cervical vertebrae and the skull were modelled as ball-socket joints with three degrees of freedom to allow for flexion/extension, lateral bending, and axial rotation. The ball-socket joint configuration was also applied to the shoulder and hip joints. A hinge joint configuration with one degree of freedom (flexion/extension) was set for the rest of the JCPs. Only the thoracic-lumbar vertebral column joint was 'locked' to restrict its articulation and, therefore, to assume minimal motion and focus on the relevant study joints. Additionally, the reflective marker positions were located on the model to match the reflective markers from the gait specimen (Figure 4-23) and allow inverse kinematics.



**Figure 4-23.** nmsBuilder model featuring bone-skin geometries and joint centres.

All 16 neck muscles that were dissected in section 4-3 were then virtually created on the bone meshes by locating their origin/insertion points following their anatomical paths. Following well-documented guidance, these muscle attachments and paths were defined (Evans and DeLahunta, 2017). A musculo-tendon unit was created on the nmsBuilder model for each muscle (Figure 4-24) as follows: splenius, semispinalis capitis (biventer cervicis), semispinalis capitis (complexus), longissimus capitis, serratus ventralis cervicis, longus capitis, omotransversarius, obliquus capitis cranialis, obliquus capitis caudalis, spinalis et semispinalis cervicis, trapezius, brachiocephalicus (cleidomastoideus), brachiocephalicus (cleidocervicalis), rhomboideus capitis, sternocephalicus, and longus colli. Likewise, the nuchal ligament was then created by locating its origin and insertion points. However, its biomechanical properties were modelled as in a previous study using resting length, stiffness, and tensile strength (Stanev et al., 2016, Charles et al., 2021). These values were calculated from the ex-vivo nuchal ligament data (section 4.4.6).



**Figure 4-24. Neck muscle attachments on nmsBuilder model.**

The muscle model approach used by nmsBuilder for musculo-tendon units is a generic Hill-type. This model requires four configuration values: optimal fibre length, tendon slack length, pennation angle, and maximum isometric force. As mentioned previously, the aim was to develop the musculoskeletal model to perform inverse



kinematics and dynamics of the gait data; in this case, the gait specimen and appropriate gait cycle identified for this purpose in section 4.2.4. Therefore, the muscle property inputs in the model need to be calculated to represent the corresponding gait specimen muscle properties. These muscle property calculations needed for the musculoskeletal model have been previously described (Allen et al., 2010, Dries et al., 2016), and were calculated from data from the 3D-reconstructed CT Specimen (CTS) (section 4.5.2 of this thesis), Cadaveric Specimen (CS) from neck dissection (section 4.3.2 of this thesis), and the Gait Specimen (GS) from which the appropriate gait cycle was identified (section 4.2.4 of this thesis) data as below:

- Fibre length: GS value calculated proportionally from CS data.

$$Fibre\ Length_{GS} = \frac{(Fibre\ Length_{CS})(Body\ Mass_{GS})^{0.33}}{(Body\ Mass_{CS})^{0.33}} \quad (Eq.1)$$

- Tendon length: GS value calculated proportionally from CS data.

$$Tendon\ Length_{GS} = \frac{(Tendon\ Length_{CS})(Body\ Mass_{GS})^{0.33}}{(Body\ Mass_{CS})^{0.33}} \quad (Eq.2)$$

- Pennation angle: CS values.
- Max isometric force: GS value calculated proportionally from CS data (Eq. 7) as below.

$$Fmax_{GS} = PCSA_{GS} \cdot \sigma_{max} \quad (Eq.3)$$

where:

$$PCSA_{GS} = \left( \frac{V_{muscle_{GS}}}{Fibre\ Length_{GS}} \right) \cos(Pennation\ Angle_{GS}) \quad (Eq.4)$$

and

$$\sigma_{max} \approx 300kNm^{-2}$$

assuming Pennation Angle GS = Pennation Angle CS,

$$\therefore Fmax_{GS} = \left( \frac{V_{muscle_{GS}}}{Fibre Length_{GS}} \right) \cos(Pennation Angle_{CS}) \cdot 300kNm^{-2} \quad (Eq.5)$$

where

$$V_{muscle_{GS}} = \frac{Body Mass_{GS} \cdot \frac{Muscle Mass_{CS}}{Body Mass_{CS}}}{1060 Kgm^{-3}} \quad (Eq.6)$$

Substituting Eq. 6 in Eq. 5,

$$Fmax_{GS} = \left( \frac{\frac{Body Mass_{GS} \cdot \frac{Muscle Mass_{CS}}{Body Mass_{CS}}}{1060 Kgm^{-3}}}{Fibre Length_{GS}} \right) \cos(Pennation Angle_{CS}) \cdot 300kNm^{-2} \quad (Eq.7)$$

For muscles with minimal or no visible tendon slack, where a scaling approach is not possible, a relatively small value was considered for the model, as previously described in a similar study (O'Neill et al., 2013b). The complete list of calculated muscle properties is shown in Table 4-6.

**Table 4-6. Muscle properties calculated for gait specimen.**

Muscle	Fibre Length GS (mm)	Tendon Slack Length GS (mm)	Pennation Angle CS ( $\alpha$ )	Maximal Isometric Force (N)
Splenius	0.2348	0.0000	0.00	144.7251
Semispinalis capitis: Biventer cervicis	0.0660	0.0000	3.33	392.0583
Semispinalis capitis: Complexus	0.1224	0.0456	3.33	117.1443
Longissimus capitis	0.0957	0.0000	1.67	219.7012
Serratus ventralis cervicis	0.1310	0.0000	3.33	351.5818
Longus capitis	0.0902	0.0000	6.67	116.6211
Omotransversarius	0.3003	0.0000	0.00	54.07306
Obliquus capitis cranialis	0.0645	0.0000	3.33	214.6813
Obliquus capitis caudalis	0.0989	0.0000	0.00	66.35141
Spinalis et semispinalis cervicis	0.1369	0.0000	6.67	209.4442
Trapezius	0.1434	0.0000	0.00	74.26557
Brachiocephalicus: Cleidomastoideus	0.3115	0.0000	1.67	55.57147
Brachiocephalicus: Cleidocervicalis	0.2707	0.0399	0.00	93.57441
Rhomboideus capitis	0.0952	0.0000	1.67	96.01846
Sternocephalicus	0.2781	0.0000	0.00	502.7721
Longus Colli	0.1495	0.0152	5.00	96.71702

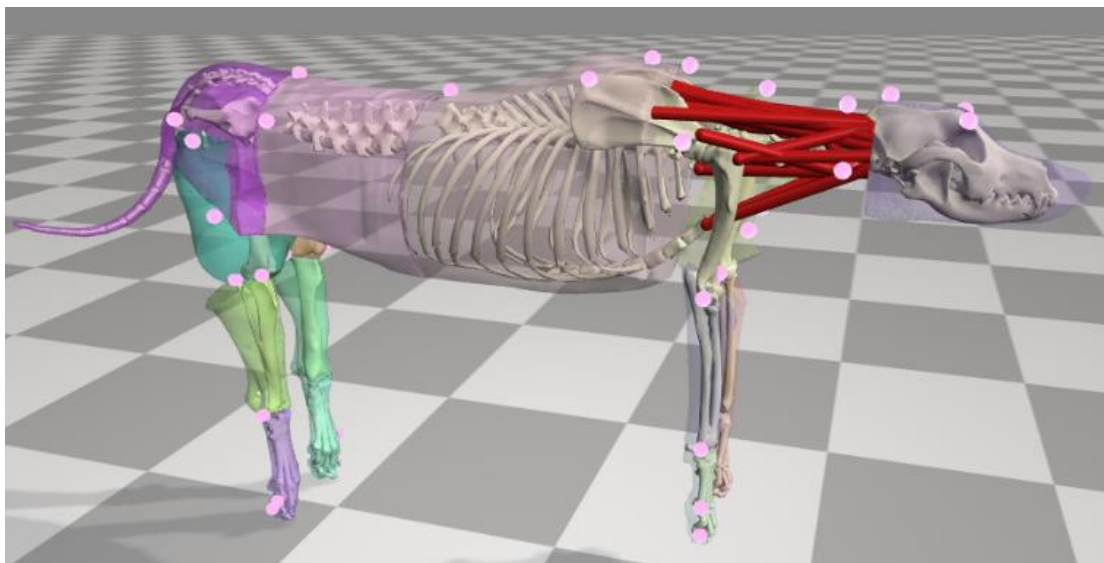
Once the muscle properties were input into the nmsBuilder model, an OpenSim model was generated and exported as a .osim file for further processing.

#### 4.6.2. OpenSim model

The .c3d file from the gait cycle previously identified for musculoskeletal modelling (section 4.2.4) was imported into Mokka software (<https://biomechanical-toolkit.github.io/mokka/>) for identification of strike events (e.g. paw/foot on and off striking the force plate events), and updated with this event configuration. Subsequently, the freely available Matlab code 'Modified-Gait-Extraction-Toolbox

([https://simtk.org/home/c3d2opensim\\_btk/](https://simtk.org/home/c3d2opensim_btk/)) was used to extract the (1) .trc file (kinematics data) needed for inverse kinematics, and (2) the .mot file (kinetics data) needed for inverse dynamics as per OpenSim guidelines (<https://simtk.org/projects/opensim/>). These .trc and .mot files are used later in the modelling process.

The .osim file exported previously from nmsBuilde was then imported into OpenSim (<https://simtk.org/projects/opensim/>). The OpenSim model was then scaled to match the size of the GS based on body weight using the built-in scale tool. The virtually-calculated body weight of the CTS was 35.35 Kg, and the weight of the GS subject 1 was 30.4 Kg. Based on the correlation of CTS-GS body proportions, a scale factor of 0.86 was used to scale down the model. Muscle properties are not scaled with this tool. Therefore, the previously calculated GS muscle properties remained the same. The scaled model is shown in Figure 4-25.



**Figure 4-25. Opensim model featuring articulated bone-skin segments, reflective marker positions, and muscle architecture of the neck.**

### 4.6.3. Inverse Kinematics

The scaled OpenSim model was then prepared for inverse kinematics. The built-in inverse kinematics tool was used to load the .trc file previously generated. This tool animates the kinematics data by matching the OpenSim reflective markers with the .trc reflective marker data (Figure 4-26) to guide the inverse dynamics process described in the next section.

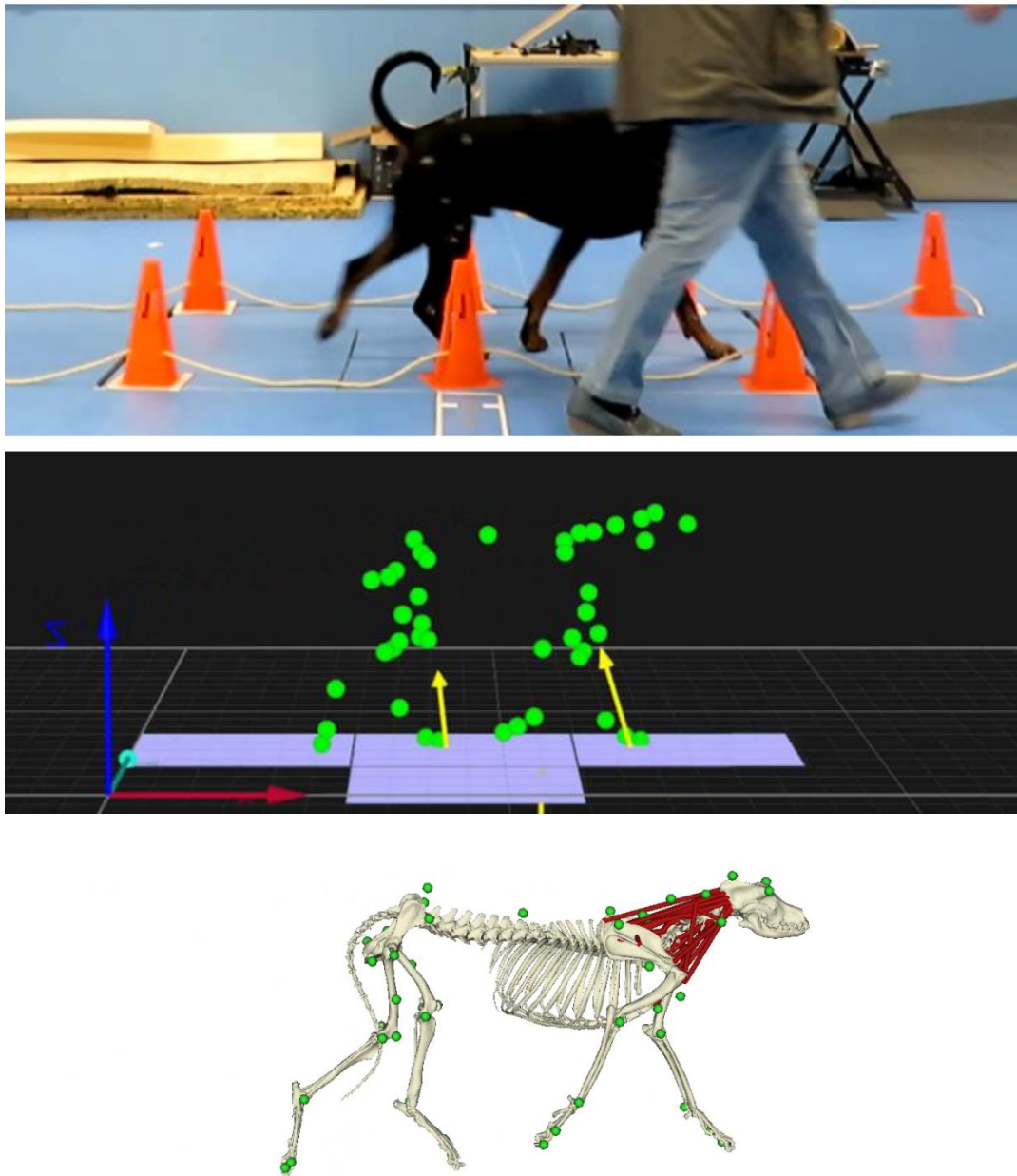
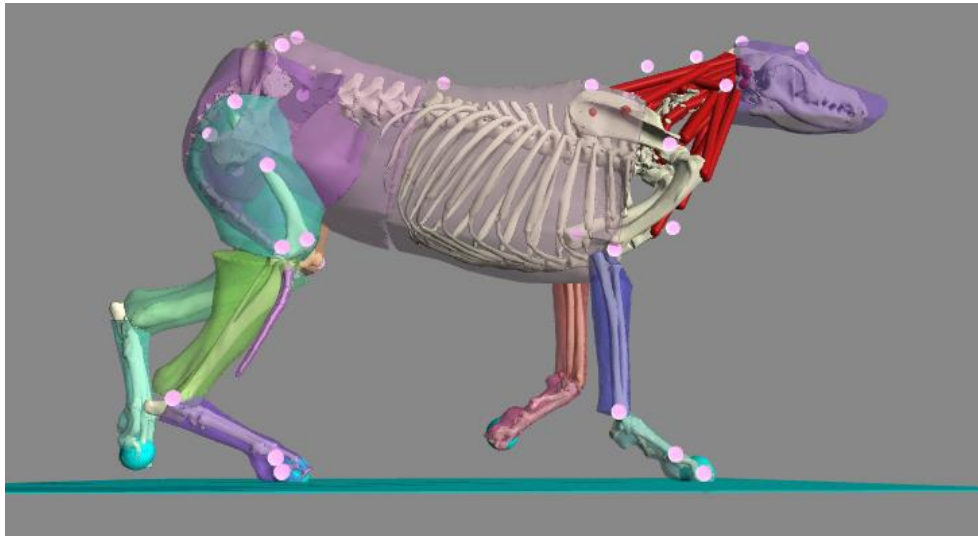


Figure 4-26. Single frame from Inverse Kinematics. (A) GS at gait lab, (B) Qualisys Track manager data, (C) Inverse kinematics representation of OpenSim model.

#### 4.6.4. Inverse Dynamics

The scaled OpenSim model was then prepared for inverse dynamics. The Ground-contact geometries need to be incorporated into the OpenSim file in order to perform inverse dynamics. Hence, spherical geometries (Figure 4-27) were added to the model by editing the .osim code.

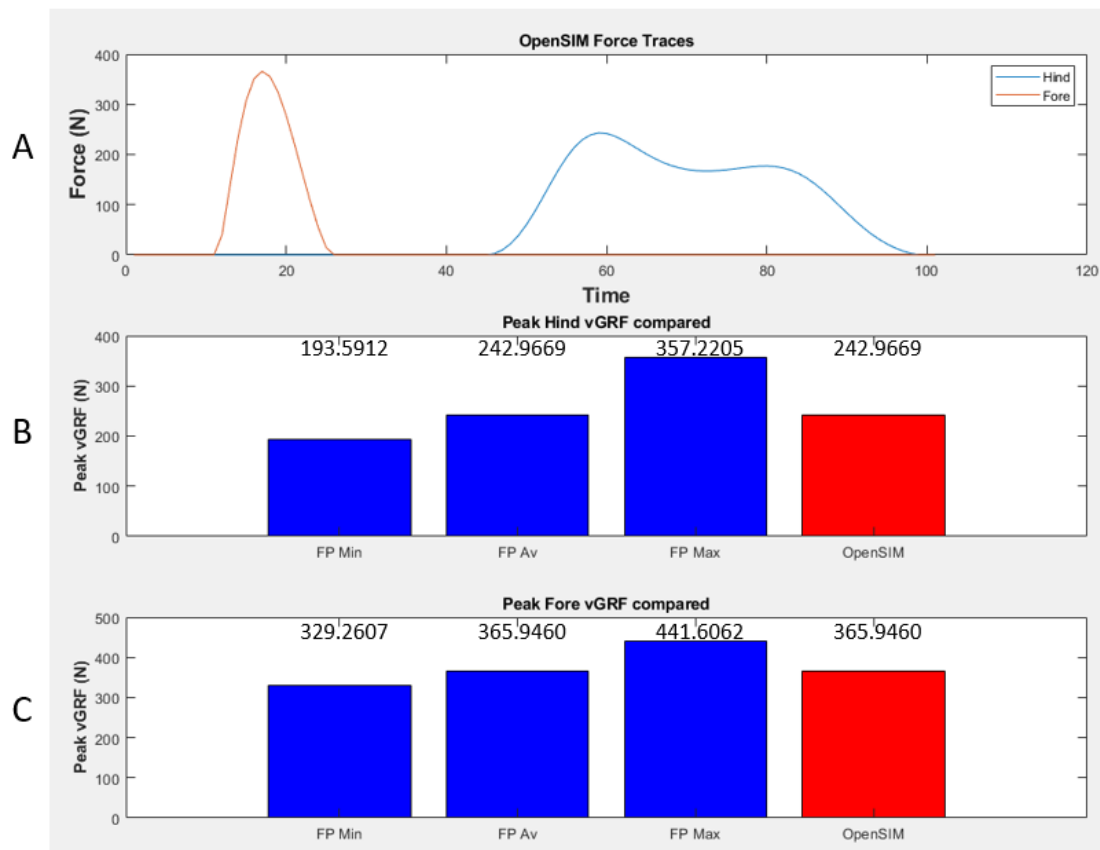


**Figure 4-27. OpenSim model animated with inverse kinematics. The contact spheres were generated at the paws and feet.**

The built-in inverse dynamics tool was then used to load the .mot file previously generated. This tool generates output files containing net forces and muscle moment arms. Once the inverse dynamics was performed, the normalised fibre length value of each muscle was verified and adjusted to lie between 0.5-1.5 (Appendix F) in order to ensure the muscles act on the appropriate section of their force-length curve over the entire gait cycle (Hicks et al., 2015).

The inverse dynamics aim to simulate the muscle forces and moments based on the kinematics data and inertial body properties (driven by the muscle properties). In order to achieve this, once the normalised fibre length values were adjusted, the .osim code was further edited by modifying the stiffness and dissipation values of the contact geometries to match the simulated output force values (OpenSim) with the

average experimental GRF values from the .mot file. The minimum (FP min), maximum (FP Max), and average (FP Av) forelimb and hindlimb experimental GRF values obtained by the force plates were calculated from the ‘clean strike’ data obtained in section 4.2.4 of this thesis. The OpenSim GRF values were then matched to the forelimb (365.94 N) and hindlimb (242.96 N) FP Av GRF values (Figure 4-28).



**Figure 4-28. Simulations of ground reaction forces. (A) An example of fore and hindlimb simulated force traces generated by the OpenSim model with inverse dynamics. (B) The OpenSim hindlimb GRF value (red bar) matched to the hindlimb FP Av GRF value (middle blue bar) of 365.94 N, (C) The OpenSim forelimb GRF value (red bar) matched to the forelimb FP Av GRF value (middle blue bar) of 242.96 N.**

Once the multi-body dynamics model matched the experimental gait data, it can be interpreted that this model replicates the experimental kinematics and kinetics, driven by the in-silico muscle and bone-skin inertia properties. Therefore, it provides estimated muscle forces and moments for implant testing.

#### 4.6.5. Summary

All findings in this chapter are summarised as follows:

- Non-invasive Gait Analysis of Neck Movements in a Normal Dog. Kinematics and kinetic data sets were gathered for gait analysis. A gait cycle was identified with ‘full’ tracking of all reflective markers and ‘clean strikes’ for musculoskeletal modelling.
- Analysis of Muscle Architecture: Neck Dissection. The muscle architecture necessary for the model was obtained. A total of 16 neck muscles were analysed.
- Ex-vivo Nuchal Ligament Test– Tensile Strength. The tensile testing provided meaningful data for developing this musculoskeletal model and other applications where tensile ligament properties are needed. Before this study, no factual information was available about the mechanical properties of the canine nuchal ligament.
- Multi-body Dynamics Model. The final multi-body dynamics model can be used to generate the basic scientific data required to optimise the development of breed-specific spinal implants for breed dogs at high risk of CSM. This model resulted in a large breed dog model, as opposed to the initial intended Doberman-specific model as described in chapter 1.



## 5. Pilot Clinical Study

### 5.1. Introduction

As described in Chapter 3, for a stabilisation system to be clinically released, it is necessary to carry out a pilot study. After proving implant stability by developing patient-specific implants and testing them using the in-silico model previously described in Chapter 4, the aim was to assess implant performance in surgical cases. Due to time constraints with live surgical cases and manufacturing turnaround times, the pilot study only included the use of the interbody spacers.

The study design presented in this chapter is a retrospective clinical study, which was carried out with the collaboration of veterinary specialists and neurosurgeons: Colin Driver, Jeremy Rose, Rory Fentem, and Andrew Tomlinson. They managed and operated the clinical cases, and helped collecting and interpreting clinical data. The objective of this pilot study was to report the medium and long-term outcome of nine dogs with disk-associated cervical spondylomyelopathy (DA-CSM), treated by instrumented interbody fusion using patient-specific end-plate conforming device that were developed following the guidelines of this thesis. The animal study was reviewed and approved by CVS Group Internal Ethical review committee. Written informed consent was obtained from the owners for the participation of their animals in this study.

---

## 5.2. Materials and Methods

### 5.2.1. Animals

The medical records of two institutions were retrospectively reviewed between January 2020 and 2023, for dogs with clinical signs and MRI findings compatible with DA-CSM, that were treated by vertebral distraction-fusion using patient-specific interbody devices. Ethical approval for the study was obtained from the main institution's internal review committee (CVS-2022-010). Data retrieved included patient signalment, clinical signs, diagnostic work-up, surgical technique and outcomes.

Neurologic examinations were scored according to the Texas Spinal Cord Injury Score (TSCIS) (Levine et al., 2009). Assessments and scoring were conducted by a board-certified neurologist or surgeon pre-operatively, post-operatively prior to discharge and at medium-term (a minimum of 2 months) follow-up. Long-term follow-up, defined as a minimum period of 9 months post-operative (Reints Bok et al., 2019), was retrospectively determined from physical examination, video analysis or pet owner telephone interview. Long-term outcome was categorised as deteriorated, stable, or improved.

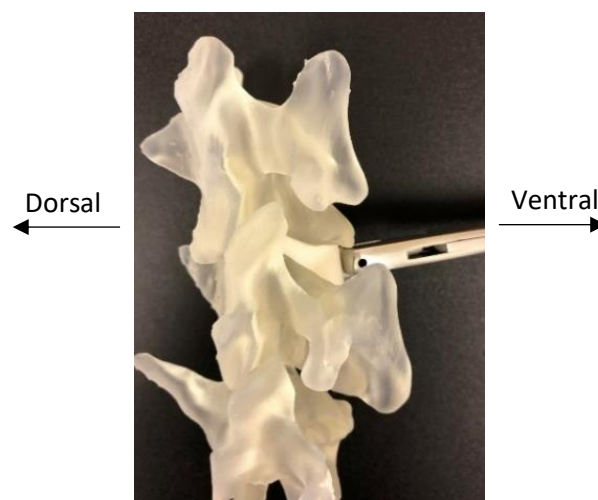
### 5.2.2. Pre-Operative Imaging

The definitive diagnosis of DA-CSM was confirmed in all cases by high-field MRI (Philips Ingenia CV, 1.5 T, or Siemens Magnetom Essenza, 1.5 T) according to published criteria (da Costa, 2010, Lewis, 1989a, Fingerroth, 2015). Kinematic and distraction imaging was not performed in the study subjects. Immediately after disease confirmation, patients were transferred to CT (Toshiba Aquilion Prime, 80 slice, or Siemens Somatom Scope, 16 slice) and were positioned in dorsal recumbency within a trough, and with the cervical spine extended such that the angle of the mandible to the sternum was an angle approximately 30° to horizontal. This position was checked by the primary surgeon and documented using digital photography for later surgical

reference. CT scans were obtained in a bone algorithm with 3D reconstruction for *in-silico* planning.

### 5.2.3. Device Design and Manufacture

Interbody devices were designed and manufactured following the guidelines described previously in this thesis. The devices were designed to measure 50% of the lateral width of the vertebral end-plate and 80% of the end-plate ventrodorsal height; these dimensions represented a compromise between end-plate coverage and ease of surgical implantation. Additionally, the devices were designed with a +10% distraction level; this marginal degree of distraction from averaged non-affected disk spaces was intended to facilitate both ease of surgical implantation and an increased post-operative distraction index. Where applicable, 3D-printed vertebral models (Figure 5-1) and surgical drill guides were designed and printed in polymer photocurable resin using stereolithography (Form 2, Formlabs; Somerville, United States) similar to methods described elsewhere (Elford et al., 2019). The aim of the vertebral models was to facilitate surgical rehearsal and plate pre-contouring to minimise surgery time.



**Figure 5-1. 3D-printed bone and spacer models, B) CpTi spacer filled with bone graft, C) Spacers implanted, D) Ventral locking plates completed the fixation.**

---

#### 5.2.4. Surgical Procedure

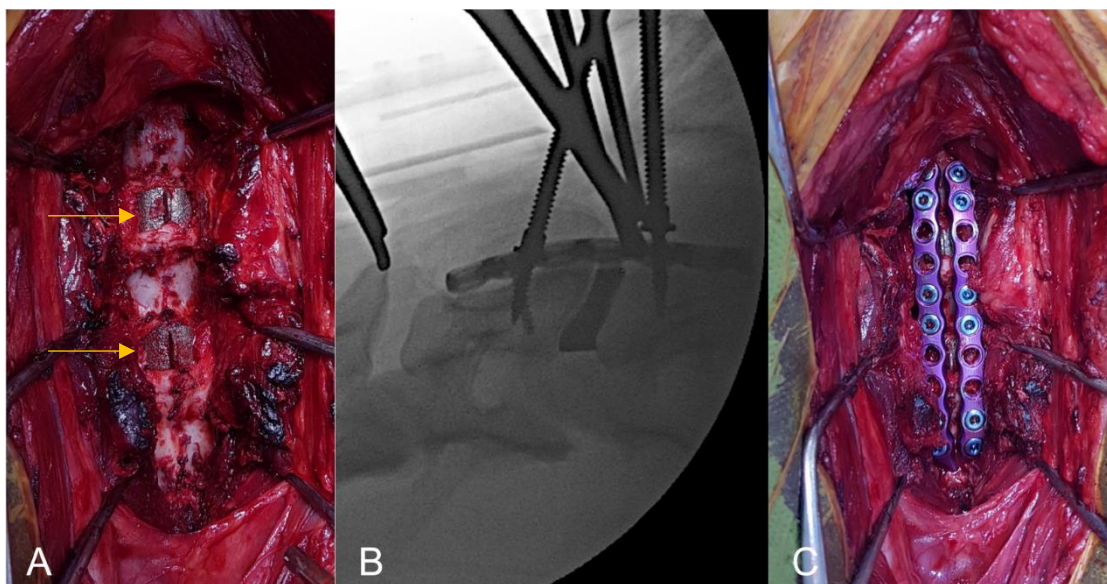
Dogs were premedicated with 0.2–0.3 mg/kg intravenous or intramuscular methadone (Comfortan® 10 mg/mL, solution for injection for Dogs and Cats, Eurovet Animal Health B.V). General anaesthesia was induced with propofol (Lipuro-Vet® 10 mg/mL solution for injection, Zoetis United Kingdom Ltd., UK) 4–6 mg/kg to effect and maintained with isoflurane (Iso-Vet® 1,000 mg/g inhalation vapor, Chanelle Pharma, Ireland). Analgesia was provided with continuous infusions of Ketamine (Narketan® 100 mg/mL solution for injection, Vetoquinol UK Ltd., United Kingdom) and Fentanyl (Fentadon® 50mcg/ml solution for injection, Dechra, UK). Cefuroxime (Zinacef GSK® Glaxo Operations UK Ltd., United Kingdom) was administered every 90 min during the procedure.

Dogs were positioned in dorsal recumbency in a position as close to pre-operative imaging as possible. A standard ventral approach to the caudal cervical vertebra for exposure of the affected disk(s) and adjacent vertebral bodies was made. Sub-total discectomy was performed, preserving fibres of the dorsal and lateral annulus fibrosus. A self-retaining Caspar vertebral distractor (Aesculap, B Braun, Germany) was used to facilitate completion of the discectomy and for gentle curettage of the cartilaginous endplates. In one case, a ventral slot of the adjacent end-plates was completed to penetrate the vertebral canal and remove compressive elements of the annulus fibrosus. The interbody device was test-fitted into the disk space and manipulated using needle holders prior to release of the distractors. Intra-operative fluoroscopy was used to confirm adequate insertion depth and end-plate conformation (Figure 5-2). Prior to insertion, the spacer was packed with cancellous autograft that was harvested from one (single segment fusion) or both (dual segment fusion) proximal humeri. Mono- or bi-cortical secondary spinal stabilisation was then performed using a method according to the preference of the surgeon using pre-operative in-silico planning, with or without the assistance of patient-specific 3D printed drill guides in the case of bi- and mono-cortical systems, respectively. Where

possible these implants were also surrounded by cancellous autograft prior to routine closure.

Post-operative care included continuation of analgesic infusions for 24 h then intravenous or intramuscular methadone according to pain scores. Oral caprofen 2 mg/kg twice daily (Carprieve<sup>®</sup>, Norbrook, Ireland) or meloxicam 0.1 mg/kg once daily (Loxicom<sup>®</sup>, Norbrook, Ireland), paracetamol 10–15 mg/kg twice daily and gabapentin 10 mg/kg three times daily (Gabapentin Noumed<sup>®</sup>, Noumed, Life sciences Ltd., United Kingdom) was also administered. Antibiotics were not continued post-operatively.

Post-operative recommendations included 3 weeks of strict rest with slowly increasing duration of controlled lead walks over the following six to 9 weeks according to the dog's ability.



**Figure 5-2.** Surgical technique, ventral view of cervical spine. (A) Intervertebral spacers can be seen *in situ* (arrowed). (B) Intra-operative fluoroscopic image demonstrating adequate positioning of interbody spacer. (C) Pre-contoured paired ventral locking plates applied to vertebrae with mono-cortical locking screws.

---

### 5.2.5. Post-Operative Imaging

CT was performed immediately post-operative and at least at medium-term follow-up, with the patient positioned as per pre-operative scans. Scans were exported and multi-planar reconstructions were reviewed using open-source DICOM (digital imaging and communications in medicine) viewing software Osirix (Pixmeo, 2010) for implant stability, vertebral interbody fusion, distraction, and subsidence.

Interbody fusion was assessed in sagittally reconstructed images, aligned along the long axis of the vertebral body and interbody spacer. An ovoid region of interest (ROI) of approximately 5mm<sup>2</sup> was created within the centre of the interbody device and fusion was considered successful when the mean Hounsfield units (HU) for endoprosthetic bone density was between 266 and 1988.

Vertebral distraction and subsidence were determined using a measurement of the distance between the cranial and caudal vertebral end-plates of the segment (McAfee et al., 2001), and a distraction index %, the method for which has previously been described utilizing the vertebral end-plates on lateral radiographs (Solano et al., 2015) and adapted here with determination of measurements taken from sagittally reconstructed CT scans. The index provides an assessment of end-plate measurements relative to individual vertebral morphometry. The end-plate measurements were calculated pre- and post-operative, then at medium-term follow-up; the indices were calculated immediately post-operative and then at medium-term follow-up. Subsidence was defined by a negative distraction index at medium-term follow-up.

Minor complications were classified as those requiring no further surgical intervention, major complications were classified by those that did. These were described and tabulated.

Where a third or fourth CT scan was performed at a minimum of 6 months follow-up, an assessment for adjacent segment pathology (ASP) was also made. ASP was defined

---

by clear intervertebral disk space narrowing, significant vertebral end-plate changes and/or the development of spondylosis deformans, that did not cause clinical signs; adjacent segment disease (ASD) was recorded as those that did cause clinical signs (Steffen et al., 2011, Reints Bok et al., 2019).

### **5.2.6. Statistical Analysis**

Continuous data sets were assessed for normality graphically and using Shapiro–Wilk tests. Mean and standard deviation (SD) were reported for normally distributed data. Categorical data are described showing the count and percentage. Paired t-tests were used to compare measurements on the same segment at two-time points. Independent t-tests were undertaken to compare mean measurements and indices across two groups. The association between two independent measurements, the variation in TSCIS and the follow up distraction index, were assessed using Pearson’s correlation coefficient (*r*).

## **5.3. Results**

### **5.3.1. Demographics and Diagnosis**

Nine medium and large breed dogs were included in this study, with mean age of  $83.7 \pm 19.8$  months and weight of  $42.7 \pm 9.5$  kg (Table 5-1). Breeds represented included three Doberman pinchers, two Great Danes, two Bernese mountain dogs, one Labrador Retriever and one border collie. There were 5 (55.6%) males and 4 (44.4%) females. All dogs were treated with analgesic medications and rest for a median period of 4 weeks (range 3–12) before non-surgical management was considered to have failed due to progression of clinical signs. All dogs were ambulatory at presentation, with typical clinical signs for DA-CSM including mild to moderate tetraparesis and generalised proprioceptive ataxia. The mean pre-operative TSCIS was  $34.6 \pm 1.98$ . All cases were diagnosed on MRI by the demonstration of focal intra-parenchymal spinal cord lesions in the C5-C7 region at the level of extra-dural cord compression and concurrent degenerative changes in the intervertebral disk, articular

facet joint and interarcuate ligaments. Five dogs were diagnosed with DA-CSM at one segment (C6-C7 in four cases, C5-6 in one) and four dogs were diagnosed with DA-CSM at two segments (C5-C6 and C6-C7), totalling 13 operated segments.

**Table 5-1. Signalment, diagnosis and neurologic scores (FN, Female Neutered; TSCIS, Texas Spinal Cord Injury Score, ME, male entire; MN, male neutered).**

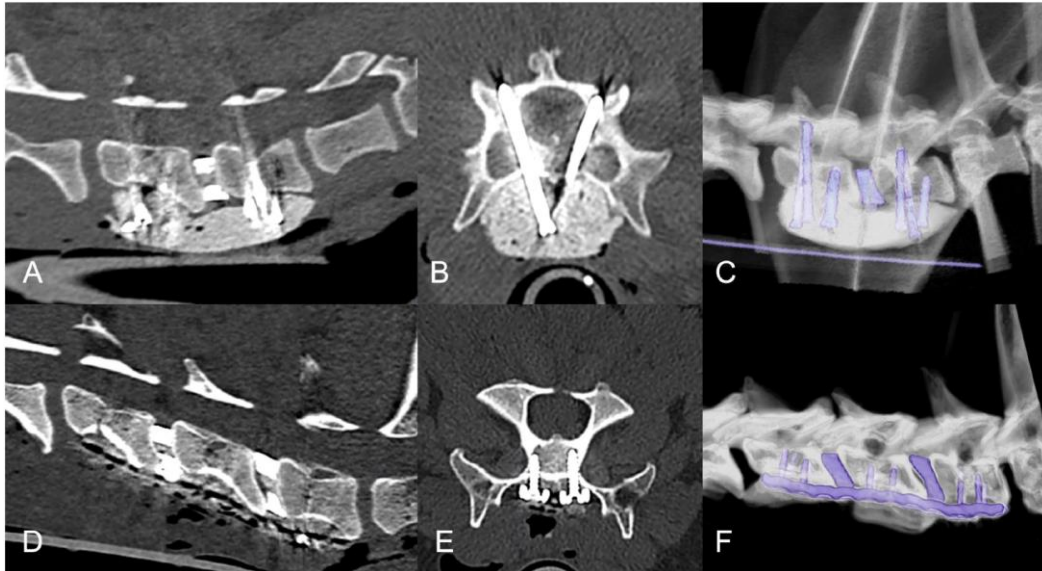
Case	Breed	Age, m	Sex	Weight (Kg)	Affected level(s)	TSCIS	
						Pre-operative	Medium-term follow-up
1	Border Collie	104	MN	28.4	C6-C7	34	35
2	Doberman	123	FN	34.4	C5-C6, C6-C7	36	36
3	Labrador Retriever	108	MN	42.0	C6-C7	32	34
4	Great Dane	72	FN	38.5	C5-C6, C6-C7	32	35
5	Great Dane	70	FN	57.6	C6-C7	33	37
6	Doberman	72	MN	41.6	C5-C6, C6-C7	37	40
7	Bernese mountain Dog	60	MN	56.9	C5-C6	36	32
8	Doberman	84	ME	41.7	C5-C6, C6-C7	36	40
9	Bernese mountain dog	80	FN	52.9	C6-C7	33	40

### 5.3.2. Surgery

All 13 interbody devices were inserted as planned (Figure 5-3). As previously described, one dog had a small ventral slot procedure contemporaneous with the implantation of the interbody device. The supporting stabilisation system utilised bi-cortical implants at 7 segments (in 5 cases); 5 segments (4 cases) with paired 2.7 or 3.5 mm bi-cortical locking screws with a single mono-cortical screw (DuPuy Synthes, Johnson and Johnson, United States) per vertebra which were enshrouded in a sculpted bolus of gentamicin-impregnated bone cement (Eurofix<sup>®</sup>, Synimed, France); and 2 segments (1 case) with a 3.5 mm pedicle screw and 3.2 mm rod system (Artemis<sup>®</sup>, Veterinary Orthopedics, United Kingdom). For the remaining 6 segments (4 cases), paired 8, 10 or 12-hole 2.7 mm locking plates and mono-cortical locking screws (Eickloxx, Eickemeyer Veterinary Equipment Ltd., United Kingdom) were utilised



(Appendix G). All bi-cortical implants were placed with the assistance of patient-specific 3D printed drill guides, whereas mono-cortical implants were placed without additional guidance. There were no notable challenges in the surgical procedure or patient anaesthesia.



**Figure 5-3. Post-operative CT imaging in cases with bi-cortical (A–C) and mono-cortical (D–F) supporting stabilisation systems. Sagittal (A,D), transverse (B,E) and three-dimensional (C,F) reconstructions with a bone algorithm.**

### 5.3.3. Clinical Outcomes

The median duration of hospitalization prior to discharge was 5 days (range 3 to 7). In three dogs, transient worsening of neck pain and mild thoracic limb lameness was evident, which resolved during hospitalization. In the case that underwent a ventral slot, transient neurologic deterioration occurred which reversed to pre-operative function within 3 days.

The medium-term follow-up examination occurred from 2 to 8 months post-operative; mean  $3.00 \pm 1.82$  months. At this point, 7 dogs had improved, 1 was stable and 1 had deteriorated with slight worsening of thoracic limb paresis and the development of pelvic limb lameness. This dog was subsequently diagnosed with

immune-mediated polyarthrititis (IMPA) following arthrocentesis of multiple joints. The mean TSCIS had improved significantly to  $36.9 \pm 2.78$  ( $p = 0.009$ ).

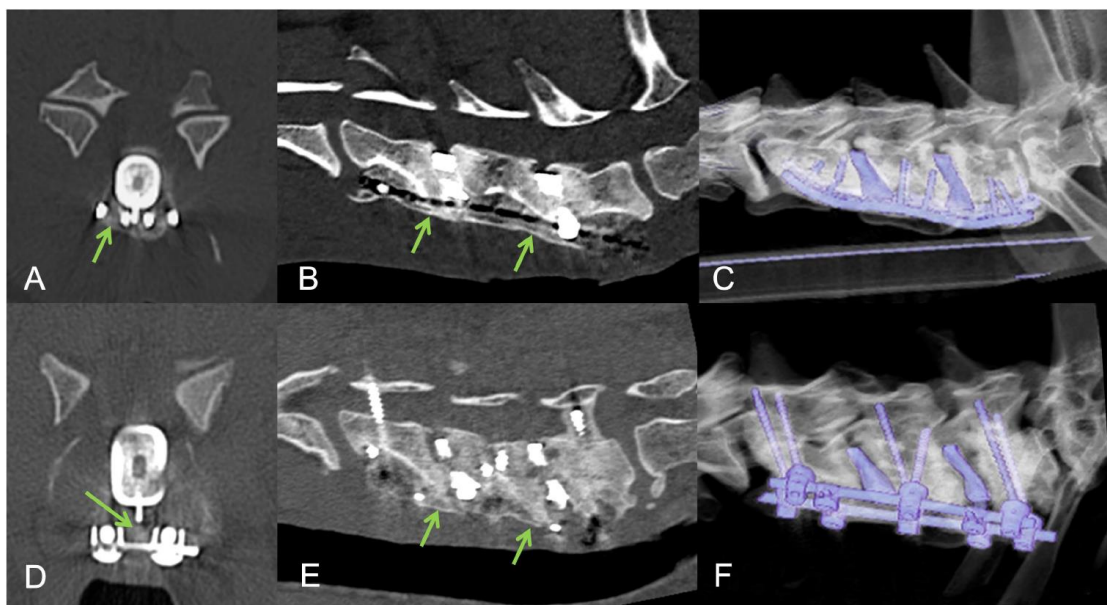
Long-term follow-up ranged from 9 to 33 months (mean duration  $14.23 \pm 8.24$  months). Improvement was seen in 8 of the 9 dogs. The dog that suffered worsened thoracic limb paresis and was diagnosed with IMPA was euthanased 9 months post-operative due to unacceptable side effects of corticosteroid therapy (polydipsia and polyuria). One dog was euthanased at 24 months post-operative for non-specific neoplasia, and one at 13 months due to the development of heart failure. One was diagnosed with gastrointestinal lymphoma 27 months post-operative and was under care for this disease without neurologic change at the last follow-up at 33 months post-operative (Appendix G).

#### **5.3.4. Radiologic Outcomes**

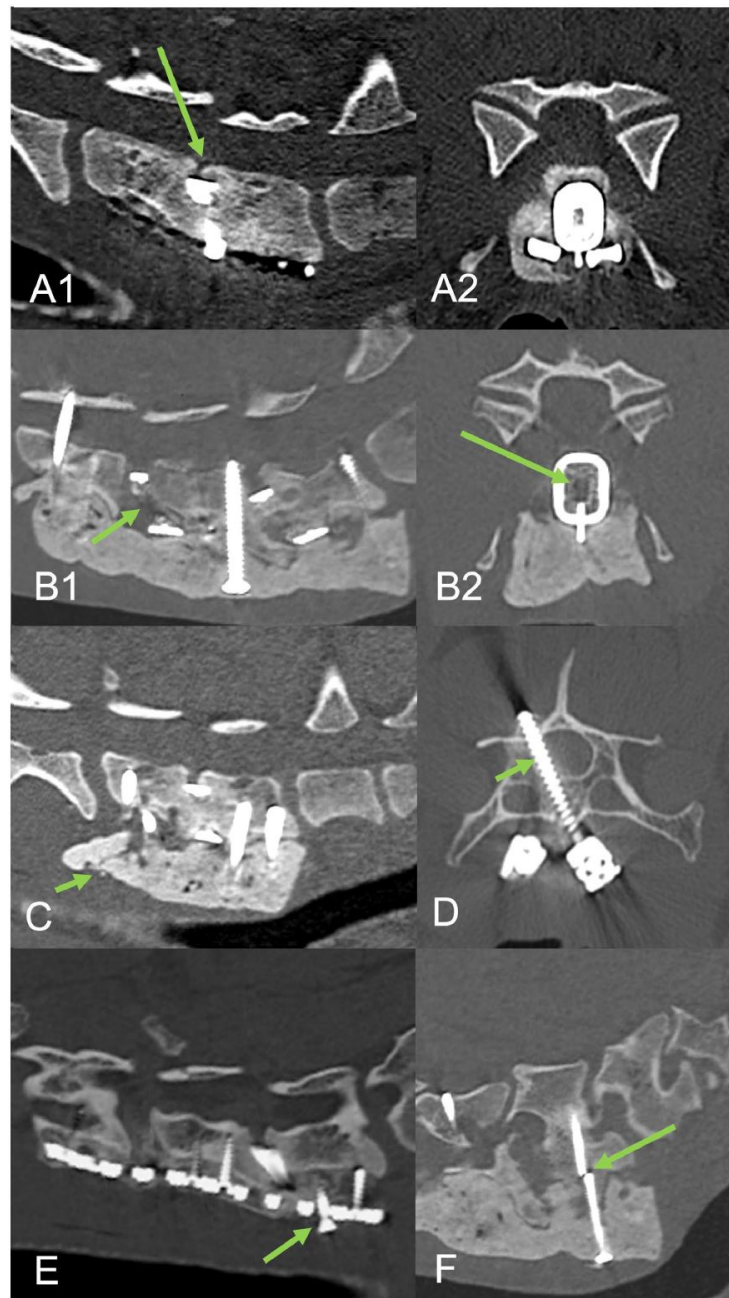
CT scans were performed immediately post-operative and at medium-term follow-up in all cases; findings are summarised in Appendix G. CT-determined interbody fusion was apparently successful in 8/9 cases (12/13 segments) (Figure 5-4); in the segment without fusion, endoprosthetic fusion appeared hampered by the ventral slot procedure performed (Figure 5-5). As locking screws and bone cement were utilised for secondary stabilisation in this case, fusion ventral to the bodies could also not be appreciated. Bony-bridging ventral to the vertebral bodies was appreciated in all cases where bone cement was not utilised.

Minor complications were evident in 7/9 cases at 7/13 segments (Figure 5-5). These included one screw breakage, one fractured bone cement, two partial vertebral canal breaches and four partial back-out of locking screws from the caudal aspect of the locking plates, all of which occurred within C7. There were no major complications. Dislodging, displacement or failure of the interbody device was not seen at any segment.

Mean end-plate measurements for pre-, post-operative and medium-term follow up were  $54.83 \pm 7.25$  mm,  $56.25 \pm 7.01$  mm and  $54.95 \pm 7.23$  mm, respectively. There was a statistically significant difference between pre- and post-operative measurements ( $p < 0.001$ ) but also comparing post-operative to follow-up measurements ( $p = 0.003$ ). Follow-up measurements did not vary significantly to pre-op ( $p = 0.787$ ). The distraction index increased in all cases immediately post-operative ( $2.69 \pm 1.67\%$ ) then reduced at follow-up in all segments ( $0.24 \pm 2.86\%$ ), but remained positive in all but three segments (Appendix G). Subsidence was therefore evident in 3/9 cases at 3/13 segments. At two segments, this subsidence appeared mild, but in one case subsidence appeared significant (distraction index  $-6.87\%$ ) and was also considered to be clinically relevant (Figure 5-5). There was no correlation between the variation of TSCIS pre- and post-operative and the distraction index at follow up ( $r = 0.3$ ,  $p = 0.328$ ).



**Figure 5-4.** Follow-up CT examinations in cases with mono-cortical (A–C) and bi-cortical (D–F) supporting stabilisation systems. Transverse (A,D), sagittal (B,E) and three-dimensional (C,F) reconstructions with a bone algorithm. Ventral bony bridging (arrowed) and endoprosthetic osseous fusion is suggested.



**Figure 5-5. Complications associated with procedure. Top row sagittal (A1) and transverse (A2) CT reconstructions from case 7 that suffered mild neurologic deterioration associated with vertebral subsidence (arrowed) despite interbody fusion. Second row sagittal (B1) and transverse (B2) CT reconstructions from case 2 demonstrating a lack of interbody fusion at C5-C6 (arrowed) adjacent to a ventral slot. Other minor complications included cement fracture with mild subsidence (C) arrowed, mild vertebral canal screw breach (D) arrowed, screw back-out with mild subsidence (E) arrowed, and screw breakage (F) arrowed.**

---

Five cases returned for a fourth CT scan between 6 and 12 months post-operative. In one case, the medium-term follow-up scan occurred at 8 months, meaning a total of 6/9 cases had scans >6 months post-operative available for assessment of ASP at 10 segments. ASP was evident at 4/9 segments, all of which involved partial bridging spondylosis deformans at the adjacent disk space. ASP did not cause clinically relevant ASD in the study subjects.

#### **5.4. Discussion**

Patient-specific endplate-conforming interbody devices with a micro-porous structure were developed and successfully implanted in nine dogs with DA-CSM alongside bi- or mono-cortical instrumentation and led to CT-determined fusion in 12 of 13 operated segments. There was a positive clinical benefit in 8 of 9 dogs and revision surgery was not required; the dog that demonstrated mild clinical deterioration might have maintained an acceptable level of function and quality of life or indeed improved, in advance of the natural progression of the disease, were it not for the development of co-morbid IMPA which affected mobility in the follow-up period. Our results compare favourably to the literature where success rates of 70–90% for surgical management of DA-CSM are reported (De Decker et al., 2012a, da Costa et al., 2006, da Costa, 2012, da Costa and Parent, 2007, Jeffery and McKee, 2001, De Decker et al., 2009, da Costa et al., 2008, De Risio et al., 2002) and the endplate confirming nature of the implant limited clinically relevant subsidence as has been reported with other interbody devices previously (da Silva et al., 2010, De Decker et al., 2011a, Steffen et al., 2011, Corlazzoli et al., 2013, Rohner et al., 2019, Joffe et al., 2019, King et al., 2020, Falzone et al., 2022).

This study represents the first description of an endplate conforming interbody device that was manufactured in titanium alloy by SLM with a micro-porous structure. Titanium alloy is an ideal material for this purpose given its rigidity, biological compatibility, corrosion resistance and MRI compatibility (Wieding et al., 2015, Niinomi et al., 2012, Ponader et al., 2008, Ernstberger et al., 2007). Scaffold properties,

such as porosity, porous size, permeability, stiffness and geometry can influence the success of bone in-growth (Mullen et al., 2009, Mullen et al., 2010). The internal portion of the current device features a scaffold with properties that closely mimics trabecular bone (Zhang et al., 2013) and which has already been successfully used in canine orthopaedic surgeries including tibial tuberosity advancement osteotomies. A potential disadvantage for patient-specific devices is the time needed to design and manufacture, meaning they are potentially not suitable for non-ambulant or emergency cases requiring more urgent surgery on a welfare basis; however, this is often not the case with DA-CSM.

Generic canine (Rohner et al., 2019, King et al., 2020) and human (Reints Bok et al., 2019) interbody spacers have been successfully employed in dogs with DA-CSM, however, the canine interbody space is geometrically more complex than in humans, and simple convex or wedge-shaped cages will not perfectly conform. This limits bone-implant contact and load distribution, which may provide a less favourable biomechanical environment compromising endplate integrity leading to implant subsidence (Zhang et al., 2016). Further, higher shear forces are present in the canine caudal cervical spine due to their naturally lordotic posture which can influence implant failure or migration (Falzone et al., 2022, Adamo, 2011). The current interbody device was created with a high-friction surface with protective solid outer wall structure, which provided excellent end-plate conformity; implant failure, migration or infection was not seen in any case.

Implant subsidence was not completely avoided, with 3/13 operated segments having a reduction in distraction index relative to pre-operative levels. This was only clinically relevant in one case with one operated segment; however, revision surgery was not considered necessary in this case as the patient remained ambulant with a relatively mild change in gait. These results compare favourably with the current literature regarding interbody device subsidence (da Silva et al., 2010, De Decker et al., 2011a, Steffen et al., 2011, Corlazzoli et al., 2013, Rohner et al., 2019, Joffe et al., 2019, King et al., 2020, Falzone et al., 2022), but direct comparison cannot be made on the basis

---

of this study. There are significant variations in the methodology for assessing implant subsidence; subsidence was assessed using previous methodology (Solano et al., 2015, Reints Bok et al., 2019) adapted from human medicine (McAfee et al., 2001) but applied to CT in follow-up. While some variation in patient positioning can be expected, the use of CT (where multi-planar reconstruction allows the fused segment to be assessed in an optimised mid-sagittal alignment) provided a potentially more accurate critique of the technique than would be possible with follow-up radiography only. Inter-observer agreement could be a source of future study to further validate these techniques.

Restoration of vertebral canal dimensions following intervertebral disk narrowing and protrusion is one of the main aims of managing DA-CSM (da Costa, 2010, Lewis, 1989a). Vertebral distraction can be beneficial in immediately decompressing the spinal cord and nerve roots (Solano et al., 2015) but over-distraction has been associated with pain in humans (Ha et al., 2013) and could in theory increase the risk of implant subsidence. A systematic approach to determining vertebral distraction was developed, allowing for a marginal degree of distraction (+10%) from averaged non-affected disk spaces. This facilitated both ease of surgical implantation and an increased post-operative distraction index in all cases. This was well tolerated with hospitalization periods being less than a week; however, 3 cases demonstrated a transient worsening of lameness which could have been related to one or multiple factors including over-distraction, surgical irritation of the nerve roots or the collection of autografts from the proximal humeri.

Supporting or 'secondary' stabilisation systems are commonly employed in canine cervical interbody fusion studies (Steffen et al., 2011, Corlazzoli et al., 2013, Rohner et al., 2019, Joffe et al., 2019, King et al., 2020, Falzone et al., 2022), primarily citing the improved rate of interbody fusion with combined cage distraction and anterior plating in man (Kaiser et al., 2002). Mono-cortical systems such as paired locking plates are most often utilised (Voss et al., 2006, Shamir et al., 2008, Bergman et al., 2008, Trotter, 2009, Steffen et al., 2011, Solano et al., 2015, Corlazzoli et al., 2013, Reints Bok et al.,

2019, Falzone et al., 2022) as the relative risk of vertebral canal penetration is low and they can provide adequate stability after ventral slot procedures (Agnello et al., 2010). Minor complications such as screw breakage and plate back-out are relatively common, as was the case in this study (4/6 operated segments). Fortunately, implant loosening might be less significant when stabilisation from fusion or bone bridging has already been accomplished (Reints Bok et al., 2019). The caudal cervical spine experiences three times more axial rotation than the cranial cervical region (Johnson et al., 2011) which may relate to more concave articular facet morphology in this region (Breit and Künzel, 2002). Biomechanical assessment of the most caudal segments following mono-cortical stabilisation or complete or sub-total discectomy is lacking. Some authors have proposed a combined dorsal and ventral approach to include trans-articular stabilisation (Corlazzoli et al., 2013, Falzone et al., 2022) or a modified slot technique with bi-cortical transpedicular screws placed with the assistance of patient-specific 3D printed drill guides (Armstrong et al., 2014). In this study, the choice of secondary stabilisation system for each case was based on implant availability, implant cost and surgeon preference. Guides were used for the placement of bi-cortical screws in combination with bone cement or rods in 7/13 segments and 3/7 experienced mild complications. The guided placement of pedicle screws with rods combines the benefits of bi-cortical fixation and the ability to lay down large amounts of cancellous autograft which assists with ventral bony bridging and potentially more rapid fusion.

A significant limitation to the study is the lack of histologic documentation of interbody fusion post-mortem, which might have been possible from one of the euthanased cases. Unfortunately, the bodies were not made available for study which was primarily related to distance of travel and euthanasia in a primary care setting. In addition, the determination of fusion was based on CT, rather than more sophisticated modalities such as  $\mu$ CT or *in-silico* subtraction techniques to reduce metallic scatter (Reints Bok et al., 2019). Ideally, a calibration phantom would be used as a control (Armstrong et al., 2014). Despite this limitation, interbody fusion was considered very likely in 12/13 segments based on the ROI Hounsfield units being compatible with



---

bone. It remains possible that individual segments lacked complete compound bone fusion and/or contained fibrous elements within the interbody spacers.

The assessment of ASP was possible in 6/9 cases, revealing 3 cases with 4/9 segments affected; fortunately, clinical signs suggestive of ASD were not reported in any cases on long-term follow up. Distraction-fusion techniques are expected to alter vertebral motion patterns. It is currently unknown whether endplate-conforming interbody devices will reduce the risk of ASP and ASD with time, relative to non-conforming spacers or cages. Current devices developed to maintain normal motion and reduce ASD, such as prosthetic disks, may be more prone to failure than distraction-fusion techniques (Falzone et al., 2022). ASP can be influenced by plates and screws impinging on adjacent segments (Reints Bok et al., 2019), which was avoided in this case series. The complete assessment for ASP and ASD with our technique is hampered by the retrospective nature of the study and a lack of uniform long-term follow up.

Other potential limitations to the study include its descriptive nature, small sample size, potential selection bias (based on financial viability and/or the selection of dogs with only mild to moderate clinical signs) and the lack of a control group. Direct comparisons to other interbody devices/spacers/cages are not possible. Further biomechanical and clinical studies would be required in dogs to confirm the suggestion that the devices provide a superior environment for stability and osseous in-growth.

In conclusion, it was reported the successful development and application of patient-specific, endplate-conforming interbody devices, featuring a micro-porous structure, for the instrumented distraction and fusion of 13 diseased spinal segments in nine dogs with DA-CSM. The technique was safe and effective, with no significant intra-operative complications. There were only minor implant-related complications on follow-up, none of which required revision surgery; in one case, subsidence was associated with mild clinical deterioration, the remaining eight cases improved.

---

## 6. Conclusion

This research has delivered patient-specific distraction-stabilisation interbody devices that have achieved satisfactory medium-term clinical outcomes, and the basis for a complete stabilisation system with anatomical bone plates which can be further instrumented with custom drill guides and pedicle screws.

Following a detailed review of different CSM stabilisation techniques and advancements in CSM distraction-stabilisation devices, diverse opportunities were identified and considered for the proposition of a stabilisation system. The Doberman was initially identified as a study breed dog for this research. However, this shifted over the course of the research to a large-breed dog approach. Novel virtual orientation and distraction techniques for canine cervical vertebrae were developed, which not only provided valuable guidelines for this research but can be implemented for other in-silico applications involving vertebrae bone-models. Additionally, a multi-body dynamics model was developed, which can provide estimated muscle forces and moments for implant optimisation.

At the time of writing, no canine-specific interbody device that includes a micro-porous structure for bone-in growth existed. Therefore, a pilot study was proposed in order to assess the clinical outcomes of the interbody spacers developed in this research. The pilot study was successfully implemented, which reported satisfactory medium-term outcomes with no major complications, with no or mild vertebral subsidence, and CT evidence of bone fusion. However, any advantage has not been definitively assessed relative to other implant systems.

In conclusion, the ultimate goal of this project was achieved while providing meaningful data for future work.

## 6.1. Perspectives on Future Applications

Future applications derived from the results presented in this thesis is as follows:

- **Patient-specific anatomical plates.** The development of this implant was put on hold due to time constraints. However, it
- **Development of stratified implants.** Once the proof-of-concept for patient-specific interbody devices is completed, stratified approaches can be considered. For this purpose, this thesis presents the development of custom devices following a systematic methodology allowing for correlation analysis of point data.
- **FEA modelling of bone-implant interfaces.** The optimisation of bone-implant constructs can be achieved by FEA models (Figure 6-1). The muscle forces and moments data from the multi-body dynamics model would drive these models.
- **Development of automated orientation technique.** At the time of writing, no other orientation technique for canine cervical vertebrae was publicly available. Once the ‘manual’ approach was assessed in this thesis, the development of an automated orientation approach may be necessary to accelerate development times. Likewise, an automated approach could also accelerate the turnaround times in terms of morphology analysis for implant designing.

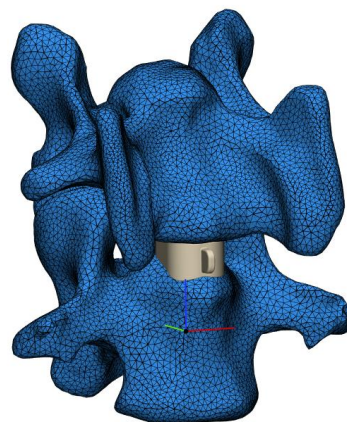


Figure 6-1. Virtual mesh of a bone-implant construct for FEA modelling.

## References

- Adamo, P. F. (2011) 'Cervical arthroplasty in two dogs with disk-associated cervical spondylomyelopathy', *Journal of the American Veterinary Medical Association*, 239(6), pp. 808-817.
- Agnello, K. A., Kapatkin, A. S., Garcia, T. C., Hayashi, K., Welihozkiy, A. T. and Stover, S. M. (2010) 'Intervertebral biomechanics of locking compression plate monocortical fixation of the canine cervical spine', *Vet Surg*, 39(8), pp. 991-1000.
- Alex, G., Alison, T. and Dan, O. N. (2018) *Breed predispositions to disease in dogs and cats*. Third Edition edn.
- Allen, V., Eley, R. M., Jones, N., Wright, J. and Hutchinson, J. R. (2010) 'Functional specialization and ontogenetic scaling of limb anatomy in Alligator mississippiensis', *J Anat*, 216(4), pp. 423-45.
- American Kennel Club (2019). Available at: <https://www.akc.org/>.
- Armstrong, J., da Costa, R. C. and Martin-Vaquero, P. (2014) 'Cervical Vertebral Trabecular Bone Mineral Density in Great Danes With and Without Osseous-Associated Cervical Spondylomyelopathy', *Journal of Veterinary Internal Medicine*, 28(6), pp. 1799-1804.
- Bates, K. T., Benson, R. B. J. and Falkingham, P. L. (2012a) 'A computational analysis of locomotor anatomy and body mass evolution in Allosauroidea (Dinosauria: Theropoda)', *Paleobiology*, 38(3), pp. 486-507.
- Bates, K. T., Maidment, S. C., Allen, V. and Barrett, P. M. (2012b) 'Computational modelling of locomotor muscle moment arms in the basal dinosaur Lesothosaurus diagnosticus: assessing convergence between birds and basal ornithischians', *J Anat*, 220(3), pp. 212-32.
- Bates, K. T. and Schachner, E. R. (2012) 'Disparity and convergence in bipedal archosaur locomotion', *Journal of The Royal Society Interface*, 9(71), pp. 1339-1353.
- Beer, P., Park, B. H., Steffen, F., Smolders, D. L. A., Pozzi, A. and Knell, S. C. (2020) 'Influence of a customized three-dimensionally printed drill guide on the accuracy of pedicle screw placement in lumbosacral vertebrae: An ex vivo study', *Vet Surg*, 49(5), pp. 977-988.

## References

---

- Bergman, R. L., Levine, J. M., Coates, J. R., Bahr, A., Hettlich, B. F. and Kerwin, S. C. (2008) 'Cervical spinal locking plate in combination with cortical ring allograft for a one level fusion in dogs with cervical spondylotic myelopathy', *Vet Surg*, 37(6), pp. 530-6.
- Birchard, S. J. and Sherding, R. G. (2006) *Saunders manual of small animal practice. [electronic book]. Online access with purchase: Elsevier (Veterinary Medicine pre-2007)* 3rd edn.: St. Louis, Mo. : Saunders Elsevier, c2006.
- Bonelli, M. A., da Costa, R. C., Martin-Vaquero, P. and Lima, C. G. (2017) 'Comparison of angle, shape, and position of articular processes in Dobermans and Great Danes with and without cervical spondylomyelopathy', *BMC Vet Res*, 13(1), pp. 77.
- Breit, S. and Künzel, W. (2002) 'Shape and orientation of articular facets of cervical vertebrae (C3-C7) in dogs denoting axial rotational ability: an osteological study', *European journal of morphology*, 40(1), pp. 43-51.
- Burbidge, H. M., Pfeiffer, D. U. and Blair, H. T. (1994) 'Canine wobbler syndrome: a study of the Dobermann pinscher in New Zealand', *N Z Vet J*, 42(6), pp. 221-8.
- Cameron, J. R. J. G. S. R. M. G. (1999) *Physics of the Body*. Second Edition edn.
- Charles, J. P., Fu, F. H. and Anderst, W. J. (2021) 'Predictions of Anterior Cruciate Ligament Dynamics From Subject-Specific Musculoskeletal Models and Dynamic Biplane Radiography', *J Biomech Eng*, 143(3).
- Chua, C. K., Leong, K. F. and Lim, C. S. (2009) *Rapid prototyping : principles and applications*. 3rd edn.: Singapore ;London : World Scientific.
- Corlazzoli, D. (2008) 'Bicortical implant insertion in caudal cervical spondylomyelopathy: a computed tomography simulation in affected Doberman Pinschers', *Vet Surg*, 37(2), pp. 178-85.
- Corlazzoli, D., Porcarelli, L. and Raimondi, F. (2013) 'Combined Dorsal And Ventral Stabilization In Traction Responsive Cervical Spondylomyelopathy', *Journal of Veterinary Internal Medicine*, 27, pp. 679-679.
- da Costa, R. (2012) 'Relationship between spinal cord signal changes and clinical and MRI findings in dogs with cervical spondylomyelopathy-102 cases', *Journal of Veterinary Internal Medicine*, 26(3), pp. 807-8.
- da Costa, R. and Parent, J. (2007) 'One-year clinical and magnetic resonance imaging follow-up Doberman Pinschers with cervical spondylomyelopathy treated

## References

---

- medically or surgically', *Journal of the American Veterinary Medical Association*, 231, pp. 243-50.
- da Costa, R. C. (2010) 'Cervical spondylomyelopathy (wobbler syndrome) in dogs', *Vet Clin North Am Small Anim Pract*, 40(5), pp. 881-913.
- da Costa, R. C. 2018. Cervical Spondylomyelopathy Update on Diagnosis - da Costa. Department of Veterinary Clinical Sciences, The Ohio State University.
- da Costa, R. C., Parent, J. M., Holmberg, D. L., Sinclair, D. and Monteith, G. (2008) 'Outcome of medical and surgical treatment in dogs with cervical spondylomyelopathy: 104 cases (1988-2004)', (no. 8), pp. 1284.
- da Costa, R. C., Parent, J. M., Partlow, G., Dobson, H., Holmberg, D. L. and Lamarre, J. (2006) 'Morphologic and morphometric magnetic resonance imaging features of Doberman Pinschers with and without clinical signs of cervical spondylomyelopathy', *American Journal Of Veterinary Research*, 67(9), pp. 1601-1612.
- da Silva, A. C., Bernard, F. and Bardet, J. F. (2010) 'Caudal cervical arthrodesis using a distractable fusion cage in a dog', *Vet Comp Orthop Traumatol*, 23(03), pp. 209-213.
- De Decker, S., Bhatti, S. F., Duchateau, L., Martle, V. A., Van Soens, I., Van Meervenne, S. A., Saunders, J. H. and Van Ham, L. M. (2009) 'Clinical evaluation of 51 dogs treated conservatively for disc-associated wobbler syndrome', *J Small Anim Pract*, 50(3), pp. 136-42.
- De Decker, S., Caemaert, J., Tshamala, M. C., Gielen, I. M. V. L., Van Bree, H. J. J., Bosmans, T., Wegge, B. and Van Ham, L. M. L. (2011a) 'Surgical Treatment of Disk-Associated Wobbler Syndrome by a Distractable Vertebral Titanium Cage in Seven Dogs', *Veterinary Surgery*, 40(5), pp. 544-554.
- De Decker, S., da Costa, R. C., Volk, H. A. and Van Ham, L. M. (2012a) 'Current insights and controversies in the pathogenesis and diagnosis of disc-associated cervical spondylomyelopathy in dogs', *Vet Rec*, 171(21), pp. 531-7.
- De Decker, S., Gielen, I. M., Duchateau, L., Volk, H. A. and Van Ham, L. M. (2012b) 'Intervertebral disk width in dogs with and without clinical signs of disk associated cervical spondylomyelopathy', *BMC Vet Res*, 8, pp. 126.
- De Decker, S., Gielen, I. M. V. L., Duchateau, L., Saunders, J. H. H., van Bree, H. J. J., Polis, I. and Van Ham, L. M. L. 2011b. Magnetic resonance imaging vertebral

canal and body ratios in Doberman Pinschers with and without disk-associated cervical spondylomyelopathy and clinically normal English Foxhounds.

De Decker, S., Gielen, I. M. V. L., Duchateau, L., Van Soens, I., Bavegems, V., Bosmans, T., van Bree, H. J. J. and Van Ham, L. M. L. (2010) 'Low-field magnetic resonance imaging findings of the caudal portion of the cervical region in clinically normal Doberman Pinschers and Foxhounds', (no. 4), pp. 428.

De Decker, S., Saunders, J. H., Duchateau, L., Pey, P. and Van Ham, L. M. L. (2011c) 'Radiographic vertebral canal and vertebral body ratios in Doberman Pinschers with and without clinical signs of caudal cervical spondylomyelopathy', (no. 7), pp. 958.

De Risio, L., Muana, K., Murray, M., Olby, N., Sharp, N. J. H. and Cuddon, P. (2002) 'Dorsal laminectomy for caudal cervical spondylomyelopathy: Postoperative recovery and long-term follow-up in 20 dogs', *Veterinary Surgery*, 31(5), pp. 418-427.

Dixon, B. C., Tomlinson, J. L. and Kraus, K. H. (1996) 'Modified distraction-stabilization technique using an interbody polymethyl methacrylate plug in dogs with caudal cervical spondylomyelopathy', *J Am Vet Med Assoc.*, 208(1):61-8.

Dries, B., Jonkers, I., Dingemanse, W., Vanwanseele, B., Vander Sloten, J., van Bree, H. and Gielen, I. (2016) 'Musculoskeletal modelling in dogs: challenges and future perspectives', *Vet Comp Orthop Traumatol*, 29(3), pp. 181-7.

Elford, J. H., Oxley, B. and Behr, S. (2019) 'Accuracy of placement of pedicle screws in the thoracolumbar spine of dogs with spinal deformities with three-dimensionally printed patient-specific drill guides', *Vet Surg.*

Ernstberger, T., Heidrich, G., Bruening, T., Kreff, S., Buchhorn, G. and Klinger, H. M. (2007) 'The interobserver-validated relevance of intervertebral spacer materials in MRI artifacting', *European Spine Journal*, 16(2), pp. 179-185.

Evans, H. E. and DeLahunta, A. (2017) *Guide to the dissection of the dog*. 8th ed. edn.: Elsevier.

Falzone, C., Tranquillo, V. and Gasparinetti, N. (2022) 'Comparison of Two Surgical Techniques for the Treatment of Canine Disc Associated-Cervical Spondylomyelopathy', *Frontiers in Veterinary Science*, 9.

Fingerroth, J. T., WB (2015) 'Is "wobbler" disease related to disc disease?', *Advances in intervertebral disc disease in dogs and cats*: Wiley-Blackwell, pp. 50-66.

## References

---

- Fossum, T. W. (2018) *Small Animal Surgery*. Philadelphia: Mosby.
- Fujioka, T., Nakata, K., Nishida, H., Sugawara, T., Konno, N., Maeda, S. and Kamishina, H. (2019) 'A novel patient-specific drill guide template for stabilization of thoracolumbar vertebrae of dogs: cadaveric study and clinical cases', *Vet Surg*, 48(3), pp. 336-342.
- Gibson, I., Rosen, D. W. and Stucker, B. *Additive manufacturing technologies. [electronic book] : 3D printing, rapid prototyping, and direct digital manufacturing. Online access with purchase: Springer* Second edn.: New York, NY : Springer, 2015.
- Guevar, J., Bleedorn, J., Cullum, T., Hetzel, S., Zlotnick, J. and Mariani, C. L. (2021) 'Accuracy and safety of three-dimensionally printed animal-specific drill guides for thoracolumbar vertebral column instrumentation in dogs: Bilateral and unilateral designs', *Vet Surg*, 50(2), pp. 336-344.
- Ha, S. M., Kim, J. H., Oh, S. H., Song, J. H., Kim, H. I. and Shin, D. A. (2013) 'Vertebral Distraction during Anterior Cervical Discectomy and Fusion Causes Postoperative Neck Pain', *J Korean Neurosurg Soc*, 53(5), pp. 288-292.
- Hamilton-Bennett, S. E., Oxley, B. and Behr, S. (2018) 'Accuracy of a patient-specific 3D printed drill guide for placement of cervical transpedicular screws', *Vet Surg*, 47(2), pp. 236-242.
- Hicks, J. L., Uchida, T. K., Seth, A., Rajagopal, A. and Delp, S. L. (2015) 'Is my model good enough? Best practices for verification and validation of musculoskeletal models and simulations of movement', *Journal of biomechanical engineering*, 137(2).
- ISB (2002) 'ISB recommendation on definitions of joint coordinate system of various joints (spine)', *Journal of Biomechanics* (35), pp. 543-548.
- Jeffery, N. D. (1995) *Handbook of small animal spinal surgery*. London : Saunders, 1995.
- Jeffery, N. D. (2010) 'Vertebral fracture and luxation in small animals', *Vet Clin North Am Small Anim Pract*, 40(5), pp. 809-28.
- Jeffery, N. D. and McKee, W. M. (2001) 'Surgery for disc-associated wobbler syndrome in the dog--an examination of the controversy', *J Small Anim Pract*, 42(12), pp. 574-81.



## References

---

- Joffe, M. R., Parr, W. C. H., Tan, C., Walsh, W. R. and Brunel, L. (2019) 'Development of a Customized Interbody Fusion Device for Treatment of Canine Disc-Associated Cervical Spondylomyelopathy', *Vet Comp Orthop Traumatol*, 32(1), pp. 79-86.
- Johnson, J. A., da Costa, R. C., Bhattacharya, S., Goel, V. and Allen, M. J. (2011) 'Kinematic motion patterns of the cranial and caudal canine cervical spine', *Vet Surg*, 40(6), pp. 720-7.
- Kaiser, M. G., Haid, R. W., Jr., Subach, B. R., Barnes, B. and Rodts, G. E., Jr. (2002) 'Anterior cervical plating enhances arthrodesis after discectomy and fusion with cortical allograft', *Neurosurgery*, 50(2), pp. 229-36; discussion 236-8.
- Kamishina, H., Sugawara, T., Nakata, K., Nishida, H., Yada, N., Fujioka, T., Nagata, Y., Doi, A., Konno, N., Uchida, F. and Maeda, S. (2019) 'Clinical application of 3D printing technology to the surgical treatment of atlantoaxial subluxation in small breed dogs', *PLoS One*, 14(5), pp. e0216445.
- Kielty, C. M. (2006) 'Elastic fibres in health and disease', *Expert Reviews in Molecular Medicine*, 8(19), pp. 1-23.
- King, J. C., Corfield, G. S., Mouatt, J. G., Kan, C. Y. and Moses, P. A. (2020) 'Surgical management and long-term outcome of dogs with cervical spondylomyelopathy with an anchored intervertebral titanium device', *Australian Veterinary Journal*, 98(4), pp. 156-163.
- Koehler, C. L., Stover, S. M., LeCouteur, R. A., Schulz, K. S. and Hawkins, D. A. (2005) 'Effect of a ventral slot procedure and of smooth or positive-profile threaded pins with polymethylmethacrylate fixation on intervertebral biomechanics at treated and adjacent canine cervical vertebral motion units', (no. 4), pp. 678.
- Koo, T. K. and Li, M. Y. (2016) 'A Guideline of Selecting and Reporting Intraclass Correlation Coefficients for Reliability Research', *J Chiropr Med*, 15(2), pp. 155-63.
- Kruth, J. P., Van Vaerenbergh, J., Mercelis, P., Lauwers, B., Froyen, L. and Rombouts, M. (2004) 'Selective laser melting of iron-based powder', *Journal of Materials Processing Technology*, 149(1-3), pp. 616-622.
- Levine, G. J., Levine, J. M., Budke, C. M., Kerwin, S. C., Au, J., Vinayak, A., Hettlich, B. F. and Slater, M. R. (2009) 'Description and repeatability of a newly developed spinal cord injury scale for dogs', *Preventive Veterinary Medicine*, 89(1), pp. 121-127.

## References

---

- Lewchalermwong, P., Suwanna, N. and Meij, B. P. (2018) 'Canine Vertebral Screw and Rod Fixation System: Design and Mechanical Testing', *Vet Comp Orthop Traumatol*, 31(2), pp. 95-101.
- Lewis, D. G. (1989a) 'Cervical spondylomyelopathy ('wobbler' syndrome) in the dog: A study based on 224 cases', *Journal of Small Animal Practice*, 30(12), pp. 657-665.
- Lewis, D. G. (1989b) 'Cervical wobbler syndrome', *Journal of Small Animal Practice*, (30), pp. 657-665.
- Lind, J. U., Busbee, T. A., Valentine, A. D., Pasqualini, F. S., Yuan, H., Yadid, M., Park, S. J., Kotikian, A., Nesmith, A. P. and Campbell, P. H. (2017) 'Instrumented cardiac microphysiological devices via multimaterial three-dimensional printing', (no. 3), pp. 303.
- Lipsitz, D., Levitski, R. E., Chauvet, A. E. and Berry, W. L. (2001) 'Magnetic resonance imaging features of cervical stenotic myelopathy in 21 dogs', *Veterinary Radiology and Ultrasound*, 42(1), pp. 20-27.
- Lorenz, M. D., Coates, J. R. and Kent, M. (2011) *Handbook of veterinary neurology. [electronic book]. Online access with purchase: Elsevier (Veterinary Medicine 2011) 5th edn.: St. Louis, Mo. : Elsevier/Saunders, c2011.*
- Lyman, R. 'Continuous dorsal laminectomy for the treatment of caudal cervical instability and malformation'. *ACVIM Forum Proceedings. Lakewood (CO): American College of Veterinary Internal Medicine*, 13-6.
- Mai, W. (2018) *Diagnostic MRI in Dogs and Cats*. CRC Press.
- Maidment, S. C. R., Bates, K. T., Falkingham, P. L., VanBuren, C., Arbour, V. and Barrett, P. M. (2014) 'Locomotion in ornithischian dinosaurs: an assessment using three-dimensional computational modelling', *Biological Reviews*, 89(3), pp. 588-617.
- Mariani, C., Zlotnick, J., Harysson, O., Marcellin, D., Malinak, K., Gavitt, A. and Guevar, J. (2020) 'Accuracy of three-dimensionally printed animal-specific drill guides for implant placement in canine thoracic vertebrae: A cadaveric study', *Veterinary Surgery*, 50.
- Materialise 2014. Mimics® Innovation Suite. Available at: <http://biomedical.materialise.com/mis>

## References

---

- McAfee, P. C., Boden, S. D., Brantigan, J. W., Fraser, R. D., Kuslich, S. D., Oxland, T. R., Panjabi, M. M., Ray, C. D. and Zdeblick, T. A. (2001) 'Symposium: A Critical Discrepancy—A Criteria of Successful Arthrodesis Following Interbody Spinal Fusions', *Spine*, 26(3).
- McDonald, C. P., Bachison, C. C., Chang, V., Bartol, S. W. and Bey, M. J. (2010) 'Three-dimensional dynamic in vivo motion of the cervical spine: assessment of measurement accuracy and preliminary findings', *Spine J*, 10(6), pp. 497-504.
- McKee, W. M., Lavelle, R. B., Richardson, J. L. and Mason, T. A. (1989) 'Vertebral distraction-fusion for cervical spondylopathy using a screw and double washer technique', *Journal of Small Animal Practice*, 31(1), pp. 21-26.
- McKee, W. M., Pink, J. J. and Gemmill, T. J. (2016) 'Cement plug technique for the management of disc-associated cervical spondylopathy in 52 Doberman Pinscher dogs', *Vet Comp Orthop Traumatol*, 29(3), pp. 195-201.
- Mendez, J. K., A. (1960) 'Density and composition of mammalian muscle', *Metabolism, Clinical and Experimental*, 9(2), pp. 184-188.
- Miller, M. E. and Evans, H. E. (1993) *Miller's anatomy of the dog*. 3rd edn.: Philadelphia ;London : W.B. Saunders, c1993.
- Mullen, L. (2009) 'The characterisation and structural optimisation of additively fabricated porous components specifically for use in orthopaedic applications'.
- Mullen, L., Stamp, R. C., Brooks, W. K., Jones, E. and Sutcliffe, C. J. (2009) 'Selective Laser Melting: A regular unit cell approach for the manufacture of porous, titanium, bone in-growth constructs, suitable for orthopedic applications', *Journal of Biomedical Materials Research Part B: Applied Biomaterials*, 89B(2), pp. 325-334.
- Mullen, L., Stamp, R. C., Fox, P., Jones, E., Ngo, C. and Sutcliffe, C. J. (2010) 'Selective laser melting: A unit cell approach for the manufacture of porous, titanium, bone in-growth constructs, suitable for orthopedic applications. II. Randomized structures', *Journal of Biomedical Materials Research Part B: Applied Biomaterials*, 92B(1), pp. 178-188.
- Newton, C. D. and Nunamaker, D. M. (1985) *Textbook of small animal orthopaedics*. Philadelphia (Pa.) : Lippincott.
- NIH 2013. ImageJ 1.48. Available at: <https://imagej.nih.gov/ij>.

## References

---

- Niinomi, M., Nakai, M. and Hieda, J. (2012) 'Development of new metallic alloys for biomedical applications', *Acta Biomaterialia*, 8(11), pp. 3888-3903.
- O'Neill, D. G., Church, D. B., McGreevy, P. D., Thomson, P. C. and Brodbelt, D. C. (2013a) 'Longevity and mortality of owned dogs in England', *Vet J*, 198(3), pp. 638-43.
- O'Neill, M. C., Lee, L.-F., Larson, S. G., Demes, B., Stern, J. T., Jr. and Umberger, B. R. (2013b) 'A three-dimensional musculoskeletal model of the chimpanzee (*Pan troglodytes*) pelvis and hind limb', *Journal of Experimental Biology*, 216(19), pp. 3709-3723.
- Oxley, B. and Behr, S. (2016) 'Stabilisation of a cranial cervical vertebral fracture using a 3D-printed patient-specific drill guide', *J Small Anim Pract*, 57(5), pp. 277.
- Peters, A. E., Geraghty, B., Bates, K. T., Akhtar, R., Readioff, R. and Comerford, E. (2022) 'Ligament mechanics of ageing and osteoarthritic human knees', *Frontiers in Bioengineering and Biotechnology*, 10.
- Pixmeo 2010. Osirix. Available at: [www.osirixviewer.com](http://www.osirixviewer.com).
- Ponader, S., Vairaktaris, E., Heintl, P., Wilmowsky, C. v., Rottmair, A., Körner, C., Singer, R. F., Holst, S., Schlegel, K. A., Neukam, F. W. and Nkenke, E. (2008) 'Effects of topographical surface modifications of electron beam melted Ti-6Al-4V titanium on human fetal osteoblasts', *Journal of Biomedical Materials Research Part A*, 84A(4), pp. 1111-1119.
- PTC 2017. CAD Software | PTC. Available at: <http://www.ptc.com/en/cad>.
- Raja, V. and Fernandes, K. J. (2008) *Reverse engineering. [electronic book] : an industrial perspective. Springer series in advanced manufacturing*: London : Springer, ©2008.
- Reints Bok, T. E., Willemsen, K., van Rijen, M. H. P., Grinwis, G. C. M., Tryfonidou, M. A. and Meij, B. P. (2019) 'Instrumented cervical fusion in nine dogs with caudal cervical spondylomyelopathy', *Vet Surg*, 48(7), pp. 1287-1298.
- Rohner, D., Kowaleski, M. P., Schwarz, G. and Forterre, F. (2019) 'Short-Term Clinical and Radiographical Outcome after Application of Anchored Intervertebral Spacers in Dogs with Disc-Associated Cervical Spondylomyelopathy', *Vet Comp Orthop Traumatol*, 32(2), pp. 158-164.

## References

---

- Rusbridge, C., Wheeler, S. J., Torrington, A. M., Pead, M. J. and Carmichael, S. (1998) 'Comparison of two surgical techniques for the management of cervical spondylomyelopathy in dobermanns', *J Small Anim Pract*, 39(9), pp. 425-31.
- Seim, H. B. and Withrow, S. J. (1982) 'Pathophysiology and diagnosis of caudal cervical spondylo-myelopathy with emphasis on the Doberman Pinscher', *Journal American Animal Hospital Association*, 18(241).
- Shamir, M. H., Chai, O. and Loeb, E. (2008) 'A method for intervertebral space distraction before stabilization combined with complete ventral slot for treatment of disc-associated wobbler syndrome in dogs', *Vet Surg*, 37(2), pp. 186-92.
- Solano, M. A., Fitzpatrick, N. and Bertran, J. (2015) 'Cervical Distraction-Stabilization Using an Intervertebral Spacer Screw and String-of Pearl (SOP) Plates in 16 Dogs With Disc-Associated Wobbler Syndrome', *Vet Surg*, 44(5), pp. 627-41.
- Stanev, D., Moustakas, K., Gliatis, J. and Koutsojannis, C. (2016) 'ACL Reconstruction Decision Support. Personalized Simulation of the Lachman Test and Custom Activities', *Methods Inf Med*, 55(1), pp. 98-105.
- Steffen, F., Voss, K. and Morgan, J. P. (2011) 'Distraction-fusion for caudal cervical spondylomyelopathy using an intervertebral cage and locking plates in 14 dogs', *Vet Surg*, 40(6), pp. 743-52.
- Stokes, I. (1994) 'Three-dimensional terminology of spinal deformity', *Spine*, 19(2), pp. 236-248.
- The Kennel Club UK 2018. Quarterly registration statistics for the working group.
- Toni, C., Oxley, B. and Behr, S. (2020) 'Atlanto-axial ventral stabilisation using 3D-printed patient-specific drill guides for placement of bicortical screws in dogs', *J Small Anim Pract*, 61(10), pp. 609-616.
- Trotter, E. J. (2009) 'Cervical spine locking plate fixation for treatment of cervical spondylotic myelopathy in large breed dogs', *Vet Surg*, 38(6), pp. 705-18.
- Tuan, J., Solano, M. A. and Fitzpatrick, N. (2019) 'Ventral distraction-stabilization in 5 continuous sites for the treatment of cervical spondylomyelopathy in a Great Dane', *Vet Surg*, 48(4), pp. 607-614.
- Tuomi, J., Paloheimo, K.-S., Vehviläinen, J., Björkstrand, R., Salmi, M., Huutilainen, E., Kontio, R., Rouse, S., Gibson, I. and Mäkitie, A. A. (2014) 'A novel classification

## References

---

- and online platform for planning and documentation of medical applications of additive manufacturing', *Surgical Innovation*, 21(6), pp. 553-559.
- Voss, K., Steffen, F. and Montavon, P. M. (2006) 'Use of the ComPact UniLock System for ventral stabilization procedures of the cervical spine', *A retrospective study*, 19(01), pp. 21-28.
- Wang, D., Wang, Y., Wu, S., Lin, H., Yang, Y., Fan, S., Gu, C., Wang, J. and Song, C. (2017) 'Customized a Ti6Al4V Bone Plate for Complex Pelvic Fracture by Selective Laser Melting', *Materials (1996-1944)*, 10(1), pp. 35.
- Wieding, J., Lindner, T., Bergschmidt, P. and Bader, R. (2015) 'Biomechanical stability of novel mechanically adapted open-porous titanium scaffolds in metatarsal bone defects of sheep', *Biomaterials*, 46, pp. 35-47.
- Wright, F., J.R., R. and A.C., P. (1973) 'Ataxia of the Great Dane caused by stenosis of the cervical vertebral canal: Comparison with similar conditions in the basset hound, doberman pinscher, ridgeback, and the thoroughbred horse.', *Vet Rec*, (92:1).
- Zhang, F., Xu, H. C., Yin, B., Xia, X. L., Ma, X. S., Wang, H. L., Yin, J., Shao, M. H., Lyu, F. Z. and Jiang, J. Y. (2016) 'Can an Endplate-conformed Cervical Cage Provide a Better Biomechanical Environment than a Typical Non-conformed Cage?: A Finite Element Model and Cadaver Study', *Orthop Surg*, 8(3), pp. 367-76.
- Zhang, Z., Jones, D., Yue, S., Lee, P. D., Jones, J. R., Sutcliffe, C. J. and Jones, E. (2013) 'Hierarchical tailoring of strut architecture to control permeability of additive manufactured titanium implants', *Materials Science and Engineering: C*, 33(7), pp. 4055-4062.

## Appendices

### Appendix A. Anatomical measurements for gait analysis.

Code	Measurement
C1	Circumference around snout
C2	Circumference around RM46-RM47 (Frontal Lobe)
C3	Circumference around RM1 (Occipital Crest)
C4	Circumference around RM4 (Cervical vertebral column_A)
C5	Circumference around RM5 (Cervical vertebral column_B)
C6	Circumference around RM6 (Cervical vertebral column_C)
C7	Circumference around RM7 (Thoracic vertebral column_A), cranially to Acromion
C8	Circumference around thorax passing caudally to Acromion
C9	Circumference around RM24 (T13)
C10	Circumference around RM25 (L7)
C11	Circumference around RM10 or RM11 (Left/Right Acromion)
C12	Circumference around RM16 or RM17 (Left/Right Mid-Humerus)
C13	Circumference around RM12-RM14 or RM13-RM15 (Left/Right Lateral-Medial Epicondyle)
C14	Circumference around RM18 or RM19 (Left/Right Ulna Styloid)
C15	Circumference around just below RM30 or RM31 (Left/Right GT)
C16	Circumference around RM44 or RM45 (Left/Right Mid-Femur)
C17	Circumference around RM36 or RM37 (Left/Right Lateral Stifle)
C18	Circumference around RM38 or RM39 (Left/Right Lateral Malleolus)
D1	Distance between snout and RM1
D2	Distance between snout and frontal lobe (RM46/RM47)
D3	Distance between frontal lobe (RM46/RM47) and occipital crest (RM1)
D4	Distance between occipital crest (RM1) and first palpable vertebra (RM7)
D5	Distance between occipital crest (RM1) and RM4
D6	Distance between RM4 and RM5
D7	Distance between RM5 and RM6
D8	Distance between RM6 and first palpable vertebra RM7
D9	Distance between first palpable vertebra (RM7) and T13 (RM24)
D10	Distance between T13 (RM24) and L7 (RM25)
D11	Distance between first palpable vertebra (RM7) and L7 (RM25)
D12	Distance between Left/Right Acromion (R10 or RM11) to Left/Right Lateral Epicondyle (RM12 or RM13)
D13	Distance between Left/Right Lateral Epicondyle (RM12 or RM13) to Left/Right Ulna Styloid (RM18 or RM19)
D14	Distance between Left/Right GT (RM30 or RM31) to Left/Right Lateral Stifle (RM36 or RM37)
D15	Distance between Left/Right Lateral Stifle (RM36 or RM37) to Left/Right Lateral Malleolus (RM38 or RM39)

Appendix B. Anatomical measurements for gait analysis (averages).

Code	Participant 1				Participant 2				Participant 3			
	N1 (cm)	N2 (cm)	N3 (cm)	Average (cm)	N1 (cm)	N2 (cm)	N3 (cm)	Average (cm)	N1 (cm)	N2 (cm)	N3 (cm)	Average (cm)
C1	23.0	24.0	24.0	23.7	30.0	30.5	30.0	30.2	24.0	23.0	23.5	23.5
C2	33.5	34.0	34.0	33.8	41.0	40.5	40.5	40.7	35.5	35.5	35.0	35.3
C3	36.5	36.0	37.0	36.5	43.0	42.5	43.5	43.0	38.0	37.0	37.5	37.5
C4	38.5	38.5	39.0	38.7	45.0	44.5	44.0	44.5	39.5	39.5	40.0	39.7
C5	39.0	39.0	39.5	39.2	49.0	51.0	51.5	50.5	40.0	42.0	41.0	41.0
C6	46.0	44.0	45.0	45.0	70.0	72.0	69.0	70.3	50.0	52.0	52.5	51.5
C7	56.0	57.0	56.0	56.3	68.0	68.0	69.0	68.3	57.0	58.0	56.0	57.0
C8	79.0	79.0	79.0	79.0	94.0	93.0	93.5	93.5	85.0	85.0	83.0	84.3
C9	67.0	68.0	69.0	68.0	72.0	72.5	72.5	72.3	68.0	66.0	67.0	67.0
C10	62.0	62.0	62.0	62.0	72.0	69.0	69.0	70.0	60.0	61.0	61.0	60.7
C11	NA	NA	NA	NA	NA	NA	NA	NA	NA	NA	NA	NA
C12	22.0	22.0	24.0	22.7	29.0	29.0	29.5	29.2	27.0	28.0	28.0	27.7
C13	18.0	17.5	17.5	17.7	24.5	24.0	24.0	24.2	21.0	21.0	21.0	21.0
C14	13.5	13.5	13.5	13.5	16.0	16.0	16.0	16.0	15.0	15.0	15.0	15.0
C15	NA	NA	NA	NA	NA	NA	NA	NA	NA	NA	NA	NA
C16	42.0	39.0	41.0	40.7	42.0	41.0	40.5	41.2	40.0	40.0	39.5	39.8
C17	27.0	27.5	26.5	27.0	32.0	33.0	34.0	33.0	26.0	26.0	26.5	26.2
C18	13.5	13.5	14.0	13.7	18.0	18.0	18.0	18.0	16.0	15.5	15.5	15.7
D1	24.5	25.0	25.0	24.8	28.0	28.0	28.5	28.2	26.0	26.0	26.0	26.0
D2	13.5	13.5	13.5	13.5	15.5	15.0	15.5	15.3	14.0	14.0	14.5	14.2
D3	10.0	10.5	10.0	10.2	13.0	12.0	12.0	12.3	12.0	11.5	12.0	11.8
D4	24.0	24.0	24.0	24.0	26.0	26.0	26.0	26.0	26.0	26.0	26.0	26.0
D5	4.0	4.0	4.0	4.0	4.3	4.3	4.3	4.3	4.3	4.3	4.3	4.3
D6	8.0	8.0	8.0	8.0	8.7	8.7	8.7	8.7	8.7	8.7	8.7	8.7
D7	8.0	8.0	8.0	8.0	8.7	8.7	8.7	8.7	8.7	8.7	8.7	8.7
D8	4.0	4.0	4.0	4.0	4.3	4.3	4.3	4.3	4.3	4.3	4.3	4.3
D9	24.5	24.0	25.0	24.5	27.5	27.5	28.0	27.7	25.0	24.5	25.0	24.8
D10	19.0	19.0	19.0	19.0	20.5	20.0	20.0	20.2	15.0	15.0	15.0	15.0
D11	43.5	43.0	44.0	43.5	48.0	48.0	47.5	47.8	40.5	40.0	40.0	40.2
D12	16.5	16.5	17.0	16.7	19.0	19.0	19.0	19.0	17.5	18.0	17.5	17.7
D13	20.0	20.5	20.5	20.3	23.5	23.5	24.0	23.7	22.0	21.5	21.5	21.7
D14	18.0	18.5	18.5	18.3	22.0	21.5	21.5	21.7	19.5	20.0	20.0	19.8
D15	18.0	18.0	18.0	18.0	21.5	21.5	21.5	21.5	19.0	19.5	20.0	19.5



Appendix C. 'Clean Strikes' recorded from the gait study of subject 1.

<b>Subject</b>	<b>Trial Set</b>	<b>Walk Trial</b>	<b>Force Plate</b>	<b>Limb</b>	<b>Frames</b>
Doberman 1	1	2	3	Right Forelimb	3476-3516
Doberman 1	1	2	1	Left Forelimb	3518-3560
Doberman 1	1	2	3	Left Hindlimb	3519-3560
Doberman 1	1	2	1	Right Hindlimb	3562-3602
Doberman 1	5	2	4	Right Hindlimb	2737-2767
Doberman 1	5	2	3	Left Hindlimb	2749-2778
Doberman 1	5	2	1	Right Forelimb	2762-2794
Doberman 1	7	1	4	Right Forelimb	724-764
Doberman 1	7	1	3	Left Forelimb	768-804
Doberman 1	7	1	4	Right Hindlimb	781-811
Doberman 1	7	1	3	Left Hindlimb	808-857
Doberman 1	7	1	1	Right Forelimb	816-859
Doberman 1	7	1	1	Right Hindlimb	865-908
Doberman 1	7	2	4	Left Forelimb	3558-3594
Doberman 1	7	2	3	Right Forelimb	3604-3639
Doberman 1	7	2	4	Left Hindlimb	3604-3639
Doberman 1	7	2	1	Left Forelimb	3641-3679
Doberman 1	7	2	3	Right Hindlimb	3649-3680
Doberman 1	7	2	1	Left Hindlimb	3685-3723
Doberman 1	8	1	4	Left Forelimb	461-490
Doberman 1	8	1	4	Left Hindlimb	510-542
Doberman 1	8	2	4	Left Forelimb	3382-3424
Doberman 1	8	2	3	Right Forelimb	3430-3471
Doberman 1	8	2	4	Left Hindlimb	3430-3468
Doberman 1	8	2	1	Left Forelimb	3471-3514
Doberman 1	8	2	3	Left Hindlimb	3473-3514
Doberman 1	8	2	1	Right Hindlimb	3520-3560
Doberman 1	9	1	3	Right Forelimb	3227-3270
Doberman 1	9	2	3	Left Hindlimb	3273-3316
Doberman 1	10	2	4	Left Forelimb	3340-3388
Doberman 1	10	2	3	Right Forelimb	3390-3437
Doberman 1	10	2	4	Right Hindlimb	3391-3434
Doberman 1	10	2	3	Left Hindlimb	3440-3483

## Appendices

### Appendix D. Muscle architecture obtained from the neck dissection.

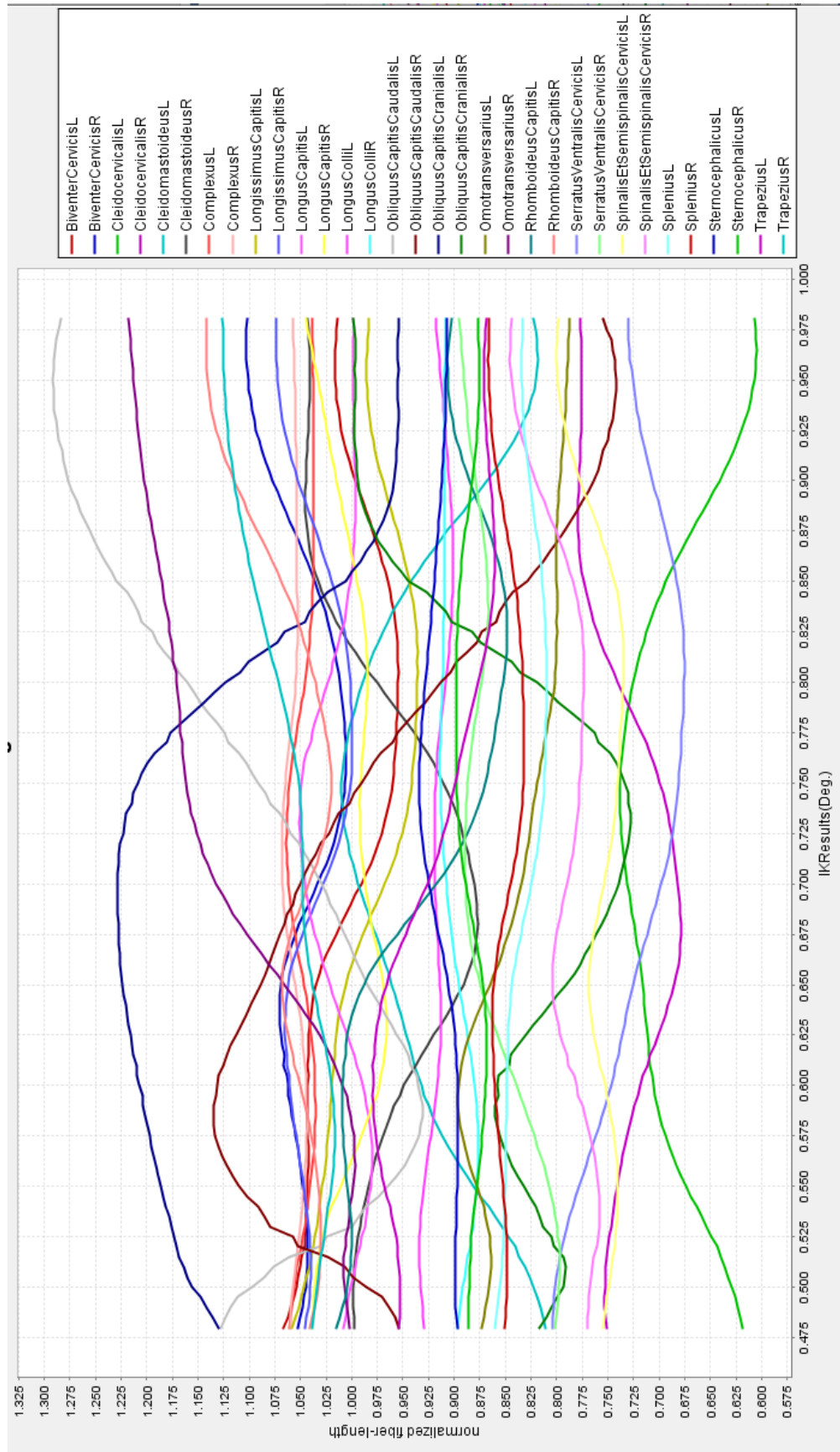
ID	Muscle	Muscle Mass (g)	Muscle Density (kg m <sup>2</sup> )	Muscle Volume (m <sup>3</sup> )	Muscle Length (mm)	Mean Fibre Length (mm)	Mean Pennation Angle (deg)
1	<b>Splenius</b>	63.2	1060	0.059623	273	190	0.00
2	<b>Semispinalis capitis: Biventer cervicis</b>	48.2	1060	0.045472	320	53	3.33
3	<b>Semispinalis capitis: Complexus</b>	26.7	1060	0.025189	234	99	3.33
4	<b>Longissimus capitis</b>	39.1	1060	0.036887	280	77	1.67
5	<b>Serratus ventralis</b>	85.8	1060	0.080943	242	106	3.33
6	<b>Longus capitis</b>	19.7	1060	0.018585	184	73	6.67
7	<b>Omotransversarius</b>	30.2	1060	0.028491	238	243	0.00
8	<b>Obliquus capitis cranialis</b>	25.8	1060	0.02434	71	52	3.33
9	<b>Obliquus capitis caudalis</b>	12.2	1060	0.011509	92	80	0.00
10	<b>Spinalis et semispinalis cervicis</b>	53.7	1060	0.05066	264	111	6.67
11	<b>Trapezius</b>	19.8	1060	0.018679	177	116	0.00
12	<b>Brachiocephalicus: Cleidomastoideus</b>	32.2	1060	0.030377	240	252	1.67
13	<b>Brachiocephalicus: Cleidocervicalis</b>	47.1	1060	0.044434	274	219	0.00
14	<b>Rhomboideus capitis</b>	17.0	1060	0.016038	173.5	77	1.67
15	<b>Sternocephalicus</b>	260.0	1060	0.245283	237	225	0.00
16	<b>Longus Colli</b>	27.0	1060	0.025472	198	121	5.00

## Appendices

### Appendix E. Full list of muscle properties: Cadaveric Specimen (CS).

Muscle	Mass CS (kg)	Body Weight Proportion	Density CS (kg/m <sup>3</sup> )	Volume CS (m <sup>3</sup> )	Muscle + tendon unit length CS	Muscle belly length CS (m)	External tendon length CS (m)	Muscle belly mass CS (kg)	Tendon mass CS (kg)	Mean Fibre Length CS (mm)	Average PA CS	Maximal Isometric Force (N)
<b>Splenius</b>	0.06	0.39	106	5.9623	0.27	0.27	0.00	0.06	0.00	0.19	0.00	94.14
	32	50	0	E-05	30	30	00	32	00	00	00	101
<b>Semispinalis capitis: Biventer cervicis</b>	0.04	0.30	106	4.5472	0.32	0.32	0.00	0.04	0.00	0.05	3.33	255.0
	82	13	0	E-05	00	00	00	82	00	34	33	268
<b>Semispinalis capitis: Complexus</b>	0.02	0.16	106	2.5189	0.25	0.23	0.02	0.02	0.00	0.09	3.33	76.20
	67	69	0	E-05	80	40	40	62	04	90	33	019
<b>Longissimus capitis</b>	0.03	0.24	106	3.6887	0.28	0.28	0.00	0.03	0.00	0.07	1.66	142.9
	91	44	0	E-05	00	00	00	91	00	74	67	116
<b>Serratus ventralis cervicis</b>	0.08	0.53	106	8.0943	0.24	0.24	0.00	0.08	0.00	0.10	3.33	228.6
	58	63	0	E-05	20	20	00	58	00	60	33	975
<b>Longus capitis</b>	0.01	0.12	106	1.8585	0.18	0.18	0.00	0.01	0.00	0.07	6.66	75.85
	97	31	0	E-05	40	40	00	97	00	30	67	99
<b>Omotransversarius</b>	0.03	0.18	106	2.8491	0.23	0.23	0.00	0.03	0.00	0.24	0.00	35.17
	02	88	0	E-05	80	80	00	02	00	30	00	354
<b>Obliquus capitis cranialis</b>	0.02	0.16	106	2.4340	0.07	0.07	0.00	0.02	0.00	0.05	3.33	139.6
	58	13	0	E-05	10	10	00	58	00	22	33	462
<b>Obliquus capitis caudalis</b>	0.01	0.07	106	1.1509	0.09	0.09	0.00	0.01	0.00	0.08	0.00	43.16
	22	63	0	E-05	20	20	00	22	00	00	00	038
<b>Spinalis et semispinalis cervicis</b>	0.05	0.33	106	5.0660	0.26	0.26	0.00	0.05	0.00	0.11	6.66	136.2
	37	56	0	E-05	40	40	00	37	00	08	67	396
<b>Trapezius</b>	0.01	0.12	106	1.8679	0.17	0.17	0.00	0.01	0.00	0.11	0.00	48.30
	98	38	0	E-05	70	70	00	98	00	60	00	839
<b>Brachiocephalicus: Cleidomastoideus</b>	0.03	0.20	106	3.0377	0.24	0.24	0.00	0.03	0.00	0.25	1.66	36.14
	22	13	0	E-05	00	00	00	22	00	20	67	822
<b>Brachiocephalicus: Cleidocervicalis</b>	0.04	0.29	106	4.4434	0.29	0.27	0.02	0.04	0.00	0.21	0.00	60.86
	71	44	0	E-05	50	40	10	66	04	90	00	844
<b>Rhomboideus capitis</b>	0.01	0.10	106	1.6038	0.17	0.17	0.00	0.01	0.00	0.07	1.66	62.45
	70	63	0	E-05	35	35	00	70	00	70	67	825
<b>Sternocephalicus</b>	0.26	1.62	106	2.4528	0.23	0.23	0.00	0.26	0.00	0.22	0.00	327.0
	00	50	0	E-04	70	70	00	00	00	50	00	44
<b>Longus Colli</b>	0.02	0.16	106	2.5472	0.20	0.19	0.00	0.02	0.00	0.12	5.00	62.91
	70	88	0	E-05	60	80	80	69	01	10	00	265

Appendix F. Adjusted normalised fibre length values for each muscle over the study gait cycle.



Appendix G. Surgical technique, radiographic follow-up and long-term outcome (ASP, adjacent segment pathology; F/U, follow-up).

Case	Affected Segment	Supportive Stabilization	End-Plate Measurements (mm)			Distraction Index %			Medium-Term CT Findings			Long-Term CT Findings		Long-Term Outcome	
			Pre-op	Post-op	F/U	Post-op	F/U	Subsidence	Fusion	Minor Complications	ASP	F/U (months)	Outcome	Cause of Euthanasia	
1	C6-C7	Screws + bone cement	43.6	45.2	42.5	3.67	-2.52	Yes	Yes	Fractured bone cement	-	10	Improved	-	
2	C5-C6	Screws + bone cement	52.83	55.1	54.5	4.3	3.16	No	No	None	-	12	Improved	-	
	C6-C7	Screws + bone cement	48.54	49.33	49.23	1.63	1.42	No	Yes	Broken screw in C7	-				
3	C6-C7	Screws + bone cement	47.98	50.53	49.39	5.31	2.94	No	Yes	None	No	9	Improved	-	
4	C5-C6	Paired locking plates	56.46	59.35	57.85	5.12	2.46	No	Yes	None	No	24	Improved	Neoplasia	
	C6-C7	Paired locking plates	49.2	50.58	49.21	2.8	0.02	No	Yes	1/12 screws backed out of plate in C7, 2/12 loose	Yes				
5	C6-C7	Paired locking plates	72.03	73.01	72.1	1.36	0.1	No	Yes	2/12 screws backed out of plate in C7	Yes	33	Improved	-	
6	C5-C6	Paired locking plates	59.21	60.68	60.55	2.48	2.26	No	Yes	None	No	20	Improved	-	
	C6-C7	Paired locking plates	55.77	55.9	54.33	0.23	-2.58	Yes	Yes	4/12 screws backed out of plate in C7	No				
7	C5-C6	Paired locking plates	58.97	59.72	54.92	1.27	-6.87	Yes*	Yes	1/8 screw backed out of plate in C7, 1/8 loose	-	9	Deteriorated	IMPA	
8	C5-C6	Pedicle screws - rod	61.3	61.6	61.2	0.49	0.16	No	Yes	Minor vertebral canal breach	Yes	13	Improved	Heart Failure	
	C6-C7	Pedicle screws - rod	53.1	55.1	54.5	3.77	2.64	No	Yes	None	Yes				
9	C6-C7	Screws + bone cement	53.8	55.2	53.9	2.6	0.19	No	Yes	None	No	12	Improved	-	

Asterisk denotes clinically relevant vertebral subsidence.